



**Fábio Duarte Vidal**

**Modelação de fenómenos de ventilação em casas passivas**

**Modelling ventilation phenomena in passive houses**





**Fábio Duarte Vidal**

**Modelação de fenómenos de ventilação em casas passivas**

Dissertação apresentada à Universidade de Aveiro para cumprimento dos requisitos necessários à obtenção do grau de Mestre em Engenharia Civil, realizada sob a orientação científica da Professora Doutora Inês Osório de Castro Meireles, Professora Auxiliar do Departamento de Engenharia Civil da Universidade de Aveiro e coorientação científica do Professor Doutor Romeu da Silva Vicente, Professor Associado do Departamento de Engenharia Civil da Universidade de Aveiro e da Professora Doutora Maria Fernanda da Silva Rodrigues, Professora Auxiliar do Departamento de Engenharia Civil da Universidade de Aveiro.





**Fábio Duarte Vidal**

**Modelling ventilation phenomena in Passive Houses**

Dissertation submitted to the University of Aveiro to fulfill the necessary requirements for the degree of Master in Civil Engineering, held under the scientific orientation of Doctor Inês Osório de Castro Meireles, Professora Auxiliar at the Department of Civil Engineering of the University of Aveiro and under the co-orientation of Doctor Romeu da Silva Vicente, Professor Associado at the Department of Civil Engineering of the University of Aveiro and Doctor Maria Fernanda da Silva Rodrigues, Professora Auxiliar at the Department of Civil Engineering of the University of Aveiro.



*Aos meus pais*





## **o júri**

presidente

**Professora Doutora Ana Luísa Pinheiro Lomelino Velosa**  
Professora Associada da Universidade de Aveiro

**Professor Doutor Vítor Faria e Sousa**  
Professor Auxiliar do Instituto Superior Técnico (arguente)

**Professor Doutor Romeu da Silva Vicente**  
Professor Associado da Universidade de Aveiro (coorientador).



## **agradecimentos**

Gostaria de agradecer a todas as pessoas que, de uma forma ou de outra, contribuíram para realização desta dissertação e que sempre me acompanharam e ajudaram durante o meu percurso académico.

Queria apresentar o meu agradecimento ao Instituto Superior Técnico, em particular ao Professor Vítor Faria e Sousa, pela disponibilização do software necessário para a realização deste trabalho e por toda a ajuda prestada.

Queria também apresentar o meu agradecimento à Modiko® e à Téketo® por permitirem que este estudo fosse realizado no seu projeto Passive House.

Agradeço à minha orientadora, a Professora Doutora Inês Meireles, por todo o conhecimento, ajuda e disponibilidade que sempre me transmitiu e pela motivação que me foi dando nos momentos mais difíceis. Agradeço também aos meus coorientadores, o Professor Doutor Romeu Vicente e a Professora Doutora Fernanda Rodrigues, também pelos conhecimentos transmitidos e por toda a ajuda que sempre me prestaram.

Um especial agradecimento ao Engenheiro Rui Oliveira pela sua enorme disponibilidade e pelas horas perdidas com a minha tese, tanto a ajudar-me nos ensaios de campo como em qualquer outra situação que eu necessitava. Em muitas situações, dispensou mais do seu tempo do que lhe era pedido e, por isso, muito obrigado.

Um enorme agradecimento aos meus amigos mais próximos, não só pela ajuda que me prestaram neste trabalho, mas por tudo. Refiro-me ao Telmo, à Regina, ao Diogo, ao Fred, ao Pica, à Silvério, ao Flávio, à Chica, ao Zero, ao Princesa, ao Pina, ao Joel e à Renata.

Por fim, agradeço a toda a minha família, em particular aos meus pais, à minha irmã, ao meu irmão, aos meus avós, à minha tia Célia e às minhas primas pequeninas por todo o apoio que me deram.



## palavras-chave

Casas passivas, Ventilação, Conforto térmico, Mecânica dos fluidos computacional (CFD), Velocidade do ar, Temperatura do ar.

## resumo

A presente dissertação visa aliar o uso de programas de simulação numérica de fluidos, mais concretamente a mecânica dos fluidos computacional (CFD), no apoio à conceção de sistemas de ventilação em casas passivas.

A construção sustentável é cada vez mais uma preocupação no mercado atual da construção, encontrando nessas casas uma alternativa muito válida no que toca a poupanças de energia neste setor. Uma casa passiva é reconhecida por obter altos níveis de conforto térmico sem necessidade de grandes consumos de energia. Para além de um isolamento térmico rigoroso, o uso de sistemas de ventilação de elevada eficiência é um dos principais fatores para atingir tais níveis de conforto. Esta dissertação pretende, por isso, fazer um estudo da circulação de ar resultante de um sistema de ventilação mecânica numa casa passiva construída em Portugal e a conseqüente análise do conforto térmico que nela se obtém, tendo sido utilizado um programa comercial de CFD, o *FLOW-3D*<sup>®</sup>.

Foi necessário realizar uma validação do programa através da comparação de valores de velocidade do ar obtidos numericamente pelo respetivo algoritmo de cálculo e experimentalmente através do registo de velocidades do ar na casa passiva objeto de estudo, tendo-se utilizado para o efeito anemómetros digitais. Por fim, após a validação descrita anteriormente, foi feita uma análise do conforto térmico do edifício em estudo com base em registos de temperatura obtidos experimentalmente e de velocidades do ar obtidos da simulação efetuada.



**keywords**

Passive houses, Ventilation, Thermal comfort, Computational Fluid Dynamics (CFD), Air velocity, Air temperature.

**abstract**

The present dissertation aims to combine the use of Computational Fluid Dynamics (CFD) software, to support the design of ventilation systems in passive houses.

Sustainable construction is an increasing concern in the current construction market, finding in these houses a valid alternative in order to enhance energy savings in this sector. A passive house is known for achieving high levels of thermal comfort without consuming too much energy. In addition to an extremely rigorous thermal insulation, the use of highly efficient ventilation systems is one of the main factors in achieving such levels of comfort. Therefore, this dissertation intends to study the circulation of air associated to the mechanical ventilation system of a passive house in Portugal and consequent analysis of its thermal comfort. To achieve such purpose, a CFD commercial program called *FLOW-3D*<sup>®</sup> will be used.

It was necessary to perform a validation of the program by comparing air velocities obtained numerically by the program and experimentally through the registration of air velocities in the studied passive house with the use of digital anemometers.

Lastly, after the validation described above, an analysis over the thermal comfort of the building was performed, based on temperature registrations obtained experimentally and velocity values obtained from the numerical simulations.





## Table of Contents

List of Figures.....	III
List of Tables.....	VII
Notation.....	IX
Chapter 1. Introduction.....	3
1.1 Background and motivation.....	3
1.2 Objectives.....	4
1.3 Methodology.....	4
1.4 Thesis outline.....	5
Chapter 2. Passive House.....	9
2.1 Passive House concept.....	9
2.2 The Passive House standard.....	10
2.2.1 Passive House Planning Package (PHPP).....	10
2.2.2 Passive House certification.....	11
2.2.3 Passive House requirements.....	12
2.3 Passive House principles.....	12
2.3.1 Thermal insulation.....	13
2.3.2 Elimination of thermal bridges.....	15
2.3.3 High insulated windows.....	18
2.3.4 Airtightness.....	19
2.3.5 Ventilation in Passive Houses.....	22
2.4 Portuguese legislation on energy performance.....	29
2.5 Thermal comfort assessment.....	31
2.5.1 Definition of comfort.....	31
2.5.2 Role of ventilation in achieving thermal comfort and indoor air quality.....	31
2.5.3 Methods for evaluating comfort.....	33
Chapter 3. Numerical Model.....	45
3.1 Computational Fluid Dynamics.....	45
3.2 Fluid motion equations.....	45
3.2.1 The continuity equation – mass is conserved.....	50
3.2.2 The momentum equation – Newton’s 2 <sup>nd</sup> law.....	51

3.2.3	The energy equation – energy is conserved .....	55
3.3	Types of flow .....	59
3.4	Turbulent flow .....	61
3.4.1	Turbulence models .....	62
3.5	Elements in a CFD code .....	64
3.5.1	Pre-processor .....	64
3.5.2	Solver .....	64
3.5.3	Post-processor .....	65
3.6	<i>FLOW-3D</i> <sup>®</sup> modelling .....	65
3.6.1	Finite volume method.....	65
3.6.2	Grid definition .....	66
3.6.3	FAVOR <sup>™</sup> method.....	71
3.6.4	Boundary conditions .....	72
Chapter 4.	Case Study.....	75
4.1	Building description.....	75
4.2	Experimental analysis .....	77
4.2.1	Experimental procedure 1 – blower door.....	78
4.2.2	Experimental procedure 2 – mechanical ventilation system.....	83
4.3	Numerical analysis.....	86
4.3.1	Numerical procedure 1 – blower door.....	86
4.3.2	Numerical procedure 2 – mechanical ventilation system.....	92
Chapter 5.	Results Analysis .....	103
5.1	Procedure 1 – blower door.....	103
5.2	Procedure 2 – mechanical ventilation system.....	108
5.3	Thermal comfort evaluation.....	121
Chapter 6.	Final Considerations.....	127
6.1	Conclusions.....	127
6.2	Future developments.....	129
References	.....	135
Appendix A	.....	145
Appendix B	.....	146
Appendix C	.....	147

## List of Figures

Figure 1 – First ever Passive House located in Darmstadt, Germany. ....	9
Figure 2 – 5 main Passive House principles. ....	13
Figure 3 – Thermographic image showing the advantages of a proper thermal insulation. ..	15
Figure 4 – Schematic illustrations of conventional thermal bridges. ....	16
Figure 5 – Highly efficient window with insulated frame and multiple low-e glazing. ....	18
Figure 6 – “Red pencil method” to assure an airtight envelope. ....	20
Figure 7 – Airtight membranes installed to prevent leakages in building’s envelope. ....	20
Figure 8 – Blower door test. ....	22
Figure 9 – Natural ventilation principles. ....	25
Figure 10 – Schematic Passive House ventilation system. ....	27
Figure 11 – Schematic illustration of an air-to-air heat exchanger. ....	27
Figure 12 – Influence of relative humidity in thermal comfort. ....	32
Figure 13 – PPD as function of PMV, presenting category B levels of comfort. ....	36
Figure 14 – Design values for the indoor operative temperature for buildings without mechanical cooling systems as function of the exponentially-weighted running mean of the outdoor temperature. ....	40
Figure 15 – Indoor operative temperature as function of the exponentially-weighted running mean of the outdoor temperature when these are below the minimum limit. ....	40
Figure 16 – Thermal comfort analysis for the cooling season of a category II building. ....	41
Figure 17 – Finite control volume. ....	46
Figure 18 – Infinitesimal fluid element. ....	47
Figure 19 – Fluid element moving in the Cartesian flow field. ....	48
Figure 20 – Graphic representations of surfaces forces. ....	53
Figure 21 – Surface forces in $x$ direction represented in an infinitesimally small, moving element. ....	53
Figure 22 – Energy fluxes in an infinitesimally small, moving fluid element, solely in the $x$ direction. ....	56
Figure 23 – Laminar flow. ....	59
Figure 24 – Turbulent flow. ....	60
Figure 25 – Flow chart of the turbulence models studied by Zhai <i>et al.</i> (2007). ....	62
Figure 26 – Representation of flow variables in a typical <i>FLOW-3D</i> <sup>®</sup> cell. ....	66

Figure 27 – Types of mesh elements. ....	67
Figure 28 – Types of hexahedral meshes. ....	68
Figure 29 – Tetrahedral unstructured mesh. ....	68
Figure 30 – Uniform grid. ....	69
Figure 31 – Non-uniform grid. ....	70
Figure 32 – Conforming mesh concept to model a thin cavity in a large solid. ....	70
Figure 33 – FAVOR <sup>TM</sup> method. ....	71
Figure 34 – Studied Passive House dwelling. ....	75
Figure 35 – Complex where the studied dwelling is inserted (in red). ....	75
Figure 36 – Plan view of the ground floor. ....	76
Figure 37 – Plan view of the 1 <sup>st</sup> floor. ....	76
Figure 38 – Hole for the ventilation duct. ....	78
Figure 39 – Identification of the space in study where the blower door test was performed (in red). ....	78
Figure 40 – 3D model of the space where the blower door test was conducted. ....	79
Figure 41 – Digital anemometer used to register air velocities in experimental procedure 1. ....	79
Figure 42 – Blower door installed to conduct the experiment. ....	80
Figure 43 – Illustration of the expected airflow caused by a depressurized blower installed at the door. ....	81
Figure 44 – Part of the grid used to mark the exact points where the anemometer registered values below the ventilation opening. ....	82
Figure 45 – Plan views of each height with the identification of the registration points below the air inlet. ....	82
Figure 46 – Slope of the ventilation duct. ....	83
Figure 47 – Thermo hygrometer used in experimental procedure 2. ....	84
Figure 48 – Anemometer used in experimental procedure 2. ....	84
Figure 49 – Ventilation grid. ....	85
Figure 50 – Representation of each measuring point. ....	86
Figure 51 – 3D model of the space in study. ....	87
Figure 52 – Partition walls approximated as baffles. ....	87
Figure 53 – 3D model representing all subcomponents that define the geometry in study. ....	89

---

Figure 54 – Mesh definition of the region in study. ....	89
Figure 55 – Mass averaged mean kinetic energy of the solution. ....	90
Figure 56 – Mass-averaged turbulent energy of the solution. ....	90
Figure 57 – Boundary conditions applied to the model.....	92
Figure 58 – 3D model of the studied house.....	93
Figure 59 – Pictures of details which helped to accurately draw the ventilation ductwork.	93
Figure 60 – Ventilation system ductwork modelled using AutoCAD software.....	94
Figure 61 – Position of the ductwork within the suspended ceilings (direction $y$ of the house). .....	95
Figure 62 – Interior content of the studied house’s 3D model. ....	95
Figure 63 – Grids considered in the convergence test.....	96
Figure 64 – Convergence process in the $z$ plan. ....	97
Figure 65 – Convergence test in the $x$ plan. ....	97
Figure 66 – Convergence test in the $y$ plan. ....	98
Figure 67 – Grid definition of the modelled house. ....	98
Figure 68 – Mass averaged mean kinetic energy of the solution. ....	99
Figure 69 – Mass-averaged turbulent energy of the solution. ....	99
Figure 70 – Numerical velocity field (m/s) in the chosen $z$ plans. ....	104
Figure 71 – Numerical velocity field (m/s) in the chosen $y$ plans.....	104
Figure 72 – Numerical velocity field (m/s) in the chosen $x$ plans.....	105
Figure 73 – Numerical velocity results (m/s) at the air outlet. ....	105
Figure 74 – Graphical analysis of the velocity results obtained experimentally by the blower door test and through numerical simulation. ....	107
Figure 75 – Grid’s fixator that blocks the airflow at point 3.....	109
Figure 76 – Velocity results (m/s) inside the ventilation ductwork. ....	110
Figure 77 – Sectional detail of the ventilation duct at $x = 4.02$ m.....	111
Figure 78 – Air velocities (m/s) at supply and extraction points in different $z$ plans.....	111
Figure 79 – Airflow directions in supply and extraction grids.....	112
Figure 80 – Sectional plans to illustrate the airflow velocities (m/s) in different areas of the model. ....	112
Figure 81 – Graphical analysis of velocity results in the living room.....	113
Figure 82 – Graphical analysis of velocity results in room 1.....	114

Figure 83 – Graphical analysis of velocity results in room 2.....	114
Figure 84 – Graphical analysis of velocity results in room 3.....	114
Figure 85 – Graphical analysis of velocity results in room 4.....	115
Figure 86 – Graphical analysis of velocity results in hallway 1.....	115
Figure 87 – Graphical analysis of velocity results in hallway 2.....	115
Figure 88 – Graphical analysis of velocity results in sanitary facility 1. ....	116
Figure 89 – Graphical analysis of velocity results in sanitary facility 2. ....	116
Figure 90 – Graphical analysis of velocity results in sanitary facility 3. ....	117
Figure 91 – Graphical analysis of velocity results in sanitary facility 4. ....	117
Figure 92 – Graphical analysis of velocity results in the kitchen.....	117
Figure 93 – Velocity field in different compartments with indication of the position of points 4. ....	120
Figure 94 – Model of a ventilation grid.....	130
Figure C. 1 – Experimental vs numerical velocities for each point in room 1.....	147
Figure C. 2 – Experimental vs numerical velocities for each point in room 2.....	147
Figure C. 3 - Experimental vs numerical velocity results for each point in room 3.....	148
Figure C. 4 – Experimental vs numerical velocity results for each point in room 4.....	148
Figure C. 5 – Experimental vs numerical velocity results for each point in hallway 1.....	149
Figure C. 6 – Experimental vs numerical velocity results for each point in hallway 2.....	149

## List of Tables

Table 1 – Thickness needed for several elements to achieve a $0.13 \text{ W}/(\text{m}^2 \cdot ^\circ\text{C})$ U-value....	14
Table 2 – Target values for pollutants in Portuguese Regulation.....	23
Table 3 – Thermal requirements established in the RCCTE against Passive House values. .....	30
Table 4 – Ventilation rates for each level of indoor air quality.....	32
Table 5 – Thermal sensation scale.....	35
Table 6 – Categories of thermal environment. ....	38
Table 7 – Description of the applicability of the thermal environment categories depicted in the EN 15251 Standard.....	39
Table 8 – Values of the constants of the standard k- $\epsilon$ and RNG k- $\epsilon$ models. ....	63
Table 9 – Design characteristics of the original house compared to the Passive House....	77
Table 10 – Technical specifications of the anemometer used in experimental procedure 1. .....	80
Table 11 – Technical specifications of the thermo hygrometers used in experimental procedure 2. ....	84
Table 12 – Technical specifications of the anemometer used in experimental procedure 2. .....	84
Table 13 – Cell sizes of each multi-block mesh for the 5 tests. ....	96
Table 14 – Average velocity values measured at each point.....	103
Table 15 – Analysis between experimental and numerical data in procedure 1. ....	106
Table 16 – Experimental velocity results for the living room and rooms 1, 2 and 3. ....	108
Table 17 – Experimental velocity results for room 4, the upstairs hallway and kitchen...	108
Table 18 – Experimental velocity results for the 4 sanitary facilities. ....	109
Table 19 – Analysis between experimental and numerical results in procedure 2.....	118
Table 20 – Thermal comfort evaluation according to ISO 7730-2006.....	122
Table 21 – Local discomfort parameters calculated according to ISO 7730-2006. ....	124
Table A. 1 – Plan coordinates of each point measured near the inlet in experimental procedure 1.....	145
Table A. 2 – Plan coordinates of the outlet point in experimental procedure 1.....	145
Table B. 1 – Numerical range of the velocity results of experimental procedure 1.....	146





## Notation

### *Roman upper case letters*

$C$	Heat exchange through convection
$D/Dt$	Substantial derivative
$E$	Heat loss by evaporation
$\vec{F}$	Force vector
$F_x$	Force in the $x$ direction
$I_{cl}$	Clothing insulation
$G$	Buoyancy term
$M$	Metabolism rate; Mach number
$R$	Heat exchange through radiation
$Re$	Reynolds number
$S$	Heat accumulation in the body
$T$	Local temperature gradient
$Tu$	Turbulence intensity
$U$	Velocity averaged over a tube's cross section
$\vec{V}$	Velocity field vector
$V^2/2$	Kinetic energy of a moving fluid per unit mass
$W$	Energy of the realized mechanical work

### *Roman lower case letters*

$\vec{a}$	Acceleration vector
$a_x$	Acceleration in the $x$ direction
$c$	Velocity of sound
$d$	Tube diameter
$e$	Internal energy of a moving fluid per unit mass
$\vec{i}, \vec{j}, \vec{k}$	Unit vectors in the $x$ , $y$ and $z$ directions respectively
$k$	Thermal conductivity; turbulent kinetic energy
$m$	Mass of the element
$p$	Pressure force

$p_a$	Water vapour partial pressure
$\dot{q}$	Rate of volumetric heat addition per unit mass
$t_a$	Air temperature
$t_{a,l}$	Local air temperature
$t_f$	Floor temperature
$\bar{t}_r$	Mean radiant temperature
$u, v, w$	$x, y$ and $z$ components of velocity respectively
$\overline{u_{m_i}}, \overline{u_{m_j}}$	Time averaged mixture velocity components in the directions $x_i$ and $x_j$ respectively
$\bar{v}_{a,l}$	Local mean air velocity
$v_a$	Air velocity

*Greek upper case letters*

$\Delta t_{a,v}$	Vertical air temperature difference between the head and feet
$\Delta t_{pr}$	Radiant thermal asymmetry

*Greek lower case letters*

$\delta m$	Mass of a moving fluid element
$\delta V$	Volume of a moving fluid element
$\varepsilon$	Dissipation rate of the turbulent kinetic energy
$\theta_{n-i}$	Running mean outdoor temperature of the previous day
$\theta_o$	Indoor operative temperature
$\theta_{rm}$	Running mean outdoor temperature
$\mu$	Fluid viscosity
$\mu_T$	Eddy dynamic viscosity
$\rho$	Fluid density
$\rho_0$	Reference density
$\tau_{xx}$	Normal stress
$\tau_{yx}$	Shear stress
$\nu$	Kinematic viscosity parameter

*Symbols*

∇ Vector operator

*Abbreviations*

CFD	Computational Fluid Dynamics
DES	Detached Eddy Simulation
DNS	Direct Numerical Simulation
DR	Draught Rate
ECM	Electronic Commuted Motor
EPBD	Energy Performance of Buildings Directive
HRV	Heat Recovery Ventilation
HVAC	Heating, Ventilating and Air Conditioning
LES	Large Eddy Simulation
NZEB	Nearly Zero Energy Building
PD	Percentage Dissatisfied
PHPP	Passive House Planning Package
PMV	Predicted Mean Vote
PPD	Predicted Percentage Dissatisfied
RANS	Reynolds-Averaged Navier-Stokes
RCCTE	<i>Regulamento das Características de Comportamento Térmico dos Edifícios</i>
RECS	<i>Regulamento de Desempenho Energético dos Edifícios de Comércio e Serviços</i>
REH	<i>Regulamento de Desempenho Energético dos Edifícios de Habitação</i>
RNG	Renormalized Group
RSECE	<i>Regulamento dos Sistemas Energéticos de Climatização em Edifícios</i>
SCE	<i>Sistema Nacional de Certificação Energética e da Qualidade do Ar interior nos Edifícios</i>



# Chapter 1

---

Introduction



# Chapter 1. Introduction

## 1.1 Background and motivation

For over 200 years, ever since the Industrial Revolution, fossil fuels have been the most important source of energy all over the world. For most of this time, the consequences of their incessant use were not taken into account. However, today it is known that not only are they a limited resource, but also a dangerous source of pollution. The scarcity of elements such as petroleum, coal and natural gas and the emission of greenhouse gases associated to their combustion, causing global warming, forces the usage of clean and renewable sources of energy.

Within the European Union, buildings represent 40% of the total energy consumption, which will only tend to grow with the expansion of this sector. Therefore, it is crucial to reduce the energy consumption in buildings and, if possible, start relying on renewable sources of energy, in order to reduce the emission of greenhouse gases. The European Council of March 2007 emphasized the need to increase energy efficiency in order to reduce in 20% the energy consumption by 2020. According to the EPBD 2010/31/EU, all buildings constructed after 2020, or after 2018 for public buildings, should be “Nearly Zero-Energy Buildings” (NZEB) (EPBD, 2010).

The Nearly Zero-Energy Building concept arises not only at a European level, but in a global context due to the significant impacts of buildings on the energy consumption and on the worldwide environment (Sousa *et al.*, 2012). A NZEB refers to a high energy performance building in which a very significant extent of its annual primary energy consumption is covered by energy from renewable sources, produced on-site or nearby. Basically, a building with these characteristics should present an annual primary energy balance near 0 kWh/(m<sup>2</sup>.year), meaning that it produces practically as much energy as it consumes (Aelenei *et al.* 2013). An efficient way to help obtain such an energy balance is through the use of passive measures. A well-established concept that implements these measures in buildings is the Passive House concept. In fact, studies performed by Aelenei *et al.* (2012) on buildings that adopted certain strategies to obtain a NZEB status, actually possess similar characteristics to Passive House buildings. Therefore, it is safe to say that the Passive House

standard is a very efficient way to enhance energy efficiency in buildings and achieve the mandatory goals in the European directive.

One of the most important aspects of a Passive House building is the thermal comfort achieved from a rigorous insulation and airtightness of their external facades. Although this comfort is seen as the biggest advantage of a Passive House building, if its total insulation is not accompanied by an efficient ventilation system, the indoor air quality will be seriously affected. For that matter, a detailed ventilation study is fundamental to combine thermal comfort and indoor air quality in Passive Houses.

A ventilation phenomenon is nothing more than a controlled circulation of air, therefore, it is included in the fluid mechanics' area of study. An instrument commonly used in this area is Computational Fluid Dynamics (CFD). Although it is widely accepted among the scientific community, it still requires studies to properly validate CFD commercial programs, which serves as motivation to the present dissertation.

## **1.2 Objectives**

The main objective of this dissertation is to validate ventilation phenomena simulations with the Computational Fluid Dynamics commercial program *FLOW-3D*<sup>®</sup>, by comparing airflow results obtained by the program with experimental data obtained in a Passive House dwelling. To properly validate the software, it is important to create a numerical model as close to the actual simulated dwelling as possible. This validation renders possible the use of CFD programs to provide support in the design of ventilation systems in passive houses. After a proper validation, it is intended to evaluate the level of thermal comfort that is obtained inside the house, based on thermal experimental data gathered on site and on numerical values resultant from the simulations.

## **1.3 Methodology**

In order to validate the *FLOW-3D*<sup>®</sup> simulations, a comparison between experimental and numerical data was carried out. For that, two separate experimental procedures and respective numerical simulations were performed. The experimental data was collected in a Passive House built in Portugal. The first consisted in installing a blower door in a sanitary facility in order to create an airflow that would be monitored using a digital anemometer. This scenario was then simulated using *FLOW-3D*<sup>®</sup> in order to extract air velocity results



which would be compared with the velocities registered by the anemometer. The second procedure had the same bases as the first, expect, instead of creating a forced airflow through a blower door, the measured air velocities were those caused by the Passive House mechanical ventilation system. A full-scale model of the dwelling was created in *FLOW-3D*<sup>®</sup> (including the ventilation system) and the velocity results were extracted and compared with the ones from the anemometer. Temperature and relative humidity data were also gathered inside the Passive House with the use of thermo hygrometers and, using the velocity results obtained numerically, based on the ISO 7730 norm, a prediction over the thermal comfort criteria was performed by calculating PMV (Predicted Mean Vote) and PPD (Predicted Percentage of Dissatisfied) indices and local discomfort parameters.

#### **1.4 Thesis outline**

The dissertation develops along 6 chapters. Chapter 1 is dedicated to the background and motivation of the dissertation, the objectives and methodology.

Chapter 2 addresses the Portuguese legislation over energy performance, presenting the evolution of the documents that regulate building's energy needs. This chapter also describes the Passive House concept, its requirements, certification and the 5 main principles that help achieve its low energy standard. Within these principles, a higher focus was done over ventilation by addressing natural and mechanical ventilation principles, heat recovery ventilation and overnight ventilation in preventing the risk of overheating. Finally, this chapter presents a thermal comfort assessment, emphasizing the role of ventilation and methods to evaluate comfort.

Chapter 3 describes the main features of the CFD software, *FLOW-3D*<sup>®</sup>. It presents the fluid's motion equations, addresses turbulent flows and turbulence models and all relevant aspects in a numerical simulation, such as the definition of geometry, grid and boundary conditions.

Chapter 4 describes the case study, namely the experimental procedures and numerical simulations that were performed.

Chapter 5 is dedicated to presenting the obtained experimental and numerical results and consequent comparison and analysis.

Finally, Chapter 6 presents the main conclusions of the research done in this dissertation and prospects for future developments.



# Chapter 2

---

Passive House



## Chapter 2. Passive House

### 2.1 Passive House concept

The Passive House concept was created in 1988 by Professor Bo Adamson from Sweden and Dr. Wolfgang Feist from Germany, in order to achieve the low energy demands in construction in the mid 80's. Their research led to the construction of the first Passive House building in Europe, located in Kranichstein, Darmstadt, Germany in 1991 (Passipedia, 2015a) and later a second building in Groß Umstadt, Germany in 1995. These buildings were intended to have a low energy consumption at a reasonable cost, but adequate to the German climate (Passive-On project, 2007). The Kranichstein, Darmstadt building was the first inhabited multi-family house in Europe to achieve a heating energy consumption of below 12 kWh/(m<sup>2</sup>.year), confirmed through years of monitoring. Figure 1 illustrates a picture of this building.



Figure 1 – First ever Passive House located in Darmstadt, Germany (Schnieders, 2003).

The lessons learned from this first prototype were used to develop the Passive House standard. The success of these constructions led to the creation of the Passive House Institute, an independent research institute located in Darmstadt, headed by Dr. Wolfgang Feist. This institute dedicates its research to energy efficient buildings mostly in Germany, but also in spreading the concept around the world. This concept is now widely disclosed, existing over 8 000 passive buildings around the world (PHI, 2015a).

According to the Passive House Institute, a Passive House is not an energy standard but an integrated concept that attends to assure the highest level of comfort. It states the following definition: “*A Passive House is a building, for which thermal comfort (ISO 7730) can be achieved solely by post-heating or post-cooling of the fresh air mass, which is required to achieve sufficient indoor air quality conditions – without the need for additional recirculation of air*”, this being a purely functional definition, with no numerical values and, therefore, valid for any climate (Passipedia, 2015b).

The Passive House Institute is responsible for the certification of Passive Houses, by emitting the “Quality-Approved Passive House” certificate. For that, there are over 30 Passive House building certifiers around the world, each having to be properly accredited by the Passive House Institute, which may certify buildings in the name of the Institute, according to the internationally recognized Passive House Standard. This is also valid for retrofits that include Passive House components, following the EnerPHit Standard. In special cases, the Institute itself may carry out the certification. In order to evaluate buildings that seek the certification, the Institute created a calculation tool named “Passive House Planning Package” that evaluates the building’s energy performance, by determining specific parameters that must obey to the Passive House requirements (IPHA, 2014).

## **2.2 The Passive House standard**

The Passive House standard consists mainly of three elements: imposition of an energy limit for heating or cooling the indoor environment, water heating and electricity; quality requirements for the users, mostly in terms of thermal comfort; and finally the use of passive systems to reach the first two elements at a profitable cost (Passive-On project, 2007). These elements are analysed by the calculation tool Passive House Planning Package.

### **2.2.1 Passive House Planning Package (PHPP)**

The PHPP was first released in 1998 and has been developed ever since, suffering alterations throughout the years, in order to accompany the evolution in construction methods. The PHPP is a calculation tool consisting of a series of spreadsheets, each with a specific purpose and calculation method. The programme is mainly based on Excel. It prepares an energy balance and calculates the annual energy demand of the building. It contains all necessary information for a proper design of a Passive House.

The PHPP forms the basis for the certification of a building as a Passive House or an EnerPHit, in the case of retrofits, and the primary results provided by this tool are (Passipedia, 2015c):

- The maximum heating load [ $\text{W}/\text{m}^2$ ] and the annual heating demand [ $\text{kWh}/(\text{m}^2\cdot\text{year})$ ].
- Thermal comfort in the summer with active cooling: maximum cooling load [ $\text{W}/\text{m}^2$ ] and annual cooling demand [ $\text{kWh}/(\text{m}^2\cdot\text{year})$ ].
- Thermal comfort in the summer with passive cooling: frequency of overheating events [%].
- Annual primary energy demand for the entire building [ $\text{kWh}/(\text{m}^2\cdot\text{year})$ ].

The PHPP is responsible for designing individual components (windows, shadings, ventilation, U-values, etc.), the heating and cooling loads, mechanical systems for the whole building (ventilation, heating, cooling and hot water provision), evaluating year-round thermal comfort and verifying the building's energy efficiency. The PHPP is composed of the following worksheets: verification, overview, climate, the overall heat transfer coefficient or U-value, areas, ground, components, windows, shading, ventilation, additional vent, annual heating demand, heating load, summVent, summer cooling, cooling units, cooling load, DHW+Distribution, PHPP – solar DHW worksheet, PV, electricity, use non-res, electricity non-res, Aux electricity, IHG, IHG non-res, PE value, compact, HP, HP ground boiler, district heating and refurbishment (IPHA, 2014; Passipedia, 2015c).

As mentioned before, the PHPP is constantly evolving since it was first created, adding more advanced calculations and new components. The latest PHPP version is the PHPP9 (2015).

### **2.2.2 Passive House certification**

In order for a building to receive the “Quality-Approved Passive House” certificate by the Passive house Institute, it must meet all requirements specified in the Passive House Planning Package. The requirements vary depending on the type of building (residential or service) and whether it is a new building or a retrofit of an existent building (IPHA, 2014). For the retrofit, there is the EnerPHit (the Passive house certificate for retrofits). The Passive House Institute developed the “EnerPHit – Quality-approved Energy Retrofit with Passive House Components” certificate due to the difficulties in achieving the Passive House standard when refurbishing an existing building. In this case, the primary principles to obtain the Passive House standard are the same as in new constructions, however, the requirements

are less demanding and are applied to the best remodelling of an existing building, or simply use Passive House components. For example, in a new construction the energy limit for heating is below 15 kWh/(m<sup>2</sup>.year), while in a retrofit its 25 kWh/(m<sup>2</sup>.year). (Passipedia, 2015d).

### **2.2.3 Passive House requirements**

The Passive House concept demands a set of requirements in order for a building to be considered a low energy consumption Passive House building, which include (Passive-On project, 2007; IPHA, 2014):

#### Heating and cooling demand

The nominal energy needs for building's heating and cooling cannot exceed the limit of 15 kWh/(m<sup>2</sup>.year) (or 10 W/m<sup>2</sup> on a peak demand) for each situation. These values must be checked with the help of the PHPP. The cooling demand has an additional climate-dependent allowance for dehumidification.

#### Primary energy demand

The primary energy consumption related to energy service applications (water heating, electrical equipment and lighting) must not exceed the limit of 120 kWh/(m<sup>2</sup>.year) according to the calculation made in the PHPP.

#### Airtightness

The building's air tightness must be verified by performing an onsite blower door test, at both pressurization and depressurization (positive and negative pressure respectively) of 50 Pa. The results for the air change rate ( $n_{50}$ ) must be below 0.6 air changes per hour (ach<sup>-1</sup>).

#### Thermal comfort

Thermal comfort requirements are set for all living areas year-round and define that in any given year, the indoor temperature should not exceed 25°C in more than 10% of the hours. In the winter, the indoor air temperature should not drop below 20°C and the minimum indoor surface temperatures of the building must be over 17°C, including at the window glazing's surface.

## **2.3 Passive House principles**

To achieve the Passive House standard and its requirements, there are 5 main principles that must be established during the planning of the building and corresponding measures must be adopted during its construction, as shown in Figure 2 (IPHA, 2014).



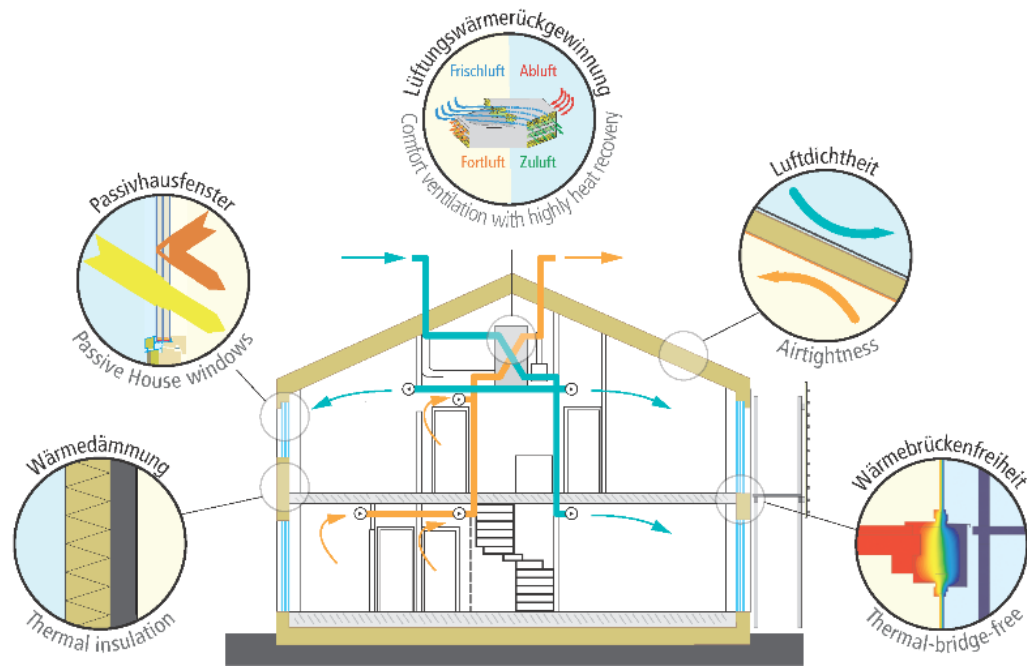


Figure 2 – 5 main Passive House principles (PHI, 2015b).

These 5 principles which help achieve the Passive House requirements are (IPHA, 2014):

- Continuous thermal insulation of the external facades.
- Total elimination of thermal bridges.
- High insulated windows (Multiple pane glazing).
- Rigorous airtightness.
- Highly efficient heat or energy recovery ventilation.

Beyond the implementation of these principles, it is also crucial to install highly efficient, low power consumption equipment. A good exploitation of solar orientation and the use of renewable sources of energy can also help achieve a low energy consumption building. The following subsections will describe the 5 Passive House principles, with a higher attention to the ventilation principle, considering that it is directly related to the area of study of this dissertation.

### 2.3.1 Thermal insulation

The performance of building's external facade is crucial when it comes to thermal comfort. A proper thermal insulation prevents interior heat losses, thus avoiding excessive energy consumption with heating or cooling. According to the Passive House standard, it is not only the insulation thickness of walls, roofs and floors that matter, but also the continuity of the insulation between these elements, meaning that there should be a total absence of

interruptions between elements. If this is not met, the appearance of thermal bridges is inevitable, leading to an increase in heat losses (Antón & Vogt, 2011).

The Passive House standard does not define a specific insulation thickness, however, the Passive House Institute has performed several studies to determine ideal thermal transmittance coefficients, or U-values [ $W/(m^2 \cdot ^\circ C)$ ], for different countries and from that, insulation types and thicknesses can be chosen. The U-value indicates the amount of heat that a surface allows to be transmitted. This means that the lower the U-value, the better the insulation, since it allows less heat loss. The Passive House Institute recommends a U-value of the building's opaque envelope between 0.1 and 0.15  $W/(m^2 \cdot ^\circ C)$  for the German reference case (Schnieders & Hermelink, 2004; Antón & Vogt, 2011) but these values may be slightly higher or lower depending on the climate. A study performed by the Passive-On project where a Portuguese Passive House proposal was presented and analysed had an insulation thickness of 150 mm for the roof and 100 mm for exterior walls, with U-values of 0.23  $W/(m^2 \cdot ^\circ C)$  and 0.32  $W/(m^2 \cdot ^\circ C)$ , respectively (Passive-On project, 2007).

Very low U-values can only be achieved using well-insulating materials. Table 1 demonstrates how thick an external building element (consisting only of the material specified) with a specific thermal conductivity should be, in order to achieve a typical Passive House U-value of 0.13  $W/(m^2 \cdot ^\circ C)$ . Note that elements with higher thermal conductivity allow higher heat losses and gains and, therefore, require thicker insulation.

Table 1 – Thickness needed for several elements to achieve a 0.13  $W/(m^2 \cdot ^\circ C)$  U-value (adapted from Passipedia, 2015e).

<b>Material</b>	<b>Thermal conductivity (<math>W/m \cdot ^\circ C</math>)</b>	<b>Thickness required for <math>U=0.13 W/(m^2 \cdot ^\circ C)</math> (m)</b>
Reinforced concrete	2.30	17.30
Solid brick	0.80	6.02
Perforated brick	0.40	3.01
Porous brick, porous concrete	0.11	0.83
Straw	0.055	0.41
Typical insulation material	0.040	0.30
High-quality conventional insulation material	0.025	0.19
Nanoporous super-insulating material (normal pressure)	0.015	0.11
vacuum insulation material (silica)	0.008	0.06
vacuum insulation material (high vacuum)	0.002	0.015

A proper thermal insulation entails the following advantages:

- Higher thermal inertia in the interior of the building. This means that it is less subject to thermal fluctuations.
- It allows to reduce the thickness of construction elements (such as bricks and concrete).
- Those construction elements are, at the same time, more protected from atmospheric agents (such as wind, rain and snow).
- A proper thermal insulation helps to achieve another Passive House principle, the elimination of thermal bridges, which will be addressed in the next subsection.
- It enhances energy savings, since the heating need is reduced.
- As mentioned before, it improves the building's thermal comfort.

Figure 3 illustrates a thermographic image of a building located in Germany, before and after a passive refurbishment. On the left, before the refurbishment, the building did not possess a proper thermal insulation, therefore, the thermography shows high levels of heat loss throughout the building's facade, while after installing insulation, the thermography shows lower superficial temperatures, due to lower heat losses.



Figure 3 – Thermographic image showing the advantages of a proper thermal insulation (adapted from IPHA, 2014).

### 2.3.2 Elimination of thermal bridges

A thermal bridge can be defined as the localized phenomenon of heat transfer in the building's facade. According to the EN ISO 10211:2007, a thermal bridge is considered the area of the building's envelope that provides less resistance, leading to high heat losses in that area. It states the following definition: *“part of the building envelope where the otherwise uniform thermal resistance is significantly changed by full or partial penetration*

of the building envelope by materials with a different thermal conductivity, and/or a change in thickness of the fabric, and/or a difference between internal and external areas, such as occur at wall/floor/ceiling junctions” (EN ISO 10211:2007). Thermal bridges usually appear when structural elements, such as beams, pillars and the top of slabs, are too close or directly connected to the outside environment without a proper insulation, but they can also occur in the presence of materials with different thermal conductivity in the building’s envelope, in the interconnection between walls and floors or ceilings, in areas where the thickness of structural elements alters, in areas where the insulation is disrupted and in other situations where there is an incorrect connection between structural elements. Also, in door and window areas, it is difficult to ensure an effective connection between the insulation and the window/door frames, which may lead to thermal bridges in these areas (Valério, 2007; Oliveira, 2013). Figure 4 illustrates different causes for thermal bridges occurrence.

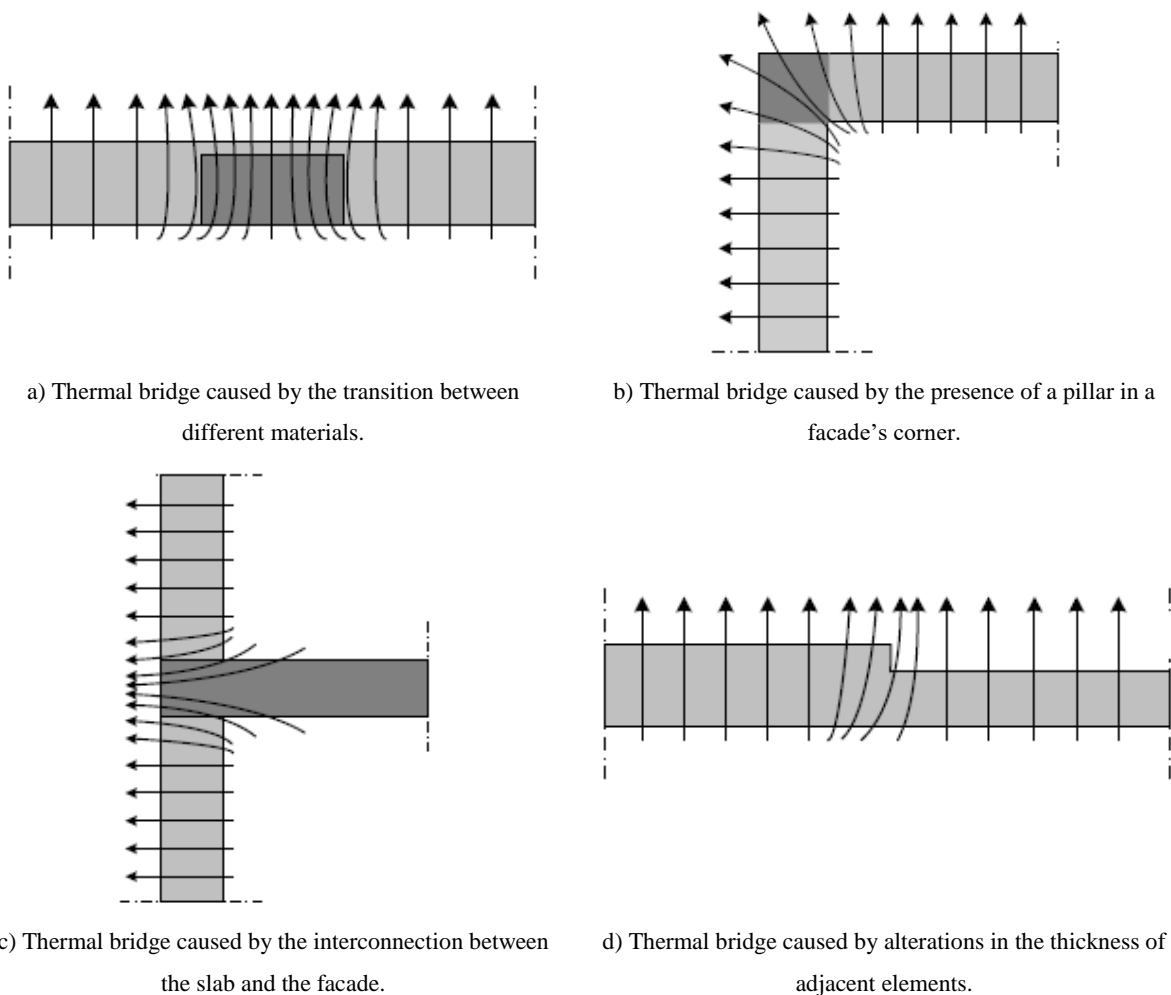


Figure 4 – Schematic illustrations of conventional thermal bridges (Valério, 2007).

Thermal bridges have a highly negative effect on the thermal performance of a building's envelope, by causing significant heat losses in the winter and undesired heat gains in the summer. They are also a cause of the diminishment of indoor air quality, since, during the heating season, the temperature of the inside surface of a thermal bridge is lower than that of its adjacent construction elements. This difference in the temperature gradient can lead to condensations and consequently to the appearance of health threatening mould (Larbi, 2005). The following points indicate some of the most important precautions to take in order to avoid thermal bridges:

- Specify and design construction details in order to support their execution.
- Application of thermal insulation in a continuous way throughout the outside of the building.
- When it is impossible to place the insulation continuously, then a material with a higher thermal resistance must be chosen.
- Install windows and doors in the same plane as the insulation layer.
- Involve part of the window/door frames with insulation.

There are two types of thermal bridges: linear (or 2D) thermal bridges and point (or 3D) thermal bridges. The first are situated at the junction of two or more building elements and are characterized by a linear thermal transmittance ( $\psi$ -value, in  $W/m^{\circ}C$ ), while the second exists where, for example, an insulated wall is perforated by a high thermal conductivity element or where there are three-dimensional corners. These are characterized by a point thermal transmittance ( $\chi$ -value, in  $W/^{\circ}C$ ). Thermal bridges can be evaluated by 3 distinct methods. It can be done experimentally, by using standardized test methods on two identical building elements (one with thermal bridges and the other without). This method is slightly uncertain, time-consuming and expensive, therefore, it is mainly used to validate simulation calculations. The evaluation can also be done using numerical methods, which are more precise, however, require a more profound knowledge in the subject, especially in order to define boundary conditions. Finally, thermal transmittance values can be consulted in catalogues, which present examples of thermal bridges with constructive details and their respective  $\psi$ -values. This is a less flexible method than calculations. Several countries present tabulated values of  $\psi$ -values for typical cases, result of detailed studies, often performed through numerical calculations and thermal modelling (Larbi, 2005). In Portugal, for example, Oliveira (2013) performed such a study according to Passive House

requirements and presented a catalogue with constructive details of several linear thermal bridges and respective  $\psi$ -values. These coefficients were calculated according to the EN ISO 10211:2007 and for each case a thermal model was done using THERM 7<sup>®</sup> software to obtain the two dimensional heat flux.

In average, thermal bridges are responsible for about 20% of the global energy losses in a regular building (Valério, 2007). However, a Passive House building adopts a thermal bridge free design which limits the linear thermal transmittance coefficient to  $\psi \leq 0.01 \text{ W/m} \cdot ^\circ\text{C}$  in all elements, leading to improved details, higher durability of construction elements and substantial energy savings (Passipedia, 2014a).

### **2.3.3 High insulated windows**

A building's glazing is the weakest area in terms of energy performance of the facade. A passive construction involves the use of high-tech windows, with the advantage of allowing a pleasant climate inside the building and a positive thermal balance, whatever the weather in question. Therefore, depending on the climate, different levels of frame insulation and different glazing characteristics can be used to guarantee thermal comfort demands in living and working spaces. A Passive House window must assure that the average temperature of internal window surfaces does not drop below  $17^\circ\text{C}$  on a cold day, without the aid of radiators placed under the windows.

The composition of such windows comprises highly insulated frames, which allow to disrupt thermal conductivity, triple low-e (low thermal emissivity) glazing (for warmer climates, a double low-e glazing may be sufficient) and an optimized installation in the wall. Low-e windows benefit the building's energy efficiency, due to their characteristics that allow greater solar gains, while keeping the heat inside. Figure 5 illustrates a typical passive house window. A well-insulated window promotes thermal comfort by preventing heat losses and therefore reduces the energy needs for heating (IPHA, 2014; Passipedia, 2014b).

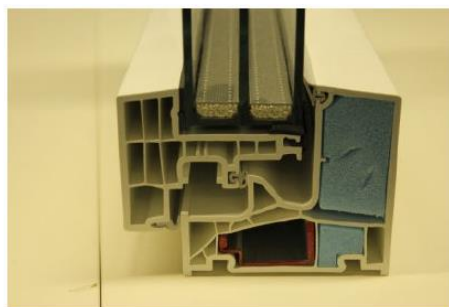


Figure 5 – Highly efficient window with insulated frame and multiple low-e glazing (Almeida, 2013).

According to Passive House standard, windows (glass and frames), must present a coefficient of thermal transmission ( $U_w$ ) below  $0.80 \text{ W}/(\text{m}^2\cdot^\circ\text{C})$  and a total solar transmittance (or g-value), which is the proportion of the solar energy available for the room, of around 50%. However, this  $U_w$  is extremely low and suitable for a very cold climate, values below  $1.6 \text{ W}/(\text{m}^2\cdot^\circ\text{C})$  are recommended for other, not so rigorous, climates.

Such high performance windows that meet the Passive House requirements are developed by an increasing number of manufacturers who offer certified Passive House windows. Note that, in Central Europe, these windows can reduce heat losses by more than 50% when compared to standard windows, enhancing heating-related energy savings (Passipedia, 2014b).

#### **2.3.4 Airtightness**

Regardless of the building's constructive system, a rigorous airtightness of its envelope facade is crucial to prevent uncontrolled airflows randomly crossing the building. These air draughts can be caused by wind or temperature variations and contribute to indoor discomfort. The undesired air intake can sometimes provide too much air or often too little, which can significantly increase or lower the building's temperature, diminishing the thermal comfort and causing uncomfortable air draughts. Structural damage may also be connected to this event, especially in timber constructions, considering that leaks in the building's envelope also allow warm, moist air to flow through the walls. When this air cools, the moisture condenses leading to the appearance of moulds. This intake can sometimes be accompanied by water, causing significant damage. Other disadvantages related to a leaky building are a poor acoustic insulation and significant heat losses. A controlled ventilation system is the ideal way to guarantee a comfortable circulation of air. Considering the existence of such a ventilation system incorporated in the building, air infiltrations may also disturb this system, making it less effective (IPHA, 2014).

The most important principle for planning an airtight building is the “continuous uninterrupted airtight building envelope” which can be obtained using the “red pencil method” (Figure 6).

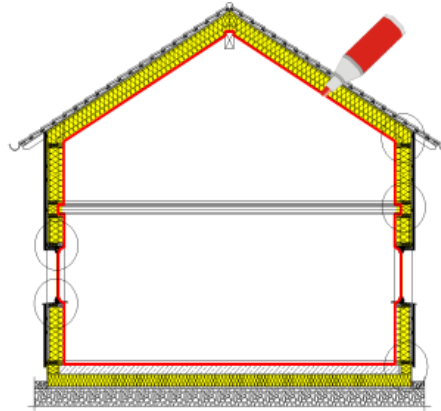


Figure 6 – “Red pencil method” to assure an airtight envelope (Passipedia, 2015f).

This principle basically means that it should be possible to trace the building’s entire envelope with a pencil without any interruptions, therefore creating an airtight layer that totally covers the building. These airtight connections should be properly detailed during the planning of the building (Passipedia, 2015f).

In order to obtain the desired airtightness, an airtight membrane should be installed in the building’s envelope, rendered compatible with each construction element. Depending on the construction type, these barriers may be formed by a parge coat (a cementitious layer usually applied over masonry or concrete walls), a vapour barrier membrane or using a timber sheet product of suitable thickness and airtightness. Every time the membrane is disrupted for any reason, for example, by a window or a door, an insulating tape should be used to connect the membrane to these elements and create a continuous hermetic barrier. Figure 7 illustrates two airtight membranes, one using a vapour barrier and the other using timber sheets. Both are properly taped to window and door elements (Mcleod *et al.*, 2011).



a) Vapour barrier membrane.



b) Timber sheet membrane.

Figure 7 – Airtight membranes installed to prevent leakages in building’s envelope (Mcleod *et al.*, 2011).



The main problems associated to the lack of infiltration control are:

- Condensation: the temperature difference between the moist inside air and the air that comes from leaks can lead to the development of molds.
- Imbalance in the mechanical ventilation system: such a system consists of a controlled constant airflow, meaning that the amount of air that enters is the same as the one that exits. When air infiltrates from a leak, it imbalances the system.
- The air that infiltrates through a leak will reduce the inside air temperature, diminishing thermal comfort.

In order to determine the building's airtightness, a pressurization test is performed. This test is denominated blower door test. This test allows to quantify airflow, determining specific leaks and heat losses associated to them. It consists of a powerful variable-speed fan installed in a doorway (Figure 8), which will controllably move air through the building, creating pressure differences between the inside and outside. Attached to the fan and the outdoors is a pressure gauge that measures the air change rate required to maintain the building at a certain pressure. The air change rate or air change per hour is the change in the building's air volume in the space of an hour. When performed in a Passive House building, the pressure at which the building should maintain is 50 Pa both in pressurization and depressurization. To meet the Passive House standard, the mean value of the air change rate obtained for pressurization and depressurization at 50 Pa ( $n_{50}$ ) should be below  $0.6 \text{ ach}^{-1}$  (air changes per hour) (Keefe, 2010; Sé, 2013).

The blower creates exaggerated airflow in the building and therefore exaggerated leaks that can be felt, for example, just by placing a hand near a window (Keefe, 2010). To determine specific leakage points and measure airflow in the building, two instruments can be used. Using an infrared camera, it is possible to see cold spots, which can result of an air leakage, while a hot sphere anemometer is also a useful tool to use during the test to determine where airflow is higher and where there is not enough flow. Also, placing the anemometer at a leakage spot, it is possible to determine the speed velocity at which air is leaking (Keefe, 2010; Sé, 2013).



Figure 8 – Blower door test (Keefe, 2010).

### **2.3.5 Ventilation in Passive Houses**

Comfort and health are very important aspects for the occupants of a building. Many indoor conditions affect comfort levels, such as the air temperature, air velocity, relative humidity and even personal factors, such as clothing and activity level. Comfort zone lies between 20 and 26°C temperature and between 30 and 60% relative humidity. Along with insulation-related aspects, an efficient ventilation system is crucial when it comes to thermal comfort and energy savings in a Passive House, since it significantly reduces the building's heat load, while, at the same time, assuring a good indoor air quality (Mlakar & Štrancar, 2011).

Although equally acknowledging the importance of all 5 Passive House principles (the first three, rigorous insulation, elimination of thermal bridges and efficient window, are related to insulation and thermal quality aspects, while airtightness and ventilation are related to each other and, not only to thermal aspects, but also to indoor air quality), as mentioned before, considering that the ventilation principle is directly related to the area of study of this dissertation, it will be analysed in higher detail.

#### **2.3.5.1 Indoor air quality**

Indoor air quality is many times associated to a proper ventilation system. Approximately 80 to 90% of people's lives are spent indoors, either in their homes, their workplace or in any other building, making it crucial to ensure a good indoor air quality. Many health problems can be caused by a deficient air quality inside buildings, such as itchy or watery eyes, blocked, stuffy or runny nose, dry throat, lethargy, tiredness, headaches and dry, itchy

or irritated skin. These symptoms are commonly associated to Sick Building Syndrome (SBD). Problems such as moulds may also occur, affecting the occupants' health (Godish, 1994; Crook & Burton, 2010; Norhidayah *et al.*, 2013). Most activities inside residential buildings are a source of pollutants caused by physiological human activity, food preparation, washing and drying of dishes and clothes, use of sanitary facilities and even smoking. Some of the main pollutants that affect the indoor quality are (Pinto *et al.*, 2007; Proença & Cano, 2010):

- **Water vapour / Relative humidity** – low values may cause dryness, skin irritation and respiratory problems, while high values can also cause discomfort and create other problems to the building, like condensations and mould development. An optimum value is between 30% and 70%.
- **Carbon dioxide (CO<sub>2</sub>)** – produced mainly by the occupants' respiration and gas combustion.
- **Carbon monoxide (CO)** – results from combustion in a low oxygen environment, which in low concentrations may cause headaches and as the concentration increases it could lead to nausea, vision problems and in last case, death.
- **Volatile organic compounds** – their major sources are the materials used in the interior lining of buildings and furniture, such as wood pellets, glues, solvents and paints. Cleaning products and tobacco are also sources of these compounds. They can cause various health problems, from simple headaches, to cardiac and respiratory problems. Some volatile organic compounds are also known as being carcinogenic.
- **Other pollutants** – formaldehyde, particles in the air, ozone, radon, microorganisms, etc.

Table 2 shows some of the recommended limit values for the pollutants mentioned in Portuguese Regulation.

Table 2 – Target values for pollutants in Portuguese Regulation (adapted from Decreto-Lei n° 79/2006).

Parameter	Target value
Carbon dioxide (CO <sub>2</sub> )	1800 mg/m <sup>3</sup>
Carbon monoxide (CO)	12.5 mg/m <sup>3</sup>
Volatile organic compounds	0.6 mg/m <sup>3</sup>
Formaldehyde	0.1 mg/m <sup>3</sup>
Particles in the air	0.15 mg/m <sup>3</sup>
Ozone	0.2 mg/m <sup>3</sup>
Radon	400 Bq/m <sup>3</sup>

In order to assure a proper indoor air quality, ventilation is vital to prevent the pollutants from exceeding the limit values and reach dangerous levels. Air admittance will dilute and remove these pollutants, control the indoor humidity and provide oxygen for the occupants.

#### 2.3.5.2 Ventilation principles

Although Passive Houses favour mechanical ventilation, considering that the fifth Passive House principle is the use of a mechanical ventilation system with heat recovery, some aspects of natural ventilation help understand ventilation phenomena, not to mention that overnight natural ventilation is also important in Passive Houses to prevent overheating events, as will be mentioned further ahead. Therefore, natural ventilation will also be addressed.

Natural ventilation was a very popular method in the past, especially considering the low energy consumption associated to this system. It relies essentially on the outdoor climate conditions. It is a process promoted by the pressure differences between both sides of windows, doors, chimneys and cracks and it may be induced by the direct wind action on the building or through the temperature difference between the indoor and outdoor. This type of ventilation is then dependent of two natural driving forces: wind and thermal buoyancy (Kleiven, 2003; Gonçalves & Graça, 2004).

When wind hits a building, an air flow is created in its surroundings, generating various static pressures that can be higher or lower than the atmospheric pressure. Generally, positive pressures are created in the building's windward side, driving air into the building through openings, and negative pressures (causing suction forces) are created in its leeward side and roof, driving air out of the building (Kleiven, 2003; Wouters & Santamouris, 2006). Regarding thermal buoyancy, this phenomenon is connected to convection movements of fluids. To different temperatures correspond different densities, therefore, the same fluid possesses lower density when it is at a higher temperature. This leads to convection movements, for example, when the air inside a room is heated, it tends to move upward, since it has lower density, while the colder air, not yet heated, tends to go downward, creating convection currents. Ventilation driven by thermal buoyancy, also known as the *chimney effect* or *stack effect*, occurs because of the density difference between the internal and external air, which are at different temperatures, creating pressure differences that pull air in and out of the building through openings in its envelope. These openings must be purposely placed to promote ventilation, otherwise, in the existence of cracks, the process is simply

considered air infiltration, which is not controlled and may cause disturbance to the natural ventilation system (Kleiven, 2003; Wouters & Santamouris 2006). Thermal buoyancy is also a relevant phenomenon in mechanical ventilation. In this type of ventilation, air is supplied at a specific temperature, however, considering the existence of numerous heat sources inside the building (whether from people, computers, etc.) the air temperature will rise, leading to convection movements that enhance ventilation.

Natural ventilation possesses 3 principles that determine how the natural driving forces are used to ventilate a building. Basically, they indicate how the air is admitted into the building and how it is exhausted out. It is important to acknowledge the role the building's airtightness has in ventilation, since infiltrations may disturb its correct functioning. These principles are: single-sided ventilation, cross-ventilation and stack ventilation. In single-sided ventilation, air admission and exhaustion is made through openings on only one side of the ventilated enclosure. There can be a single opening where the admission and exhaustion is made, e.g. a window, or there can be openings at different heights, which enhances the ventilation rate by taking advantage of the buoyancy effect. In cross-ventilation, air admission and exhaustion is made through openings, such as windows, hatches or grills, placed on opposite sides of the building. The air flow is induced by wind pressure differentials between both sides, therefore moving from the windward to the leeward side of the building. During its movement across the building, the air flow can ventilate several rooms through open doors or grills. Finally, in stack-ventilation, air is admitted through openings in the facade and exhausted at a higher level, usually through the roof. This type of ventilation usually implicates that air enters at a low level and is driven by warm air rising to the top, being exhausted out. If the outlet is placed in a wind-induced under-pressure, the stack-ventilation will be more effective, since air will be sucked out (Kleiven, 2003; Heiselberg, 2006). Figure 9 illustrates these 3 ventilation principles.

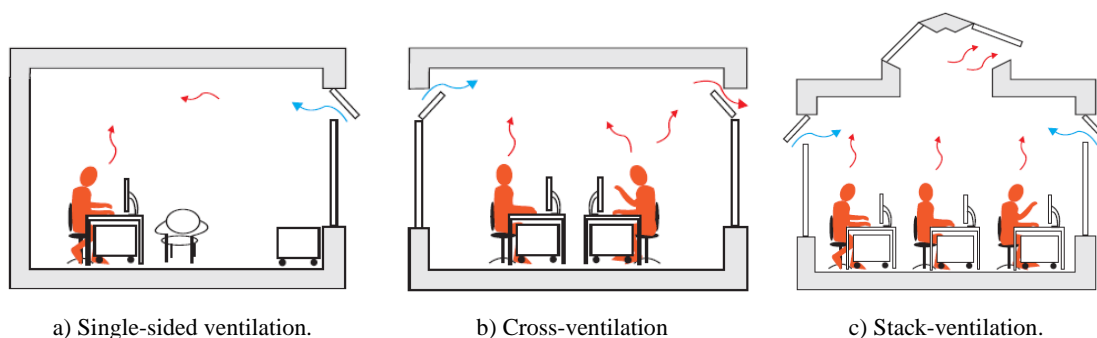


Figure 9 – Natural ventilation principles (Trend, 2014).

Note that any of these principles can also be applied to mechanical ventilation. Instead of admitting and exhausting outside air through openings in the facade, air is supplied and extracted mechanically through grids. Usually, the most common principle is cross-ventilation, since air is supplied at one or numerous points, travels throughout the building, and is extracted away from the supply areas.

#### 2.3.5.3 Passive House heat recovery ventilation

Despite the advantages of natural ventilation in terms of energy consumption, its dependence on environmental conditions makes it difficult to obtain a fully user controlled system, that meets the occupant's needs at all times and in any season of the year. Plus, it lacks the possibility of air treatment, where, especially in cold climates, heating of the supply air is essential. That is why the Passive House standard requires an efficient mechanical heat recovery ventilation system (HRV).

In a Passive House dwelling, the ventilation is done by a centralized system that allows heat recovery. Basically, this system is comprised of the following 4 components: outdoor air admission; air extraction; air supply and air exhaustion.

Outdoor air is admitted into the building through ducts, while contaminated air is extracted from kitchens and sanitary facilities. This air, which has higher temperature, will transfer heat to the admission air through a heat exchanger device that will then be supplied to the main compartments, such as rooms and living rooms. The ventilation principle used is cross-ventilation, meaning that the pre-heated air is supplied in a certain main compartment and will then travel across the house through air passages, ventilating all other compartments. The air is then exhausted out on the opposite side of the building (Feist, 2006; IPHA, 2014). This whole process must be conducted from the centralized ventilation unit, which contains high performance blowers (Passive House standard commonly use so-called *ECM electronic commuted motors*) and an air-to-air heat exchanger of very high performance (over 75%) to transfer heat from the extracted to the supplied air.

Filters must also be installed on both sides of the system, more importantly where air is admitted. The ventilation unit and all ductwork must have a proper thermal insulation and silencers. It must be provided of an anti-icing system for cold climates and a controllable bypass system for the airflow to avoid the heat exchanger in the summer, where heat recovery may not be necessary. In countries with extreme winter conditions, in addition to the heat recovery system, a mechanical pre-heating of the supplied air may also be installed

in the ventilation unit. Plus, a subsoil duct system can be installed to pre-heat the outdoor air by taking advantage of geothermal energy before reaching the ventilation unit (Feist, 2006; Wouters and Santamouris, 2006; IPHA, 2014).

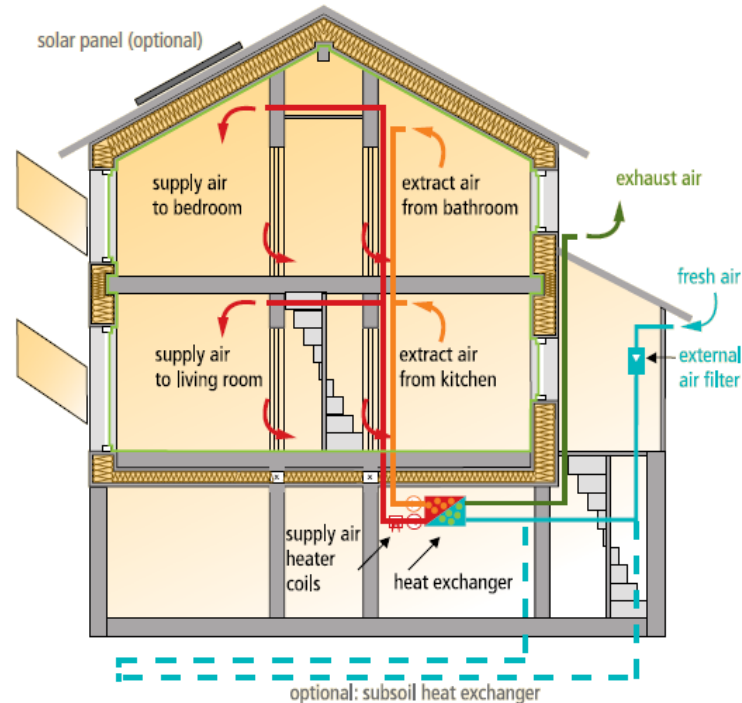


Figure 10 – Schematic Passive House ventilation system (IPHA, 2014).

Figure 11 is a schematic illustration of an air-to-air heat exchanger, where the extracted air transfers heat to the outside fresh air, before being supplied in rooms and living rooms (Feist, 2006; IPHA, 2014).

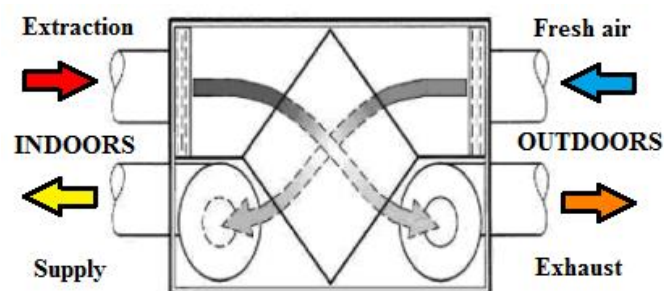


Figure 11 – Schematic illustration of an air-to-air heat exchanger (adapted from Wouters & Santamouris, 2006).

To demonstrate the efficiency of these systems, on a cold winter day with an outdoor temperature of, for example, 0°C, by using the stale extract air that can reach 20°C and considering internal heat gains, the cold incoming air can be heated to at least 16°C without any active heating (IPHA, 2014).

#### 2.3.5.4 Night-time ventilation in preventing the risk of overheating

The Passive House standard was initially developed for countries in Central Europe, where space cooling is not a high necessity, therefore, the standard configuration of their ventilation system is usually designed for heating purposes, which must be changed in cases where cooling is needed. Nevertheless, in warm climate countries, during the summer, the risk of overheating events is much higher in a passive building than in a standard building (Badescu *et al.*, 2010). Considering the increase in internal energy gains inside a building from several heat sources, such as cooking, computers, resident's activity and metabolism, which are difficult to be released, significantly raises the internal temperature, leading to overheating and to a reduction in thermal comfort in the summer. A simple approach to release this excessive heat involves ventilating during the night, when the outside temperature is lower than the internal temperatures. Architects and engineers are still hesitant when it comes to applying the night-time ventilation technique, due to uncertainties in the prediction of flow rates related to natural ventilation, however, considering that it is a simple and, above all, energy-efficient approach, numerous authors have performed studies to predict such flows and determine the efficiency of opening a window during the night to decrease the overheating rate (Artmann *et al.*, 2008; Badescu *et al.*, 2010; Mlakar & Štrancar, 2011).

During the summer, heavy and highly insulated external walls in passive dwellings tend to delay the heat transfer from the outside to the inside spaces. Plus, considering a building with a big internal mass, the increase in the air temperature is very slow. This slow heating of the building means that, in the summer, the maximal internal temperature is only reached at the late hours of the day, when the outside temperatures are already low. This is why a proper ventilation to remove excessive heat is so efficient during the night (Shaviv *et al.*, 2001). Artmann *et al.* (2008) concluded that increased flow rates in night ventilation significantly reduce overheating degree hours, until a certain critical value of air flow rate (that depends on building construction and heat gains) to which there is no further improvement in overheating reduction. Shaviv *et al.* (2001) concluded that, by applying night ventilation, it is possible to achieve a reduction of 3 to 6°C in a heavy construction building without the aid of an air conditioning unit.



## 2.4 Portuguese legislation on energy performance

In Portugal, the first legal instrument that imposed requirements on the design of new buildings was the *Regulamento das Características de Comportamento Térmico dos Edifícios* (RCCTE), approved in 1990 by the decree law n°40/90. Its main goal was to satisfy thermal comfort conditions in buildings without excessive energy needs, both in the summer or in the winter, while ensuring the minimization of anomalies caused by surface condensations. Later came into force the *Regulamento dos Sistemas Energéticos de Climatização em Edifícios* (RSECE), approved in 1998 by the decree law n°118/98, aiming to improve building's energy efficiency (Jorge, 2013).

In 2006, a reformulation was carried out on both these regulations through the decree law n° 80/2006 for the RCCTE and through the decree law n° 79/2006 for the RSECE. This last regulation established, among other requirements, levels for the indoor air quality and limits for the most common pollutants of the air inside buildings (Decreto-Lei n° 79/2006). The new RCCTE presented higher demands by strictly defining an air renewal rate, in order to ensure an adequate indoor air quality. These reformulations also took into account the European Directive 2002/91/CE, by updating the regulations to satisfy requirements related to the new social, economic and energetic reality, which required a higher thermal quality in buildings (Jorge, 2013). To comply with this regulation, a few aspects must be taken into account, such as: meeting the building envelope's thermal requirements, meeting ventilation requirements and meeting the limits of energy needs for heating and cooling. For that, this new regulation updated the values of specific thermal requirements. Some of these values are shown in Table 3, including, for different climatic zones defined in the document, thermal transmittance coefficients (or U-values) of walls and roofs, reference temperatures and relative humidity and the recently defined air renewal rate, as well as Passive House values to serve as comparison. Other important values established in this document are solar and shading factors and linear thermal transmittance coefficients for conventional thermal bridges (Decreto-Lei n° 80/2006). Another regulation, the *Sistema Nacional de Certificação Energética e da Qualidade do Ar Interior nos Edifícios* (SCE), was approved by the decree law n°78/2006, which partially transposed the European Directive 2002/91/CE into national law (Jorge, 2013). It establishes the implementation of an energy certification system in order to inform citizens on the thermal quality of buildings at its construction phase or at the time of sale or lease.

Table 3 – Thermal requirements established in the RCCTE against Passive House values (Decreto-Lei nº 80/2006).

		Climatic zone		Passive House
Reference U-values (W/m <sup>2</sup> .°C)	Walls	I1	0.70	0.10 – 0.15
		I2	0.60	
		I3	0.50	
	Roofs	I1	0.50	
		I2	0.45	
		I3	0.40	
Maximum U-values (W/m <sup>2</sup> .°C)	Walls	I1	1.80	
		I2	1.60	
		I3	1.45	
	Roofs	I1	1.25	
		I2	1.00	
		I3	0.90	
Warming season	Reference temperature	20°C		20°C
Cooling season	Reference temperature	25°C		25°C
	Relative humidity	50%		-
Reference air renewal rate		0.6 h <sup>-1</sup>		0.6 h <sup>-1</sup>

In 2013, to comply with the requirements of the Energy Performance Building Directive 2010/31/EU, a revision over the national thermal and energy legislation was performed with the publishing of the decree law nº118/2013, that includes, in a single document, the SCE, the *Regulamento de Desempenho Energético dos Edifícios de Habitação* (REH) and the *Regulamento de Desempenho Energético dos Edifícios de Comércio e Serviços* (RECS), revoking the previous decree laws nº 78/2006, 79/2006 and 80/2006 (Decreto-Lei nº 118/2013; Jorge, 2013).

Despite the Portuguese legislation tending towards energy performance enhancement, there is not yet an actual document which presents the definition of a NZEB in Portugal. However, and although there are no registered advances in the EPBD requirements, the new legislation published in 2013 by decree law nº118/2013, paves the path towards Nearly Zero-Energy Buildings and sets up a roadmap that progressively tightens the Energy Performance requirements until 2020. Nevertheless, the legislation on its own won't be enough to push the market towards the EPBD recast goals (ADENE, 2013), and that is why the ever-growing implementation of the Passive House concept in Portugal is crucial to achieve such energy demands.

## **2.5 Thermal comfort assessment**

### **2.5.1 Definition of comfort**

According to the ASHRAE Standard 55, thermal comfort is defined as the condition of the mind which expresses satisfaction with the thermal environment. Thermal comfort is a human sensation, which makes it subjective. The feeling of comfort is directly related to occupation, environmental, psychological and sociological factors (Loomans, 1998; Matias, 2000; Figueiredo, 2014). One of the greatest requirements to obtain the sensation of comfort is to maintain a thermal balance between the human body and the surrounding environment. That implies preserving the internal body temperature at  $37 \pm 0.8^{\circ}\text{C}$ . However, thermal balance and thermal comfort are not the same, since it is possible to achieve a thermal balance under uncomfortable conditions thanks to the human body's thermoregulation mechanisms. Therefore, physiologically, thermal comfort can be defined as the condition in which the human's thermoregulation mechanisms are at a state of minimum activity (Matias, 2000). P. O. Fanger's model from 1972, indicated that the human response to the indoor thermal environment depends on the following environmental factors: air temperature, air velocity, mean radiant temperature and relative humidity and the following personal factors: physical activity level and the metabolic rate and personal clothing insulation (Matias, 2000; Mlakar & Štrancar, 2011; Figueiredo, 2014).

The standards that define thermal comfort in buildings are: the ASHRAE Standard 55, the ISO 7730 and the EN 15251.

### **2.5.2 Role of ventilation in achieving thermal comfort and indoor air quality**

Ventilation presents a primary role in the occupants' sensation of indoor comfort. It enables the following needs (Pinto, 2000; Ruivo, 2010):

- Promotion of oxygen for the occupants to breathe (0.1 to 0.9 l/s).
- Dilution of pollutants and odours to satisfying values.
- Control of the indoor humidity to avoid condensations and the appearance of moulds (considering that, generally, the indoor humidity is higher than the one outdoors).
- Control over the amount of particles in the air.
- Removal or placement of thermal loads (amount of heat that must be placed or removed from a specific area of the building in order to assure thermal comfort conditions).

- Prevention of thermal asymmetries.

The human’s sensorial perception of air quality can be expressed according to the percentage of people that consider the indoor air quality to be unacceptable. Therefore, it is possible to determine the ventilation requirements based on the level of dissatisfied people. There can be considered 3 levels of indoor quality: A, B and C, which represent, respectively, 15%, 20% and 30% of dissatisfaction. For each category, it is possible to present the ventilation rate to assure that the percentage of dissatisfied people does not exceed those values, as shown in Table 4.

Table 4 – Ventilation rates for each level of indoor air quality (Viegas, 2000).

Category	Perception of air quality (dissatisfaction)	Ventilation rate (m <sup>3</sup> /h.standard person)
A	15%	36
B	20%	25.2
C	30%	14.4

Ventilation corrects the level of water vapour (relative humidity) and adjusts the air temperature. Figure 12 presents the admissible value ranges of the air’s temperature and relative humidity according to the ASHRAE (1997) recommendations, inserted in a psychrometric chart.

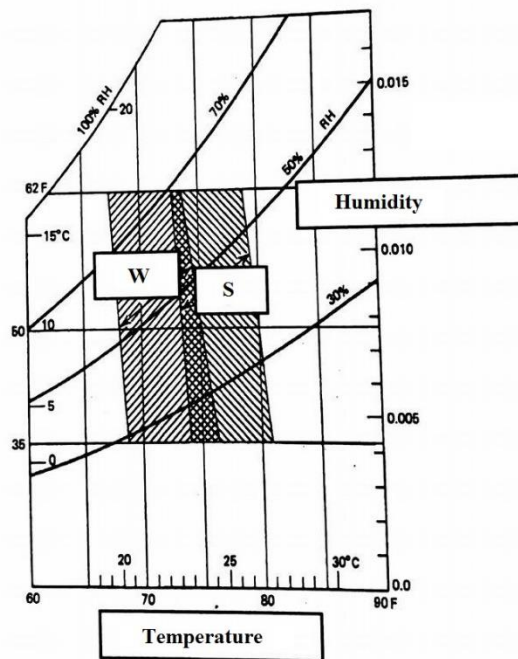


Figure 12 – Influence of relative humidity in thermal comfort (adapted from Viegas, 2000).

This psychrometric chart presents the comfort zones for the winter (w) and the summer (s) regarding temperature and relative humidity.

### 2.5.3 Methods for evaluating comfort

Researchers have been studying people’s thermal and psychological responses to environmental conditions for the purpose of developing mathematical models to predict the average acceptability of an indoor climate. Two types of models assess thermal comfort: analytical and adaptive models (Loomans, 1998; Figueiredo, 2014).

#### 2.5.3.1 Analytical model approach

The analytical model, also known as the “rational” approach to thermal comfort, explains people’s response to the thermal environment using the physics and the physiology of heat transfer (Nicol & Humphreys, 2002). It was therefore developed using heat balance principles and it is a method of calculation of steady state thermal comfort obtained from experimental data from climate chamber research under steady state conditions (Loomans, 1998; Figueiredo, 2014).

As a living organism, the human body produces heat and interacts with its surrounding environment through heat exchange. Considering the energy production of a human being and the constant thermal exchanges with the environment, a general equation that manages this thermodynamic process of energy exchange can be obtained. This is called the body’s energy balance equation and is given by (Matias, 2000):

$$S = M - W - E \pm R \pm C \quad (1)$$

Where S is the heat accumulation in the body, M the metabolism rate, W the corresponding energy of the realized mechanical work, E the heat loss by evaporation, R the heat exchange through radiation and C the heat exchange through convection.

Considering that the human body possesses a low mechanical efficiency and the majority of the energy produced is dissipated as heat, the energy fraction of the equation, W, can be considered null ( $W = 0$ ) in most cases. The metabolism rate, which represents the body’s energy production via consumption of food, can be obtained by tabulated values for different physical activities. The evaporation heat losses are mainly caused by perspiration and sweat and the heat exchanges through radiation and convection are related to the heat transfer from the skin to the outer surface of the clothed body and vice-versa. These last parameters are

therefore influenced by the thermal resistance of clothing, which can also be obtained from tabulated values (Matias, 2000).

Considering this heat balance equation and the environmental and personal factors that influence the human response to the indoor thermal environment specified by Fanger's model and referred earlier, the analytical approach to evaluate thermal comfort developed thermal indices to combine, in a single parameter, all these factors. There are numerous indices that integrate such factors that affect thermal comfort, with particular emphases to the following:

- Predicted Mean Vote (PMV).
- Predicted Percentage of Dissatisfied (PPD).

These indices are described in the International Norm ISO 7730: “*Ergonomics of the thermal environment – Analytical determination and interpretation of thermal comfort using calculation of the PMV and PPD indices and local thermal comfort criteria*”. The ISO 7730 was developed in parallel with the revised ASHRAE 55 and specifies methods for the measurement and evaluation of the moderate and extreme thermal environments, using these indices.

The PMV index characterizes an individual's thermal sensation based on the factors studied by Fanger. Therefore, the parameters that influence the PMV are the metabolism rate ( $M$ ) and the body's heat accumulation ( $S$ ), which depends on parameters such as clothing (clothing insulation,  $I_{cl}$ , clothing surface area factor,  $f_{cl}$ , and the clothing surface temperature,  $t_{cl}$ ), air temperature ( $t_a$ ), mean radiant temperature ( $\bar{t}_r$ ), air velocity ( $v_a$ ) and relative humidity through the water vapour partial pressure ( $p_a$ ). The PMV is then given by (ISO 7730-2006):

$$PMV = (0.303 \times e^{-0.036M} + 0.028) \times S \quad (2)$$

And, following the ISO 7730-2006, Rodrigues *et al.* (2009) and Matias (2000), the parameters in Equation 1 can be developed and the heat accumulation in the body,  $S$ , extends to the following equation:

$$S = \left\{ \begin{array}{l} (M - W) - 3.05 \times 10^{-3} \times [5733 - 6.99 \times (M - W) - p_a] - \\ - 0.42 \times [(M - W) - 58.15] - 1.7 \times 10^{-5} \times M \times (5867 - p_a) - \\ - 0.0014 \times M \times (34 - t_a) - 3.96 \times 10^{-8} \times f_{cl} \times \\ \times [(t_{cl} + 273)^4 - (\bar{t}_r + 273)^4] - f_{cl} \times h_c \times (t_{cl} - t_a) \end{array} \right\} \quad (3)$$

With:

$$t_{cl} = 35.7 - 0.028 \times (M - W) - I_{cl} \times \left\{ \begin{array}{l} 3.96 \times 10^{-8} \times f_{cl} \times \\ + f_{cl} \times h_c \times (t_{cl} - t_a) \end{array} \right\} \times [(t_{cl} + 273)^4 - (\bar{t}_r + 273)^4] + \quad (4)$$

$$h_c = \begin{cases} 2.38 \times |t_{cl} - t_a|^{0.25} & \text{for } 2.38 \times |t_{cl} - t_a|^{0.25} > 12.1 \times \sqrt{v_a} \\ 12.1 \times \sqrt{v_a} & \text{for } 2.38 \times |t_{cl} - t_a|^{0.25} < 12.1 \times \sqrt{v_a} \end{cases} \quad (5)$$

$$f_{cl} = \begin{cases} 1.00 + 1.290 \times I_{cl} & \text{for } I_{cl} \leq 0.078 \text{ m}^2 \cdot \text{K/W} \\ 1.05 + 0.645 \times I_{cl} & \text{for } I_{cl} > 0.078 \text{ m}^2 \cdot \text{K/W} \end{cases} \quad (6)$$

$$p_a = \frac{p_{as} \times RH}{100} \quad (7)$$

$$p_{as} = 610.5 e^{\left(\frac{17.269 \times t_a}{237.3 + t_a}\right)} \quad \text{for } t_a \geq 0^\circ\text{C} \quad (8)$$

Where  $h_c$  is the convective heat transfer coefficient,  $p_{as}$  is the water vapour saturation pressure at a specific temperature and  $RH$  the relative humidity. As mentioned earlier, the metabolism rate and clothing insulation are obtained through tabulated values.

In alternative, the ISO 7730 Norm also presents tables with PMV values for different combinations of activity, clothing, relative velocity and operative temperature. The index value can also be obtained by direct measurement (ISO 7730-2006).

The PMV quantifies the general opinion of a large group of people, by predicting the mean value of their votes according to the 7-point thermal sensation scale present in Table 5.

Table 5 – Thermal sensation scale (adapted from ISO 7730-2006).

+3	Hot
+2	Warm
+1	Slightly warm
0	Neutral
-1	Slightly cool
-2	Cool
-3	Cold

The index should only be used for values between +2 (warm sensation) and -2 (cool sensation), and the main parameters mentioned before should be within certain limits, also indicated in the norm (ISO 7730-2006).

The PPD index seeks to predict the percentage of thermally dissatisfied people and is obtained from the PMV index. According to the Norm, these are the people who would choose any of the following scales from Table 5: -3 (cold), -2 (cool), +2 (warm) and +3 (hot). The PPD value can be given by (ISO 7730-2006):

$$PPD = 100 - 95 \times e^{(-0.03353 \times PMV^4 - 0.2179 \times PMV^2)} \quad (9)$$

This equation, that determines the PPD index, can be graphically represented as function of the PMV, as shown in Figure 13. The Norm indicates the distribution of individual thermal sensation votes for different PMV values, based on experiments involving 1300 individuals. It also presents recommended values for various thermal criteria, including PMV and respective PPD values, for 3 categories of thermal environment: categories A, B and C. Category A possesses the highest levels of comfort, therefore, the hardest to achieve, while category C possesses the lowest acceptable levels of comfort. Category B, being the intermediate case, will be used as reference, considering that it requires good levels of comfort that can be reasonably achieved. This category recommends a PMV index between -0.5 and +0.5, which corresponds a PPD of below 10% (Figure 13). That means that less than 10% of the occupants feel thermally dissatisfied (ISO 7730-2006). At the end of this subsection, after presenting all thermal criteria, the limits for each category will be presented.

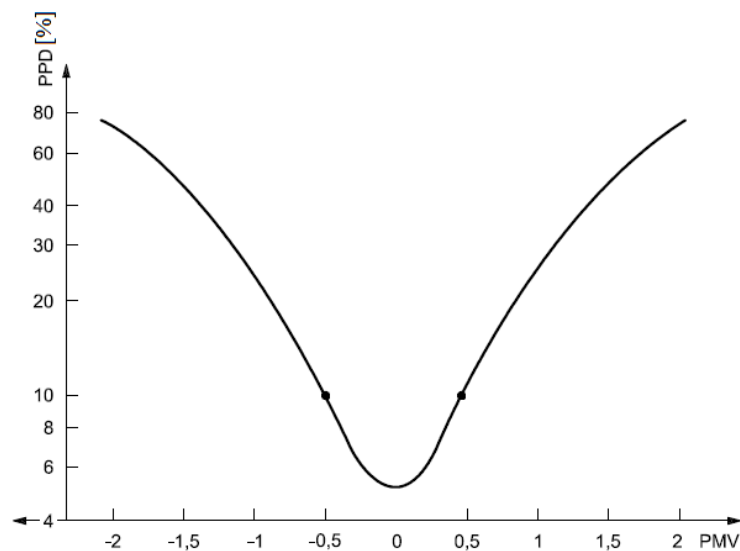


Figure 13 – PPD as function of PMV, presenting category B levels of comfort (adapted from ISO 7730-2006).



### Local discomfort

Beyond the recommended limits specified in the ISO 7730 Norm for the PMV and PPD thermal indices, this Norm also evaluates a phenomenon called “local discomfort” and specifies limits for some factors that cause this type of discomfort.

The sensation of thermal comfort, as defined in subsection 2.5.1, refers to a comfort state of the whole body. That is a direct relation between the human body and the environmental surroundings. This relation is caused by heat exchanges that can take place through convection, radiation, conduction or evaporation (mainly through perspiration and sweat). However, an individual can consider the ambient temperature to be pleasant, and yet, feel discomfort due to draughts or an excessive cooling or heating of a particular part of the body. This is called “local discomfort”. The 4 factors that cause local discomfort are (Matias, 2000; ISO 7730-2006):

- Radiant temperature asymmetry.
- Air draughts.
- Warm and cool floors.
- Vertical air temperature difference.

An asymmetry in the indoor radiant temperature usually occurs near windows, walls or lightings. For example, on a cold day, in a well heated room, when an occupant is sitting with his back turned to a window, he might feel cold on his back. That is a local discomfort caused by a radiant temperature asymmetry. There are 4 types of asymmetries: warm and cool ceiling and warm and cool wall. The ISO 7730 Norm, determines an index called Percentage Dissatisfied (PD) for each of these types through 4 different empirical equations, each depending on the value of the radiant thermal asymmetry ( $\Delta t_{pr}$ ) in question. To achieve a category B of thermal environment, the PD for radiant asymmetry should be below 5%, which corresponds a radiant thermal asymmetry of below 5°C for warm ceilings, below 14°C for cool ceilings, below 23°C for warm walls and below 10°C for cool walls (ISO 7730-2006).

Air draughts are probably the most common cause of local discomfort. The ISO 7730-2006 Norm indicates the equation to calculate the Draught Rate (DR), which depends on the local air temperature ( $t_{a,l}$ ), the local mean air velocity ( $\bar{v}_{a,l}$ ) and the local turbulence intensity ( $Tu$ ),

which can be considered 40% if unknown. To achieve category B, the DR must be below 20% (ISO 7730-2006).

When the floor is too cool or too warm, this causes an uncomfortable feeling in the occupant’s feet, especially when wearing light indoor shoes. Therefore, the Norm indicates the equation that calculates the PD for this type of local discomfort, which depends solely on the floor temperature ( $t_f$ ). For category B, the PD must be below 10%, which corresponds to a floor surface temperature range of 19 to 20°C (ISO 7730-2006).

When the temperature difference between an individual’s head and ankle is too high, it may cause discomfort. The Norm presents the equation that calculates the PD in this situation, which depends exclusively on the vertical air temperature difference between the head and feet ( $\Delta t_{a,v}$ ). For category B, the PD must be below 5%, which corresponds to a vertical air temperature difference (between 1.1 and 0.1 m above the floor) of below 3°C (ISO 7730-2006).

Summarizing the thermal comfort criteria using the analytical approach, Table 6 presents the limits of each thermal index for the 3 categories of thermal environment.

Table 6 – Categories of thermal environment (adapted from ISO 7730-2006).

Category	Thermal state of the body as a whole		Local discomfort			
	PPD %	PMV	DR %	PD % caused by		
				vertical air temperature difference	warm or cool floor	radiant asymmetry
A	< 6	-0.2 < PMV < +0.2	< 10	< 3	< 10	< 5
B	< 10	-0.5 < PMV < +0.5	< 20	< 5	< 10	< 5
C	< 15	-0.7 < PMV < +0.7	< 30	< 10	< 15	< 10

### 2.5.3.2 Adaptive model approach

The adaptive approach to thermal comfort expresses the natural tendency that people have to adapt to changing conditions to their environment. It derives from studies conducted in the field, where researchers gather thermal environment data, according to subjects’ thermal response about their everyday lives. They present a “comfort vote” based on a scale similar to the one in Table 5 from the ISO 7730 and ASHRAE 55. Then, using statistical methods to analyse the data, researchers aim to find the temperature or combination of thermal variables (air temperature, velocity and humidity) to which subjects consider comfortable or

neutral. This is then used to predict the comfort conditions that can be considered in other situations (Nicol & Humphreys, 2002).

The EN 15251 Standard: “*Indoor environmental input parameters for design and assessment of energy performance of buildings addressing indoor air quality, thermal environment, lighting and acoustics*”, analysis and quantifies indoor thermal comfort according to the adaptive approach (Figueiredo, 2014).

The Standard presents the equation for calculating the operating comfort temperature, which depends on the running mean outdoor temperature, and is given by (EN 15251-2007):

$$\theta_o = 0.33 \times \theta_{rm} + 18.8 \quad (10)$$

Where  $\theta_o$  is the indoor operative temperature and  $\theta_{rm}$  the Running mean outdoor temperature. The running mean outdoor temperature is calculated based on the values of daily average temperatures of the previous week, and is given by (EN 15251-2007):

$$\theta_{rm} = \frac{(\theta_{n-1} + 0.8 \times \theta_{n-2} + 0.6 \times \theta_{n-3} + 0.5 \times \theta_{n-4} + 0.4 \times \theta_{n-5} + 0.3 \times \theta_{n-6} + 0.2 \times \theta_{n-7})}{3.8} \quad (11)$$

Where  $\theta_{n-i}$  is the running mean outdoor temperature of the previous day.

The EN 15251 Standard catalogues the thermal environments into four categories, as shown in Table 7, where a description of the applicability of each category is presented.

Table 7 – Description of the applicability of the thermal environment categories depicted in the EN 15251 Standard (adapted from Olesen, 2007).

Category	Description
I	High level of expectation and is recommended for spaces occupied by very sensitive and fragile persons with special requirements like handicapped, sick, very young children and elderly persons.
II	Normal level of expectation and should be used for new buildings and renovations.
III	An acceptable, moderate level of expectation and may be used for existing buildings.
IV	Values outside the criteria for the above categories. This category should only be accepted for a limited part of the year.

In buildings without a mechanical cooling system, based on a weekly running average of the outside air temperature, the Standard defines curves of the recommended criterion for the indoor temperature, as shown in Figure 14. It defines the indoor operative temperature ( $\theta_o$ ) as function of the exponentially-weighted running mean of the outdoor temperature ( $\theta_{rm}$ ) for each of the categories mentioned in Table 7, with the exception of category IV, considering that it is not acceptable for most of the year. The graphic shows the upper (in shades of red)

and lower (in shades of blue) limits for the building's operative temperature. The Norm presents 3 equations, one for each category, to calculate the minimum and maximum values of the operative temperature. The upper limit is only applied for a running mean temperature of  $10^{\circ}\text{C} < \theta_{rm} < 30^{\circ}\text{C}$  and the lower limit for  $15^{\circ}\text{C} < \theta_{rm} < 30^{\circ}\text{C}$ .

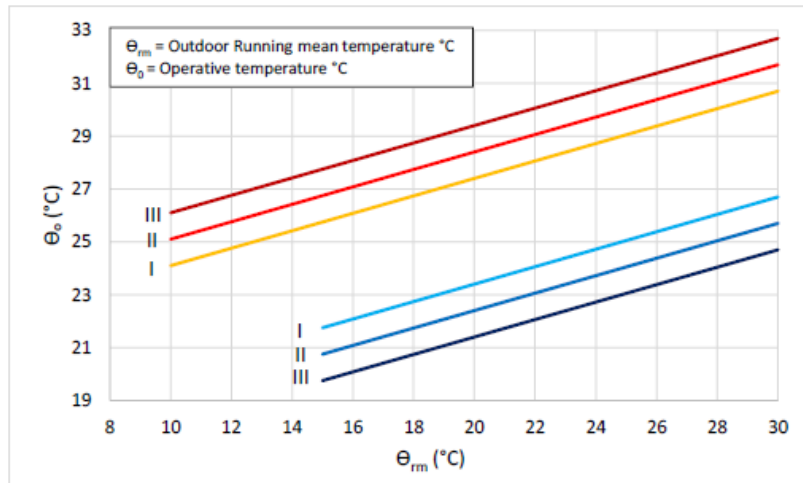


Figure 14 – Design values for the indoor operative temperature for buildings without mechanical cooling systems as function of the exponentially-weighted running mean of the outdoor temperature (EN 15251-2007).

For running mean outdoor temperatures below these limits ( $10^{\circ}\text{C}$  for upper limit and  $15^{\circ}\text{C}$  for lower limit), the maximum and minimum acceptable limits are considered constant, as shown in Figure 15.

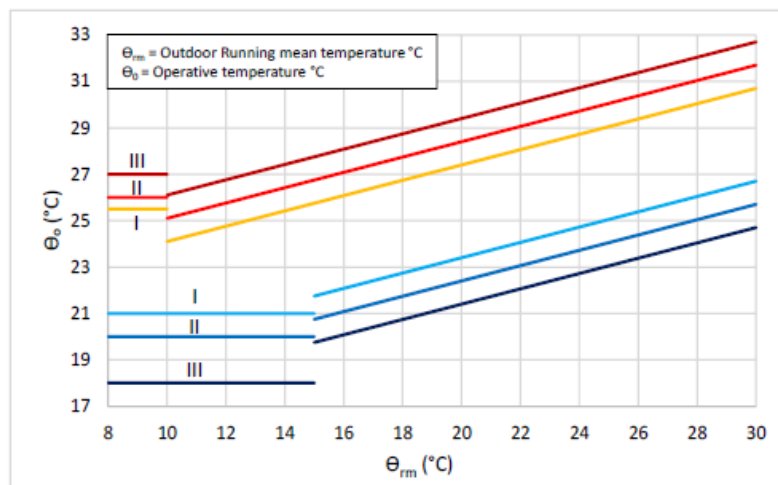


Figure 15 – Indoor operative temperature as function of the exponentially-weighted running mean of the outdoor temperature when these are below the minimum limit (EN 15251-2007).

Thermal comfort criterion is defined when the temperature distribution is within the upper and lower limits of each category. Figueiredo (2014) performed a thermal comfort analysis of the cooling season for a category II dwelling. Part of the results obtained are presented in Figure 16.

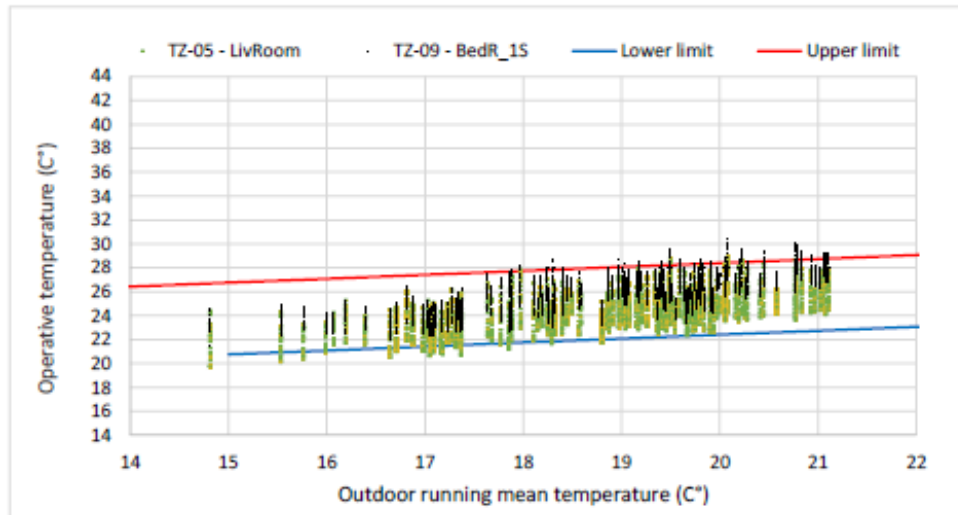


Figure 16 – Thermal comfort analysis for the cooling season of a category II building (Figueiredo, 2014).



# Chapter 3

---

Numerical Model





## Chapter 3. Numerical Model

### 3.1 Computational Fluid Dynamics

Computational Fluid Dynamics is a tool that performs computer-based simulations involving fluid flow and heat transfer. It is used in various areas of study, for example (Versteeg & Malalasekera, 1995):

- Aerodynamics of aircraft and vehicles.
- Hydrodynamics of ships.
- Electrical and electronic engineering.
- External and internal environment of buildings: wing loading and heating/ventilation.
- Marine engineering: loads on off-shore structures.
- Environmental engineering: distribution of pollutants.

CFD is a field in fluid mechanics that makes use of numerical methods and algorithms with the purpose of simulating a fluid's motion and its interaction with other surfaces or objects in which they contact (Sousa, 2012). The main instrument that allows the existence and growth of CFD is the high-speed digital computer. For that matter, it is safe to say that the CFD community has highly contributed for the development of supercomputers with high levels of storage and execution speed. This is essential since a CFD solution may require a repetitive manipulation of millions of numbers (Wendt, 2009).

Before understanding how a CFD code works, it is important to acknowledge the basic physical principles that back up the calculations performed in a CFD simulation.

### 3.2 Fluid motion equations

The discretization of the governing equations of fluid dynamics behind the *Computational Fluid Dynamics* software presented in this section is mainly based on the description done by Wendt (2009).

In order to obtain the basic equations of fluid motion, one must first choose the appropriate fundamental physical principle from the laws of physics, these being (Versteeg & Malalasekera, 1995; Wendt, 2009):

- The mass conservation law.
- The momentum conservation law (Newton's 2<sup>nd</sup> Law).
- The energy conservation law.

These principles must then be applied to a suitable flow model to extract the mathematical equations included in them. However, the definition of a suitable model of the flow is not a simple task. The fact that a fluid is an inconsistent, rather flimsy material, that is, totally deformable under stress, makes it hard to visualize or grab hold of. In order to physically define the fluid model and therefore apply the physical principles, two models may be considered: the finite control volume model and the infinitesimal fluid element model (Wendt, 2009).

#### Finite control volume

Consider a flow field of any kind as represented in Figure 17, where a closed volume exists within a finite region of the flow. That volume is referred to as *control volume*,  $V$ , and the surface that delimits this volume is referred to as *control surface*,  $S$ .

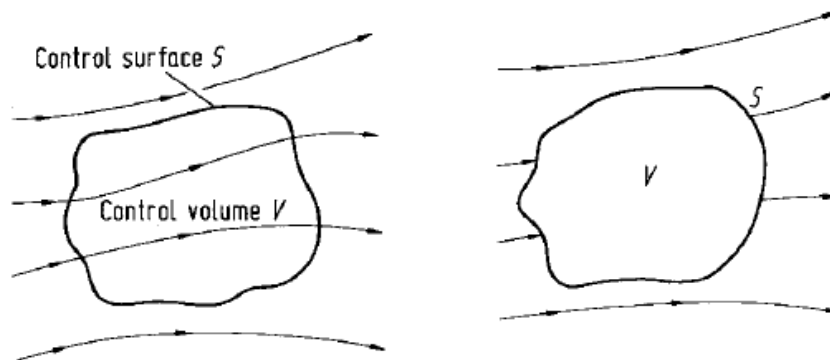


Figure 17 – Finite control volume (Wendt, 2009).

As Figure 17 demonstrates, there are two possible approaches. On the left, the control volume is fixed in space and the fluid, represented by the streamlines, moves through it. On the right, the control volume moves, accompanying the flow, meaning there are always the same fluid particles inside the volume.

The fundamental physical principles are applied to the fluid inside the control volume and, in the case where the volume is fixed in space, applied to the fluid that crosses the control surface. This allows to focus solely on the fluid inside the finite region of the volume, rather than the whole flow field. When the fluid flow equations are obtained directly from the application of the fundamental physical principles to the finite control volume, they come in

integral form, which can then be manipulated into obtaining partial differential equations. In either form, the equations obtained from the finite control volume fixed in space are called the *conservation* form, while the equations obtained from the finite control volume moving with the fluid are called *non-conservation* form of the governing equations.

### Infinitesimal fluid element

Considering a flow field of any kind as represented in Figure 18, where an infinitesimally small fluid element exists within the flow, with a differential volume,  $dV$ .

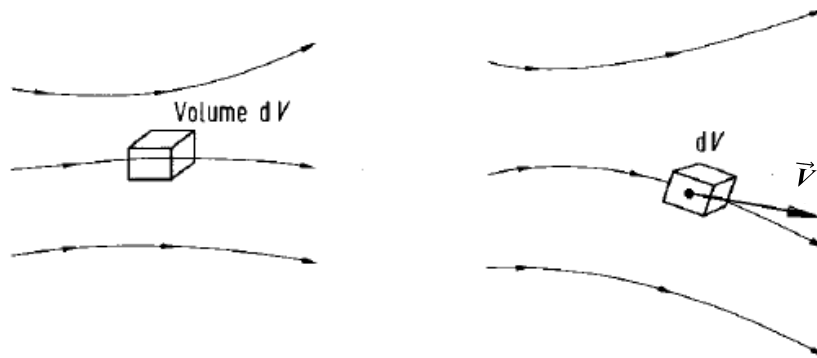


Figure 18 – Infinitesimal fluid element (Wendt, 2009).

Just like the finite control volume model, the fluid element can be considered fixed in space with the fluid running through it (left of Figure 18) or it can be moving along a streamline with a velocity vector  $\vec{V}$ , which corresponds to the flow velocity at each point (right of Figure 18). Again, whatever approach that is used, this model allows to apply the fundamental physical principles to the considered fluid element, rather than the flow field in its total.

In this case, this method leads directly to the partial differential equation form of the fundamental equations. As in the finite control volume, the conservation and non-conservation form are achieved by considering the fluid element fixed in space and moving through the streamline respectively.

It is important to refer that both conservation and non-conservation forms are equivalent. In fact, by manipulating one form, it is possible to obtain the other. Although both forms yield the same results, in CFD it is sometimes important to distinguish one from the other.

### Substantial derivative

The notion of substantial derivative is important to be established before deriving the governing equations. Physically, the substantial derivative is the time rate of change following a moving fluid element. Therefore, in order to demonstrate the substantial

derivative, the infinitesimally small fluid element moving with the flow (right of Figure 18) will be adopted. It is considered that the fluid element moves through a Cartesian space, as represented in Figure 19. To the  $x$ ,  $y$  and  $z$  axes correspond the unit vectors  $\vec{i}$ ,  $\vec{j}$  and  $\vec{k}$  respectively. The velocity field vector is then given by:

$$\vec{V} = u\vec{i} + v\vec{j} + w\vec{k} \quad (12)$$

Where the  $x$ ,  $y$ , and  $z$  components of velocity are respectively given by:

$$u = u(x, y, z, t) \quad (13)$$

$$v = v(x, y, z, t) \quad (14)$$

$$w = w(x, y, z, t) \quad (15)$$

Since the flow is considered unsteady, the velocity components are in function of space, but also time, represented by  $t$ . Applying the same analogy to the density field ( $\rho$ ):

$$\rho = \rho(x, y, z, t) \quad (16)$$

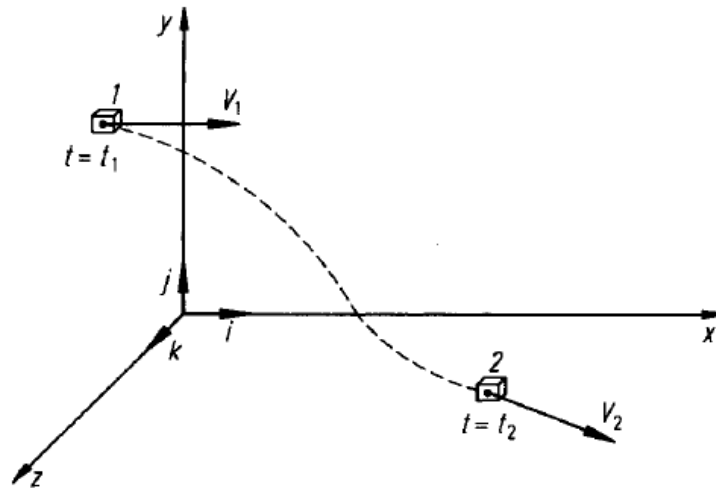


Figure 19 – Fluid element moving in the Cartesian flow field (Wendt, 2009).

Figure 19 shows the infinitesimal fluid element moving from a position 1, at time  $t_1$ , to position 2, at time  $t_2$ . The density field for each time is respectively:

$$\rho_1 = \rho(x_1, y_1, z_1, t_1) \quad (17)$$

$$\rho_2 = \rho(x_2, y_2, z_2, t_2) \quad (18)$$

This function can be expanded in a Taylor's series about point 1 as follows:

$$\rho_2 = \rho_1 + \left(\frac{\partial \rho}{\partial x}\right)_1 (x_2 - x_1) + \left(\frac{\partial \rho}{\partial y}\right)_1 (y_2 - y_1) + \left(\frac{\partial \rho}{\partial z}\right)_1 (z_2 - z_1) + \left(\frac{\partial \rho}{\partial t}\right)_1 (t_2 - t_1) + \text{Higher order terms} \quad (19)$$

Dividing the given equation by  $(t_2 - t_1)$ , and ignoring the higher order terms, the following expression is obtained:

$$\frac{\rho_2 - \rho_1}{t_2 - t_1} = \left(\frac{\partial \rho}{\partial x}\right)_1 \left(\frac{x_2 - x_1}{t_2 - t_1}\right) + \left(\frac{\partial \rho}{\partial y}\right)_1 \left(\frac{y_2 - y_1}{t_2 - t_1}\right) + \left(\frac{\partial \rho}{\partial z}\right)_1 \left(\frac{z_2 - z_1}{t_2 - t_1}\right) + \left(\frac{\partial \rho}{\partial t}\right)_1 \quad (20)$$

By examining the limit as  $t_2$  approaches  $t_1$ , the term on the left becomes:

$$\lim_{t_2 \rightarrow t_1} \left(\frac{\rho_2 - \rho_1}{t_2 - t_1}\right) = \frac{D\rho}{Dt} \quad (21)$$

Where  $D\rho/Dt$  is the time rate of change of density of the given fluid element as it moves through space. By definition, the symbol  $D/Dt$  is called the substantial derivate.

By applying the same limit to the other terms:

$$\lim_{t_2 \rightarrow t_1} \left(\frac{x_2 - x_1}{t_2 - t_1}\right) \equiv u \quad (22)$$

$$\lim_{t_2 \rightarrow t_1} \left(\frac{y_2 - y_1}{t_2 - t_1}\right) \equiv v \quad (23)$$

$$\lim_{t_2 \rightarrow t_1} \left(\frac{z_2 - z_1}{t_2 - t_1}\right) \equiv w \quad (24)$$

Applying these results to Equations 20 and 21, the following is obtained:

$$\frac{D\rho}{Dt} = u \frac{\partial \rho}{\partial x} + v \frac{\partial \rho}{\partial y} + w \frac{\partial \rho}{\partial z} + \frac{\partial \rho}{\partial t} \quad (25)$$

By Equation 25, it is possible to determine the general expression for the substantial derivative in Cartesian coordinates:

$$\frac{D}{Dt} \equiv \frac{\partial}{\partial t} + u \frac{\partial}{\partial x} + v \frac{\partial}{\partial y} + w \frac{\partial}{\partial z} \quad (26)$$

The vector operator  $\nabla$ , in Cartesian coordinates, is defined as:

$$\nabla \equiv i \frac{\partial}{\partial x} + j \frac{\partial}{\partial y} + k \frac{\partial}{\partial z} \quad (27)$$

Considering Equation 12 and by replacing the vector operator in Equation 26, the expression below is obtained:

$$\frac{D}{Dt} \equiv \frac{\partial}{\partial t} + (\nabla \cdot \vec{V}) \quad (28)$$

This is the substantial derivative in vector notation, making it valid for any coordinate system.

As mentioned before, the substantial derivative ( $D/Dt$ ) is physically the time rate of change following a moving element, thus Equation 28 can be divided in two parts: the *local derivative* ( $\partial/\partial t$ ), which is physically the time rate of change at a fixed point, and the *convective derivative* ( $\nabla \cdot \vec{V}$ ), which is physically the time rate of change due to the movement of the fluid element from one location to another in the flow field.

The substantial derivative was demonstrated through the density field, but it is also applied to any flow field variable, such as static pressure, temperature, velocity, and others.

### 3.2.1 The continuity equation – mass is conserved

In order to demonstrate the application of the conservation of mass principle, the infinitesimal fluid element moving with the flow (right of Figure 18) will be used. As mentioned before, by applying this model, the equation will be obtained directly in partial differential form (due to the application of the infinitesimal fluid element model) and will present the non-conservation form of the equation (by choosing the model to be moving with the flow). The conservation form of the equation will also be presented but without demonstration, since both forms are equivalent.

Considering a moving fluid element, with a fixed mass given by  $\delta m$ , if the element's volume is represented by  $\delta V$ , then the expression of the mass is:

$$\delta m = \rho \delta V \quad (29)$$

Since the principle states that mass is conserved, then the time rate of change of the mass of the fluid element as it moves along the flow, or substantial derivative applied to the infinitesimal mass, is zero, as shown below:

$$\frac{D(\delta m)}{Dt} = 0 \quad (30)$$

Replacing Equation 29 in Equation 30 and mathematically solving the derivative, the following expression is obtained:

$$\frac{D(\rho\delta V)}{Dt} = \delta V \frac{D\rho}{Dt} + \rho \frac{D(\delta V)}{Dt} = 0 \quad (31)$$

Dividing Equation 31 by  $\delta V$ :

$$\frac{D\rho}{Dt} + \rho \left[ \frac{1}{\delta V} \frac{D(\delta V)}{Dt} \right] = 0 \quad (32)$$

By considering that the physical meaning of  $(\nabla \cdot \vec{V})$  in the substantial derivative (Equation 28) is the time rate of change of the volume of a moving fluid element per unit volume and is given by:

$$\nabla \cdot \vec{V} = \frac{1}{\delta V} \frac{D(\delta V)}{Dt} \quad (33)$$

Then, by replacing in Equation 32, the continuity equation in the *non-conservation* form is obtained:

$$\frac{D\rho}{Dt} + \rho \nabla \cdot \vec{V} = 0 \quad (34)$$

If one chooses to apply the model of a finite control volume to be fixed in space, then it is also possible to obtain the continuity equation but in its conservation form. In this case, as mentioned earlier, the equation is directly obtained in integral form and can then be manipulated in order to be obtained as a partial differential equation. The partial differential continuity equation in conservation form can be given by:

$$\frac{\partial \rho}{\partial t} + \nabla \cdot (\rho \vec{V}) = 0 \quad (35)$$

### 3.2.2 The momentum equation – Newton's 2<sup>nd</sup> law

The fundamental physical principle applied here is the momentum conservation, also known as Newton's 2<sup>nd</sup> law, given by:

$$\vec{F} = m\vec{a} \quad (36)$$

For the flow model, the moving fluid element (right of Figure 18) will be considered. The relation between the net force of the fluid element and its acceleration described in Newton's

2<sup>nd</sup> law is a vector relation. Thus, it can be divided into three scalar relations along the  $x$ ,  $y$  and  $z$  axes. Considering only the  $x$  component, Newton's 2<sup>nd</sup> law can be written as:

$$F_x = ma_x \quad (37)$$

This force has mainly two sources (Versteeg & Malalasekera, 1995; Wendt, 2009):

- Body forces – which act directly on the fluid element's volumetric mass (e.g. gravitational, electric and magnetic forces).
- Surface forces – which act directly on the fluid element's surface. These can be divided into two forces: (a) pressure forces, due to the pressure distribution that the outside fluid causes on the fluid element, and (b) shear and normal stress distributions caused by the outside fluid pushing the surface of the element through friction (also known as viscous forces).

#### Body forces

A fluid element's volume is given by:  $(dx \, dy \, dz)$ . The body force per unit mass acting on the fluid element will be denoted  $\vec{f}$ , with  $f_x$  being its  $x$  component. Therefore:

$$\left\{ \begin{array}{l} \text{Body force on the} \\ \text{fluid element acting} \\ \text{in the } x \text{ direction} \end{array} \right\} = f_x m \quad (38)$$

And,

$$m = \rho(dx \, dy \, dz) \quad (39)$$

Replacing Equation 39 in Equation 38, the body force is given by:

$$\left\{ \begin{array}{l} \text{Body force on the} \\ \text{fluid element acting} \\ \text{in the } x \text{ direction} \end{array} \right\} = \rho f_x(dx \, dy \, dz) \quad (40)$$

#### Surface forces

There are two types of surface forces: shear and normal stresses, as represented in Figure 20. In the graphical representations shown in the figure, the shear stress (Figure 20a) is denoted by  $\tau_{yx}$  and the normal stress (Figure 20b) by  $\tau_{xx}$ .



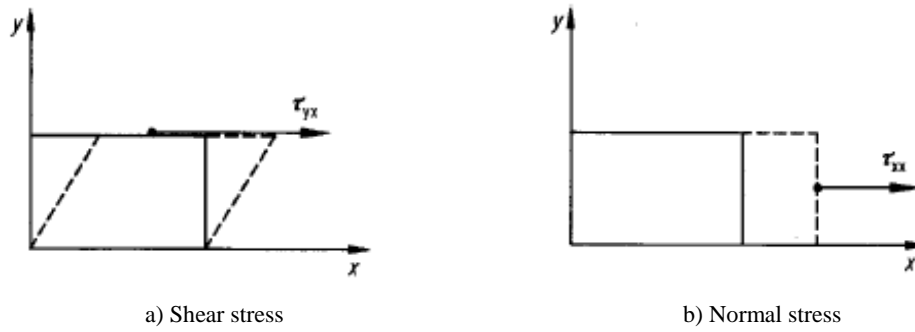


Figure 20 – Graphic representations of surfaces forces (Wendt, 2009).

Figure 21 represents all surface forces applied on an infinitesimally small, moving fluid element, namely pressure forces, shear and normal stresses. Note that, for simplification, only  $x$  direction forces are represented. The three velocity components,  $u$ ,  $v$  and  $w$  positively increase according to the axes shown.

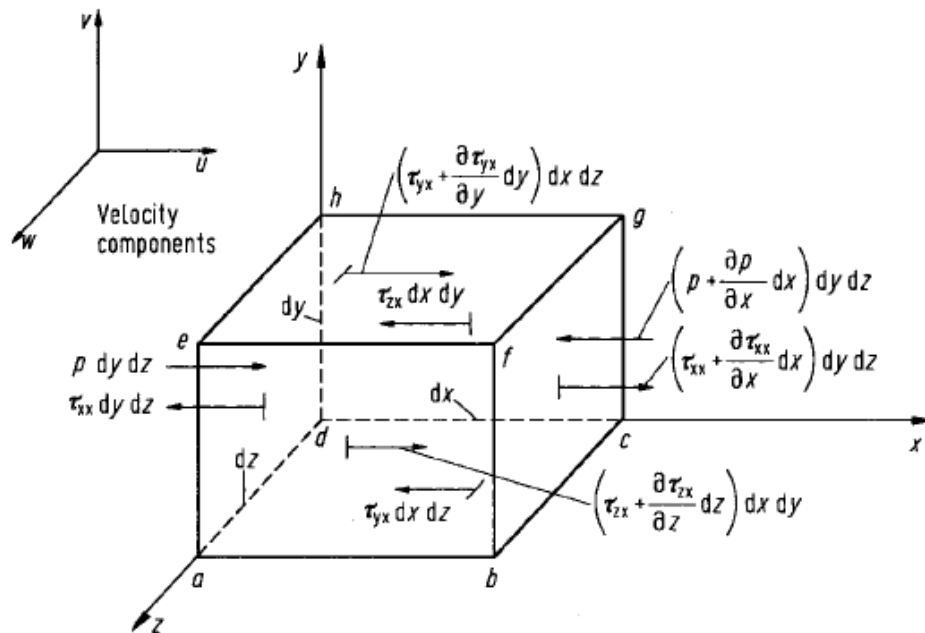


Figure 21 – Surface forces in  $x$  direction represented in an infinitesimally small, moving element (adapted from Wendt, 2009).

The convention used is that  $\tau_{ij}$  represents a stress in the  $j$  direction exerted on a plane perpendicular to the  $i$  axis and  $p$  represents pressure forces. Note that surface forces have contrary directions in opposite faces. As an example, consider the  $adhe$  face of the cube. In this face, in  $x$  direction, there is a shear stress  $\tau_{xx} dy dz$ . Note that  $dy dz$  refers to the  $y0z$  plane. There is also a pressure force applied on the face, represented by  $p dy dz$ . Face  $bcgf$  is a distance  $dx$  from the  $adhe$  face, thus, the shear stress in this face is  $[\tau_{xx} + (\partial \tau_{xx} / \partial x) dx] dy dz$

and the pressure force is  $[p+(\partial p/\partial x)dx] dy dz$ . The same applies to all other faces of the element (Versteeg & Malalasekera, 1995; Wendt, 2009).

By summing all forces represented in Figure 21, bearing in mind the direction of each force relative to the positive convention of the axes, the following expression is obtained (Versteeg & Malalasekera, 1995; Wendt, 2009):

$$\begin{aligned} \left\{ \begin{array}{l} \text{Net surface force} \\ \text{in the } x \text{ direction} \end{array} \right\} &= \left[ p - \left( p + \frac{\partial p}{\partial x} dx \right) \right] dy dz + \left[ \left( \tau_{xx} + \frac{\partial \tau_{xx}}{\partial x} dx \right) - \tau_{xx} \right] dy dz + \\ &+ \left[ \left( \tau_{yx} + \frac{\partial \tau_{yx}}{\partial y} dy \right) - \tau_{yx} \right] dx dz + \left[ \left( \tau_{zx} + \frac{\partial \tau_{zx}}{\partial z} dz \right) - \tau_{zx} \right] dx dy \end{aligned} \quad (41)$$

Simplifying the equation above, the net surface force can be given by:

$$\left\{ \begin{array}{l} \text{Net surface force} \\ \text{in the } x \text{ direction} \end{array} \right\} = \left( -\frac{\partial p}{\partial x} + \frac{\partial \tau_{xx}}{\partial x} + \frac{\partial \tau_{yx}}{\partial y} + \frac{\partial \tau_{zx}}{\partial z} \right) dx dy dz \quad (42)$$

In order to obtain the total force in the  $x$  direction,  $F_x$ , one must sum the body and surface forces, that is, Equations 40 and 42 respectively. The total force is then given by:

$$F_x = \left( -\frac{\partial p}{\partial x} + \frac{\partial \tau_{xx}}{\partial x} + \frac{\partial \tau_{yx}}{\partial y} + \frac{\partial \tau_{zx}}{\partial z} \right) dx dy dz + \rho f_x (dx dy dz) \quad (43)$$

This represents the left side of Newton's 2<sup>nd</sup> law (Equation 37). To complete the expression, the mass of the fluid element is given by Equation 39 and its acceleration, being the time rate of change of its velocity, is equal to:

$$a_x = \frac{Du}{Dt} \quad (44)$$

Since  $F_x = ma_x$ , then, after simplification, it can be written as following:

$$\left( -\frac{\partial p}{\partial x} + \frac{\partial \tau_{xx}}{\partial x} + \frac{\partial \tau_{yx}}{\partial y} + \frac{\partial \tau_{zx}}{\partial z} \right) + \rho f_x = \rho \frac{Du}{Dt} \quad (45)$$

This equation represents the momentum equation in the  $x$  direction. The momentum equation can then be written for all three directions (Versteeg & Malalasekera, 1995; Wendt, 2009):

$$x: \rho \frac{Du}{Dt} = \left( -\frac{\partial p}{\partial x} + \frac{\partial \tau_{xx}}{\partial x} + \frac{\partial \tau_{yx}}{\partial y} + \frac{\partial \tau_{zx}}{\partial z} \right) + \rho f_x \quad (46)$$

$$y: \rho \frac{Du}{Dt} = \left( -\frac{\partial p}{\partial y} + \frac{\partial \tau_{xy}}{\partial x} + \frac{\partial \tau_{yy}}{\partial y} + \frac{\partial \tau_{zy}}{\partial z} \right) + \rho f_y \quad (47)$$

$$z: \rho \frac{Du}{Dt} = \left( -\frac{\partial p}{\partial z} + \frac{\partial \tau_{xz}}{\partial x} + \frac{\partial \tau_{yz}}{\partial y} + \frac{\partial \tau_{zz}}{\partial z} \right) + \rho f_z \quad (48)$$

These three scalar equations are called the *Navier-Stokes equations* for each direction. As mentioned before, they were obtained directly in partial differential form and are in the non-conservation form of the equations. Through manipulation, the conservation form of the equations can also be obtained, although they are equivalent to the ones before.

### 3.2.3 The energy equation – energy is conserved

Once again, the infinitesimal element moving with the flow (right of Figure 18) will be used to derive the energy equation.

The first law of thermodynamics is a statement of the energy conservation principle. When this statement is applied to the moving fluid element shown in Figure 18, the rate of change of energy inside the fluid element (A) is equal to the net flux of heat into the element (B) plus the rate of working done on the element due to body and surface forces (C), as shown in the equation below:

$$A = B + C \quad (49)$$

Considering the  $C$  parameter in the equation above, the rate of work done only by the body forces acting on the fluid element moving at a velocity  $\vec{V}$  is:

$$\left\{ \begin{array}{l} \text{Rate of work} \\ \text{done by the body forces} \end{array} \right\} = \rho \vec{f} \cdot \vec{V}(dx \, dy \, dz) \quad (50)$$

Regarding the surface forces (which are the pressure forces and shear and normal stresses) represented in Figure 21 solely in the  $x$  direction, the rate of work done on the moving fluid element by these forces in the  $x$  direction is given by the multiplication of the  $x$  component of velocity,  $u$ , and the forces mentioned. For example, considering the pressure component in face *adhe* given by  $p \, dy \, dz$ , the rate of work done by this pressure force is  $u \, p \, dy \, dz$ . Figure 22 illustrates the work rate done by each surface force in the  $x$  direction in every face. Forces in the positive  $x$  direction have a positive work rate, while forces in the negative  $x$  direction have a negative work rate.

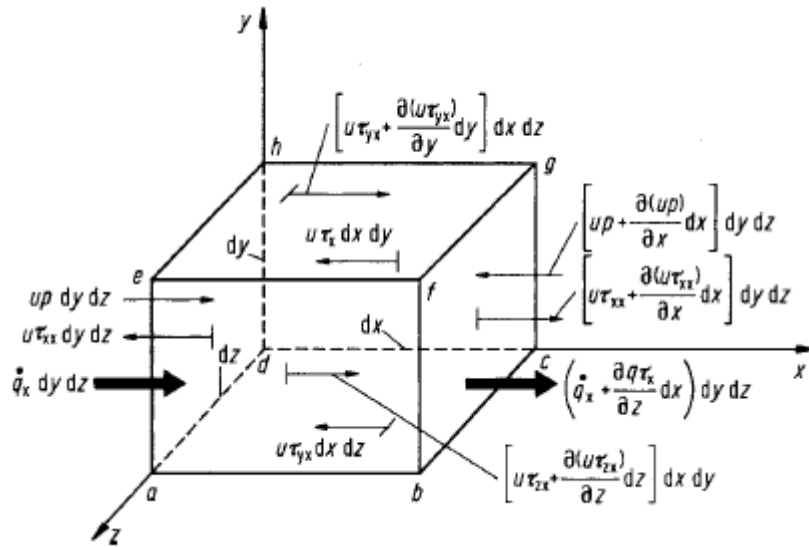


Figure 22 – Energy fluxes in an infinitesimally small, moving fluid element, solely in the  $x$  direction (Wendt, 2009).

Adding all the surface forces, taking into account the direction of each one, and after simplifications, the net rate of work done on the moving fluid element due to these forces results in:

$$\left\{ \begin{array}{l} \text{Net rate of work} \\ \text{of surface forces} \\ \text{in the } x \text{ direction} \end{array} \right\} = \left[ -\frac{\partial(up)}{\partial x} + \frac{\partial(u\tau_{xx})}{\partial x} + \frac{\partial(u\tau_{yx})}{\partial y} + \frac{\partial(u\tau_{zx})}{\partial z} \right] dx dy dz \quad (51)$$

The expression above only considers the surface forces in the  $x$  direction. By also adding the surface forces in the  $y$  and  $z$  directions and by considering the rate of work done by the body forces given in Equation 50, the net rate of work done on the moving fluid element, denoted by  $C$  in Equation 49, is given by:

$$C = \left[ \begin{array}{l} -\left( \frac{\partial(up)}{\partial x} + \frac{\partial(vp)}{\partial y} + \frac{\partial(wp)}{\partial z} \right) + \frac{\partial(u\tau_{xx})}{\partial x} + \frac{\partial(u\tau_{yx})}{\partial y} + \frac{\partial(u\tau_{zx})}{\partial z} \\ + \frac{\partial(v\tau_{xy})}{\partial x} + \frac{\partial(v\tau_{yy})}{\partial y} + \frac{\partial(v\tau_{zy})}{\partial z} + \\ \frac{\partial(w\tau_{xz})}{\partial x} + \frac{\partial(w\tau_{yz})}{\partial y} + \frac{\partial(w\tau_{zz})}{\partial z} \end{array} \right] dx dy dz + \rho \vec{f} \cdot \vec{V} dx dy dz \quad (52)$$

Considering Equations 12 and 37, the first 3 terms on the right of the equation above are equal to  $\nabla \cdot (p\vec{V})$ .

Returning to Equation 49, in regard to the  $B$  parcel, which is the net flux of heat into the element, this flux can be caused by volumetric heating (absorption or emission of radiation)

and by heat transfer across the surface (thermal conduction). In Figure 22,  $\dot{q}$  is defined as the rate of volumetric heat addition per unit mass, therefore, considering the mass of the moving fluid element to be  $\rho dx dy dz$  (Equation 39), the volumetric heating of the element is given by:

$$\left\{ \begin{array}{l} \text{Volumetric heating} \\ \text{of the element} \end{array} \right\} = \rho \dot{q} dx dy dz \quad (53)$$

Figure 22 represents the transferred heat in the x direction by thermal conduction into the moving fluid element across face *adhe* ( $\dot{q}_x dy dz$ ) and out of the element across face *bcgf* ( $[\dot{q}_x + (\partial\dot{q}_x/\partial x)dx]dydz$ ). Therefore, the net heat transferred in the x direction into the fluid element by thermal conduction is:

$$\left[ \dot{q}_x - \left( \dot{q}_x + \frac{\partial\dot{q}_x}{\partial x} dx \right) \right] dy dz = - \frac{\partial\dot{q}_x}{\partial x} dx dy dz \quad (54)$$

Considering the heat transfer by conduction in all 3 directions and in all faces shown in Figure 22, the heating of the fluid element by thermal conduction is:

$$\left\{ \begin{array}{l} \text{Heating of the} \\ \text{fluid element by} \\ \text{thermal conduction} \end{array} \right\} = - \left( \frac{\partial\dot{q}_x}{\partial x} + \frac{\partial\dot{q}_y}{\partial y} + \frac{\partial\dot{q}_z}{\partial z} \right) dx dy dz \quad (55)$$

Since the net flux of heat into the element ( $B$ ) is given by the sum of volumetric heating and thermal conduction, then, considering Equations 53 and Equation 55,  $B$  is given by:

$$B = \left[ \rho \dot{q} - \left( \frac{\partial\dot{q}_x}{\partial x} + \frac{\partial\dot{q}_y}{\partial y} + \frac{\partial\dot{q}_z}{\partial z} \right) \right] dx dy dz \quad (56)$$

Heat transfer by thermal conductivity is proportional to the local temperature gradient ( $T$ ), hence, in the x direction its value is obtained by:

$$\dot{q}_x = -k \frac{\partial T}{\partial x} \quad (57)$$

Where  $k$  represents the thermal conductivity. Considering the same for directions y and z, by substituting the thermal conductivity heat transfer in Equation 56, the expression below for  $B$  is obtained:

$$B = \left[ \rho \dot{q} + \frac{\partial}{\partial x} \left( k \frac{\partial T}{\partial x} \right) + \frac{\partial}{\partial y} \left( k \frac{\partial T}{\partial y} \right) + \frac{\partial}{\partial z} \left( k \frac{\partial T}{\partial z} \right) \right] dx dy dz \quad (58)$$

The lasting parameter of Equation 49 is parcel A, which is the rate of change of energy inside the fluid element. Firstly, considering that the moving fluid element approach is being used, then the time rate of change is given by the substantial derivative. The total energy of a moving fluid per unit mass is the sum of its internal energy per unit mass ( $e$ ) and its kinetic energy per unit mass ( $V^2/2$ ), therefore, and considering that the fluid's mass is  $\rho dx dy dz$  (Equation 39), the A parcel is given by the following expression:

$$A = \rho \frac{D}{Dt} \left( e + \frac{V^2}{2} \right) dx dy dz \quad (59)$$

By substituting the A, B and C parcels (given in Equations 59, 58 and 52 respectively) in Equation 49, the final form of the energy equation is obtained as below:

$$\begin{aligned} \rho \frac{D}{Dt} \left( e + \frac{V^2}{2} \right) = & \rho \dot{q} + \frac{\partial}{\partial x} \left( k \frac{\partial T}{\partial x} \right) + \frac{\partial}{\partial y} \left( k \frac{\partial T}{\partial y} \right) + \frac{\partial}{\partial z} \left( k \frac{\partial T}{\partial z} \right) - \\ & - \frac{\partial(u\dot{p})}{\partial x} - \frac{\partial(v\dot{p})}{\partial y} - \frac{\partial(w\dot{p})}{\partial z} + \frac{\partial(u\tau_{xx})}{\partial x} + \frac{\partial(u\tau_{yx})}{\partial y} + \\ & + \frac{\partial(u\tau_{zx})}{\partial z} + \frac{\partial(v\tau_{xy})}{\partial x} + \frac{\partial(v\tau_{yy})}{\partial y} + \frac{\partial(v\tau_{zy})}{\partial z} + \\ & + \frac{\partial(w\tau_{xz})}{\partial x} + \frac{\partial(w\tau_{yz})}{\partial y} + \frac{\partial(w\tau_{zz})}{\partial z} + \rho \vec{f} \cdot \vec{V} \end{aligned} \quad (60)$$

Since the principle of a moving fluid element was considered, Equation 60 presents the non-conservation form of the energy equation. As mentioned previously, through manipulation it is possible to obtain the conservation form of these equations, however, since they are equivalent, they will not be presented. The equation is also presented in terms of total energy ( $e + V^2/2$ ), while it is often written in a form that just involves the internal energy,  $e$ . For that, Equations 46, 47 and 48 should be multiplied by  $u$ ,  $v$  and  $w$  respectively. These resultant expressions should be added and, considering that  $u^2 + v^2 + w^2 = V^2$ , the following is obtained:

$$\begin{aligned} \rho \frac{DV^2/2}{Dt} = & -u \frac{\partial p}{\partial x} - v \frac{\partial p}{\partial y} - w \frac{\partial p}{\partial z} + u \left( \frac{\partial \tau_{xx}}{\partial x} + \frac{\partial \tau_{yx}}{\partial y} + \frac{\partial \tau_{zx}}{\partial z} \right) + \\ & + v \left( \frac{\partial \tau_{xy}}{\partial x} + \frac{\partial \tau_{yy}}{\partial y} + \frac{\partial \tau_{zy}}{\partial z} \right) + w \left( \frac{\partial \tau_{xz}}{\partial x} + \frac{\partial \tau_{yz}}{\partial y} + \frac{\partial \tau_{zz}}{\partial z} \right) + \\ & + \rho (uf_x + vf_y + wf_z) \end{aligned} \quad (61)$$

By subtracting Equation 61 from Equation 60 and considering  $\rho \vec{f} \cdot \vec{V} = \rho (uf_x + vf_y + wf_z)$ , the energy equation in terms of total energy results in the following:

$$\begin{aligned} \rho \frac{De}{Dt} = & \rho \dot{q} + \frac{\partial}{\partial x} \left( k \frac{\partial T}{\partial x} \right) + \frac{\partial}{\partial y} \left( k \frac{\partial T}{\partial y} \right) + \frac{\partial}{\partial z} \left( k \frac{\partial T}{\partial z} \right) - \\ & - p \left( \frac{\partial u}{\partial x} + \frac{\partial v}{\partial y} + \frac{\partial w}{\partial z} \right) + \tau_{xx} \frac{\partial u}{\partial x} + \tau_{yx} \frac{\partial u}{\partial y} + \tau_{zx} \frac{\partial u}{\partial z} + \\ & + \tau_{xy} \frac{\partial v}{\partial x} + \tau_{yy} \frac{\partial v}{\partial y} + \tau_{zy} \frac{\partial v}{\partial z} + \tau_{xz} \frac{\partial w}{\partial x} + \\ & + \tau_{yz} \frac{\partial w}{\partial y} + \tau_{zz} \frac{\partial w}{\partial z} \end{aligned} \quad (62)$$

Note that this equation continues in the non-conservation form and that the body force terms have cancelled.

### 3.3 Types of flow

There are two types of flow: laminar and turbulent. The difference between them was demonstrated by Osborne Reynolds in 1883, by injecting a stream of dye into a water flow through a tube at different flow rates. At a low flow rate, the dye stream followed a relatively straight and orderly path. Macroscopically, this means that the flow moves in parallel layers, without ever mixing or overturning. This is called a laminar flow, as shown in Figure 23 (Kundu *et al.*, 2012).

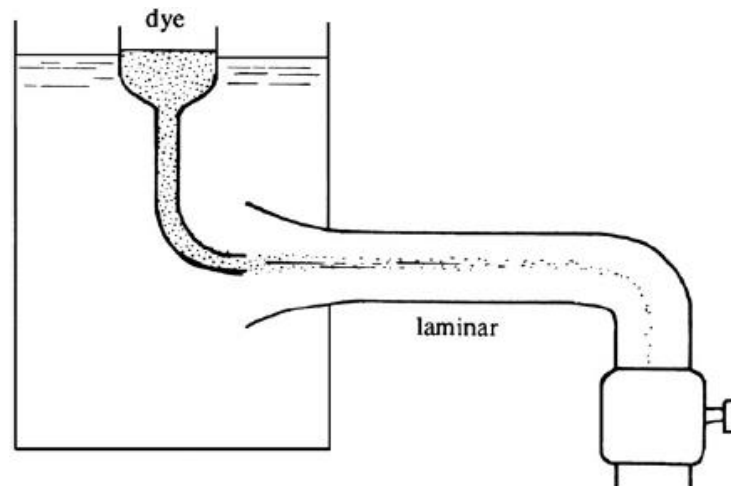


Figure 23 – Laminar flow (Kundu *et al.*, 2012).

When the flow rate was increased beyond a certain value, the dye stream became irregular, spreading disorderly throughout the section of the tube, indicating unsteady macroscopic

mixing motions. This is called a turbulent flow, as illustrated in Figure 24 (Kundu *et al.*, 2012).

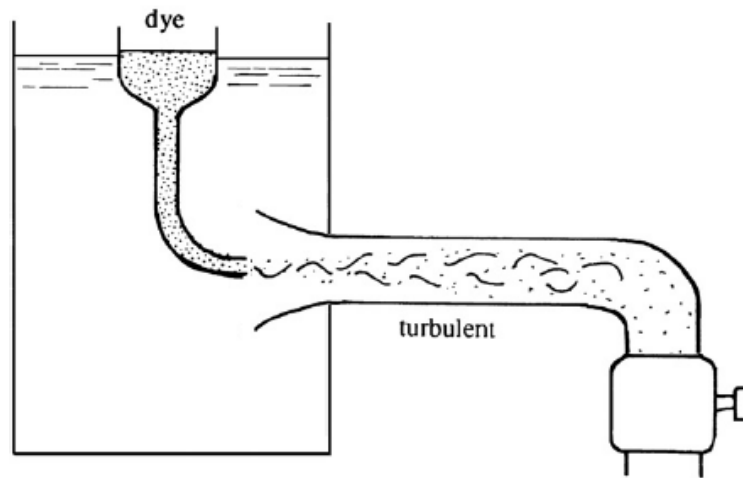


Figure 24 – Turbulent flow (adapted from Kundu *et al.*, 2012).

As mentioned before, the flow becomes turbulent when the flow rate reaches a certain specific value. The transition from laminar to turbulent flow can then be specified by calculating a parameter called the Reynolds number,  $Re$ , given by (Kundu *et al.*, 2012):

$$Re = \frac{\rho U d}{\mu} \quad (63)$$

Where  $d$  represents the tube diameter,  $U$  represents the velocity averaged over the tube's cross section,  $\rho$  represents the fluid's density and  $\mu$  represents the fluid's viscosity. Considering the kinematic viscosity parameter, which is the propensity for vorticity to diffuse through a fluid and is given by  $\nu = \mu/\rho$ . That way, the Reynolds number can also be given by (Kundu *et al.*, 2012):

$$Re = \frac{U d}{\nu} \quad (64)$$

The transition from laminar to turbulent flow occurs at Reynolds number around 2000 to 3000. In nature and in most practical engineering situations, flows are in fact turbulent. This is valid in phenomena such as atmospheric winds, ocean currents, water delivery systems, flows past cars, aircrafts, ships, etc., flows through turbines and engines and, more specifically related to this dissertation, airflows in residential and non-residential buildings (Versteeg & Malalasekera, 1995; Kundu *et al.*, 2012). For that matter, turbulent flows will be studied in higher detail.



### 3.4 Turbulent flow

A turbulent flow is far more complex than a laminar flow, since there are significant variations in kinetic energy and momentum and mass transfer can occur (Carvalho, 2002; Meireles, 2011). It is characterized by having unpredictable fluctuations, leading to the formation of vortices of various sizes. The biggest vortices are caused by the flow's kinetic energy and will transfer that energy to smaller vortices, until it is dissipated because of the fluid's viscosity (Carvalho, 2002; Meireles, 2011). In that way, Kundu *et al.* (2012) define turbulence as “*a dissipative flow state characterized by nonlinear fluctuating three-dimensional vorticity*”. Although acknowledging the simplicity in this definition, it states the main characteristics of a turbulent flow (Kundu *et al.*, 2012).

Although hard to define, it is important not to confuse turbulence with randomness. Even in a turbulent flow, the basic physical principles mentioned in subsection 3.2 are valid, which means that mass, momentum and energy are conserved. These are the main characteristics of turbulence, proving that it is not a random event (Kundu *et al.*, 2012):

- *Fluctuations* – a turbulent flow presents fluctuations in velocity, pressure, temperature, etc., which seem to be irregular and unpredictable.
- *Nonlinearity* – as mentioned before, a flow goes from laminar to turbulent when the Reynolds number exceeds a certain value. This transition is a nonlinear process. Even after reaching an equilibrium state, disturbances may still occur causing the flow to become unpredictable.
- *Vorticity* – a turbulent flow contains fluctuating vorticity. It is possible to observe swirls of different sizes that deform, coalesce, divide, and spin. Important spinning structures present in a turbulent flow are called eddies. An eddy is basically the swirling motion of a fluid and its size range increases with higher Reynolds number.
- *Dissipation* – as stated, a vortex transfers kinetic energy to smaller vortices until the fluid's viscosity causes this energy to dissipate in the form of heat.
- *Diffusivity* – this type of flow is characterized by agitating motions of the fluid, leading to the mixing and diffusion of species, momentum and heat.

Despite its seemingly unpredictable behaviour, it is still possible to achieve useful and relatively precise predictions using empirical models and numerical simulation.

### 3.4.1 Turbulence models

A turbulence model is a computational procedure intended to solve the complex prediction of a turbulent flow. The most used CFD turbulence models to take into account are: Direct Numerical Simulation (DNS), Large Eddy Simulation (LES), and Reynolds-Averaged Navier-Stokes (RANS) equations. DNS is the least feasible approach, since it performs extremely long simulations and requires a very large computing power, mostly unavailable in personal computers. For most situations, LES models are still too expensive, computationally speaking, and RANS models sometimes lack accuracy due to their intrinsic simplifications. So, more recently, a development in turbulence modeling by coupling RANS and LES models resulted in the Detached Eddy Simulation (DES) method, solving these problems. Therefore, only LES, RANS and DES turbulence models will be considered (Sousa, 2012).

Zhai *et al.* (2007) performed a study on a numerous of RANS, LES and DES models, having identified eight prevalent models. Among the RANS models tested, Indoor zero-equation, RNG k- $\epsilon$ , standard k- $\epsilon$ , LRN-LS, SST k- $\omega$ , v2f-dav and RSM-IP were identified for their elevated accuracy and performance. In the LES models, the LES-Dyn model had the best performance and the DES-SA model was identified among the DES models. Generally, the RANS models are the most commonly used, in particular the standard k- $\epsilon$  and the RNG k- $\epsilon$  (Chen, 2009). Figure 25 presents a flow chart of the models studied and identified.

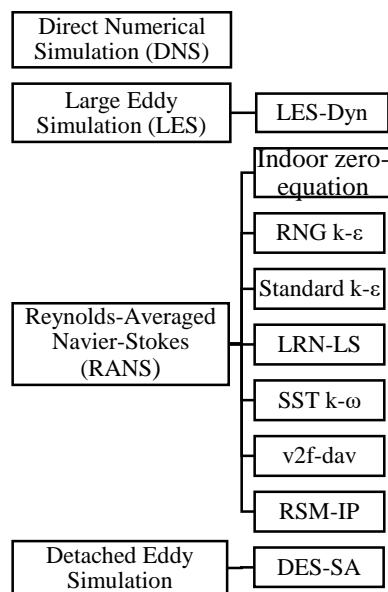


Figure 25 – Flow chart of the turbulence models studied by Zhai *et al.* (2007).

Regarding the RNG k-ε and standard k-ε models, these will be presented in higher detail. Each of these turbulence models consider transport equations for the flow’s turbulent kinetic energy ( $k$ ) and the dissipation rate of the turbulent kinetic energy ( $\varepsilon$ ). The transport equation for  $k$  is given by (Meireles, 2011):

$$\rho_0 \left[ \underbrace{\frac{\partial k}{\partial t}}_{\text{Rate of change}} + \underbrace{\overline{u_{m_j}} \frac{\partial k}{\partial x_j}}_{\text{Convective transport}} \right] = \underbrace{\frac{\partial}{\partial x_j} \left( \frac{\mu_T}{\sigma_k} \frac{\partial k}{\partial x_j} \right)}_{\text{Diffusive transport}} + \underbrace{\mu_T \left( \frac{\partial \overline{u_{m_i}}}{\partial x_j} + \frac{\partial \overline{u_{m_j}}}{\partial x_i} \right) \frac{\partial \overline{u_{m_j}}}{\partial x_j}}_{\text{Production of shear}} + \underbrace{G - \rho_0 \varepsilon}_{\text{Viscous dissipation}} \quad (65)$$

The transport equation for  $\varepsilon$  is given by (Meireles, 2011):

$$\rho_0 \left[ \underbrace{\frac{\partial \varepsilon}{\partial t}}_{\text{Rate of change}} + \underbrace{\overline{u_{m_j}} \frac{\partial \varepsilon}{\partial x_j}}_{\text{Convective transport}} \right] = \underbrace{\frac{\partial}{\partial x_j} \left( \frac{\mu_T}{\sigma_\varepsilon} \frac{\partial \varepsilon}{\partial x_j} \right)}_{\text{Diffusive transport}} + \underbrace{C_{1\varepsilon} \frac{\varepsilon}{k} \left[ \mu_T \left( \frac{\partial \overline{u_{m_i}}}{\partial x_j} + \frac{\partial \overline{u_{m_j}}}{\partial x_i} \right) \frac{\partial \overline{u_{m_i}}}{\partial x_j} + C_{3\varepsilon} G \right]}_{\text{Generation – destruction}} - \rho_0 C_{2\varepsilon} \frac{\varepsilon^2}{k} \quad (66)$$

Where  $\overline{u_{m_i}}$  and  $\overline{u_{m_j}}$  are the time-averaged mixture velocity components in the directions  $x_i$  and  $x_j$  respectively,  $\mu_T$  is the eddy dynamic viscosity,  $\rho_0$  is the reference density,  $G$  corresponds to the buoyancy term and  $\sigma_k$ ,  $\sigma_\varepsilon$ ,  $C_{1\varepsilon}$ ,  $C_{2\varepsilon}$  and  $C_{3\varepsilon}$  are constants. The main difference between the RNG k-ε and standard k-ε models lies in the way these constants are obtained. In the standard k-ε model they are obtained experimentally while in the RNG k-ε model they are derived explicitly, making this last model more accurate. The values of each constant are presented in Table 8 for each model.

Table 8 – Values of the constants of the standard k-ε and RNG k-ε models (adapted from Meireles, 2011).

Constants	Standard k-ε model	RNG k-ε model
$\sigma_k$	1.00	0.72
$\sigma_\varepsilon$	1.30	0.72
$C_{1\varepsilon}$	1.44	1.42
$C_{2\varepsilon}$	1.92	Function of $k$ , $\varepsilon$ and shear rate
$C_{3\varepsilon}$	0.20	0.20

### **3.5 Elements in a CFD code**

After understanding the basic physical principles behind a CFD simulation and the characteristics of the flow it intends to simulate, this section addresses to how a CFD code works. As mentioned earlier, a CFD code solves numerical algorithms to predict a fluid flow, presenting a detailed user interface where problem parameters are inputted and results are examined. There are three main elements in a CFD code (Versteeg & Malalasekera, 1995):

- i) Pre-processor.
- ii) Solver.
- iii) Post-processor.

#### **3.5.1 Pre-processor**

The first step in a CFD simulation is the pre-processor. This consists in entering the flow problem's parameters in the software's interface. This may include (Versteeg & Malalasekera, 1995):

- Definition of the geometry of the region in study. This can be done by using the software's primitive geometry generator or by importing the model from another software.
- Grid generation. This consists of dividing the domain in order to create a grid (or mesh) of smaller cells.
- Selection of the physical and chemical phenomena that will be modelled.
- Definition of the fluid's properties.
- Definition of boundary conditions for each grid.

After inputting the necessary parameters for the flow problem, these will be transformed into a form suitable for use by the solver.

#### **3.5.2 Solver**

In this stage of the CFD code, the physical processes previously defined will be solved using numerical techniques. Three numerical solution techniques can be considered: the finite element, the finite difference and spectral methods. The solver processes these numerical methods by following the steps below (Versteeg & Malalasekera, 1995):

- Use of simple functions to approximate flow variables that are previously unknown.

- Substitution of these approximated parameters in the problem's governing flow equations and posterior mathematical manipulation of such equations.
- Algebraic resolution of the equations.

Considering these steps, the three numerical solution techniques mentioned differ in the approximations made to the flow variables and in the way they are substituted into the equations. The CFD commercial software available for this study is *FLOW-3D*<sup>®</sup>. The technique used in this software is called the *finite volume method* which was developed as a special finite difference formulation. This technique is actually the most well-established CFD technique and is also used in other commercial CFD codes, such as: FLUENT, PHOENICS and STAR-CD (Versteeg & Malalasekera, 1995; Savage & Johnson, 2001).

### 3.5.3 Post-processor

The step following the solver process is the analysis of the results. For that, the post-processor of a CFD software is provided of data visualization tools, such as (Versteeg & Malalasekera, 1995):

- Domain geometry and grid display.
- Vector plots.
- 2D and 3D surface plots.
- Line and shaded contour plots.
- View manipulation (translation, rotation, scaling, etc.).
- Particle tracking.
- Colour postscript output.

It is also possible to obtain a more dynamic display of the results through animations and results may also be exported to another software in order to be analysed beyond the code.

## 3.6 *FLOW-3D*<sup>®</sup> modelling

### 3.6.1 Finite volume method

As mentioned before, *FLOW-3D*<sup>®</sup> commercial program solves the RANS equations using the finite volume method. These are the main steps in its numerical algorithm (Versteeg & Malalasekera, 1995):

- Integration of the fundamental fluid flow equations over all the solution domain's finite control volumes.
- Substitution in the integrated equations of terms that represent flow processes such as convection, diffusion and sources by numerical approximations, in order to convert the integral equations into algebraic equations.
- Use of an iterative method to solve the algebraic equations.

In the finite volume method, the computational domain is subdivided into a grid of hexahedral cells of various sizes that do not overlap in a Cartesian reference, which means that to each cell corresponds the average values of the flow variables, such as pressure and velocity. The flow's variables, such as pressure ( $P$ ), fluid fractions ( $F$ ), fractional volumes ( $V_F$ ), density ( $\rho$ ), internal energy ( $I$ ), turbulence quantities ( $q$ ), dissipation ( $D$ ) and viscosity ( $\mu$ ) are located at the center of each cell, except for the velocities in each direction ( $u$ ,  $v$  and  $w$ ) and the fractional areas ( $A_x$ ,  $A_y$  and  $A_z$ ), which are located at the center of the cell's faces (Savage & Johnson, 2001; Flow Science, 2015). Figure 26 demonstrates the location of the flow variables in a typical *FLOW-3D*<sup>®</sup> cell.

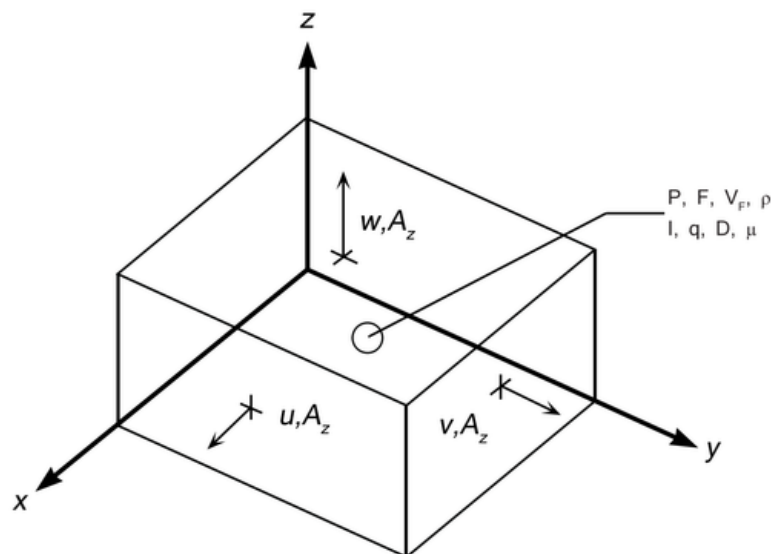


Figure 26 – Representation of flow variables in a typical *FLOW-3D*<sup>®</sup> cell (Flow Science, 2015).

### 3.6.2 Grid definition

As mentioned earlier, the grid generation is one of the main steps in the pre-processor. After defining the geometry of the computational domain, the CFD model requires a proper division into subdomains (elements, control volumes, etc.) in order to numerically solve the physical flow phenomenon. This process results in a mesh of cells overlapping the

computational domain (Ferziger & Perić, 2002). This is a relevant stage since the results of a flow simulation (for example velocity, temperature or pressure values) are defined at each cell of the grid. For that matter, the higher the number of cells, the more accurate the results will be. Of course, it is important to acknowledge that a very high number of cells also requires a higher computational capacity and execution time. An optimum mesh is one that is very refined in areas where large variations are expected, therefore a higher accuracy is required, and coarser where variations aren't significant (Versteeg & Malalasekera, 1995). Considering the importance of grid refinement in order to obtain accurate results, but still acknowledging the time and computational limitations in the use of a grid with a very high number of cells, Franke *et al.* (2007) described the refinement process in the following steps:

- i) Run a simple calculation with the studied model, in order to acknowledge the available computational capacity.
- ii) Generate a simple mesh in the model and run an initial simulation.
- iii) Extract the results from the studied zone.
- iv) Then, the previously defined mesh must be refined and the results are again extracted.
- v) This should be an iterative process, until an agreement is reached considering the results obtained.

There are commonly three types of mesh elements in CFD solvers: hexahedral element (6 faces, 8 corners and 12 edges), tetrahedral element (4 faces, 4 corners and 6 edges) and pyramidal or wedge shaped (5 faces, 5 corners and 8 edges) as shown in Figure 27 (Pordal, 2006).

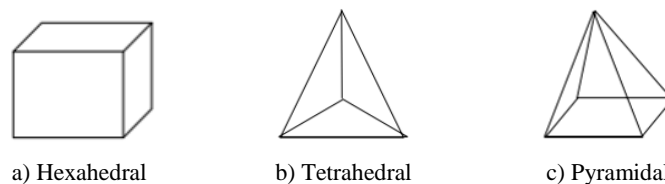


Figure 27 – Types of mesh elements (adapted from Pordal, 2006).

Generally, two types of hexahedral meshes can be considered: single-block structured mesh, when the hexahedral elements are arranged in a rectangular form and multi-block structured mesh, considering a number of structured blocks (Figure 28). In a structured mesh, a grid cell can be identified by a unique three-dimensional index  $(i, j, k)$  (Pordal, 2006; Ferziger & Perić, 2002). Multi-block grids are important considering that certain models, due to their

complexity, may require a very large number of grid cells, leading to inaccuracy and an excessive simulation time. To avoid such problems, *FLOW-3D*<sup>®</sup> allows the generation of multi-block grids, in order to only apply grid blocks in specific areas where the flow will occur and therefore avoid excessive grid cells and minimize the simulation time. When creating a multi-block, it is important to assure that the boundaries of each block are properly connected to the adjacent block, in order to avoid discontinuities in the domain (Silva, 2013).

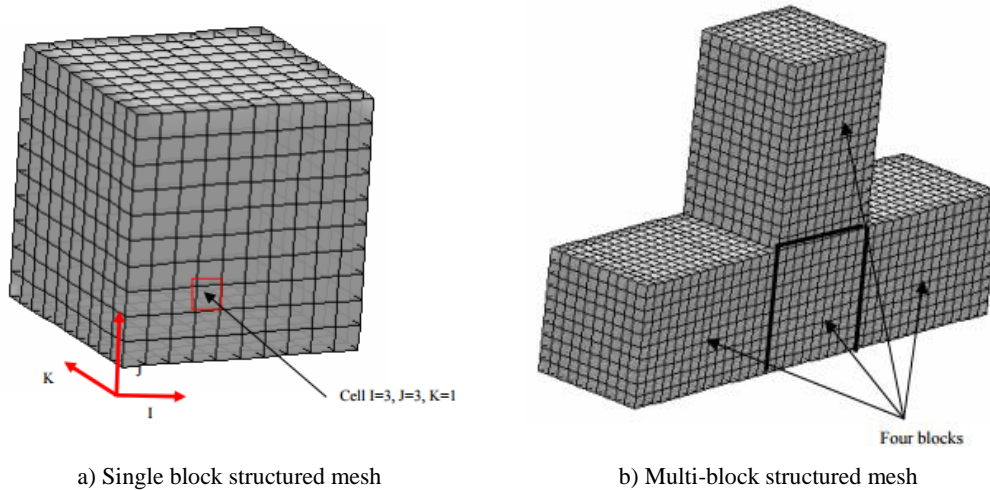


Figure 28 – Types of hexahedral meshes (Pordal, 2006).

When using a tetrahedral type mesh, the grid obtained is called an unstructured mesh (Figure 29). In this case, a unique three-dimensional index cannot be used to identify a grid cell. This type of mesh is mostly used to define complex three-dimensional geometries because it is a more flexible type of grid (Ferziger & Perić, 2002; Pordal, 2006).

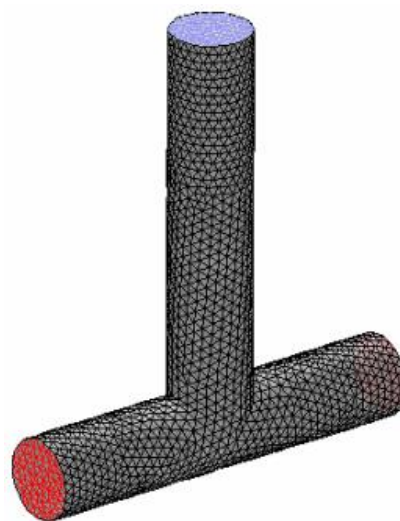


Figure 29 – Tetrahedral unstructured mesh (Pordal, 2006).



A mesh can also be defined by its orthogonality. This means that the grid cells can be orthogonal or non-orthogonal. A grid's orthogonality is determined by the angle between crossing grid lines. When they form a straight angle (90 degrees) the grid is orthogonal. The hexahedral single-block structured mesh presented above in Figure 28 is an example of an orthogonal mesh. When the lines do not constitute a straight angle between each other, then the mesh is non-orthogonal. A tetrahedral mesh, as shown in Figure 29, is a common non-orthogonal mesh, although hexahedral meshes can also share this characteristic (Olsen, 1999). An orthogonal mesh has the advantage of simplifying the discretization of the differential equations, which leads to less approximations in order to obtain algebraic equations and, therefore, higher accuracy in the results. On the other hand, the non-orthogonality leads to the appearance of secondary terms that tend to reduce the stability in the iterative processes. This leads to an increase in both programming difficulty and in the cost and time of solving the equations. Besides that, a non-orthogonal grid can produce unphysical solutions which can affect the accuracy and efficiency of the algorithm. However, in order to define complex geometries, a non-orthogonal mesh is the best solution since it is adaptable to any geometry (Ferziger & Perić, 2002).

*FLOW-3D*<sup>®</sup> always defines geometries using an orthogonal grid. For more complex geometries, the programme uses a method called FAVOR<sup>™</sup> which will further be described in subsection 3.6.3. Considering the orthogonal grid used by the programme, it can also be characterized by its uniformity. A grid is considered uniform when the spacing between grid cells is constantly the same and, therefore, cells are all the same size (Figure 30). When this spacing alters within the grid, leading to the existence of cells with different sizes, it is considered non-uniform (Figure 31). Uniform grids are simpler and more regular, while non-uniformity allows the refinement of the grid in specific areas that require a higher accuracy in the results (Wendt, 2009).

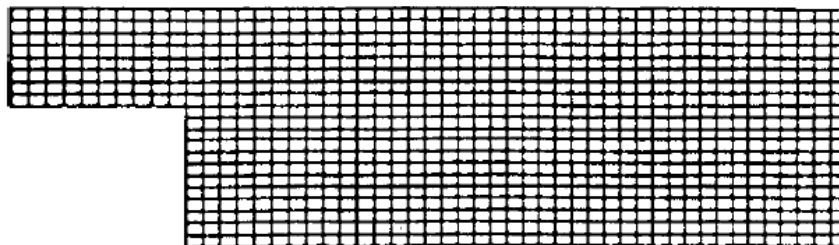


Figure 30 – Uniform grid (Wendt, 2009).

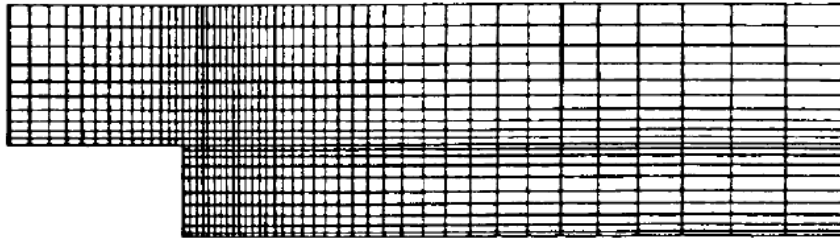


Figure 31 – Non-uniform grid (Wendt, 2009).

Two other aspects should also be considered by the user that is generating a grid: smoothness in a non-uniform grid, which means that the change in cell size should be gradual, and the aspect ratio, which is the ratio between a cell's longest edge length and its shortest edge length. The ideal aspect ratio is equal to 1, which is obtained in cubic cells, and should not exceed 3. It is recommended that the ratio between adjacent cell sizes should be as close to unity as possible, and not exceed 1.25. In multi-block meshes, a ratio of 2 to 1 should be considered as the acceptable maximum to avoid significant inter-block accuracy loss (Flow Science, 2015).

A more recent aspect introduced in latest versions of the *FLOW-3D*<sup>®</sup> software is the conforming mesh concept. It is used when it is necessary to model thin cavity regions that stretch over a large portion of the computational domain. In these cases, highly refined grids are needed in the thin cavity regions, while the surrounding solid elements may only require a coarse grid resolution. The conforming mesh is intended to address these issues by resolving only the cavity and a uniform layer of solid around it. This results in an overlaid two-block mesh which delivers an accurate solution in both domains, as shown in Figure 32 (Flow Science, 2015).

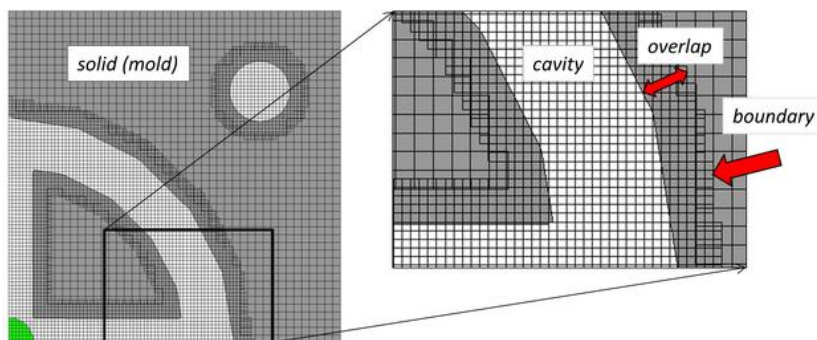


Figure 32 – Conforming mesh concept to model a thin cavity in a large solid (Flow Science, 2015).

The conforming mesh concept can also be applied in order for meshes to conform to a solid region (instead of void). This is useful in problems where it is required to accurately capture a very thin solid region surrounded by fluid (Flow Science, 2015).

### 3.6.3 FAVOR™ method

The *Fractional Area/Volume Obstacle Representation*, or simply FAVOR™ method, is the technique used by the *FLOW-3D*® software to incorporate geometries into the governing equations by means of the computational grid. When the grid is defined in the pre-processor, it generates area fractions for each cell face and determines which corners of the face are inside the geometry that was introduced. Therefore, there are three situations that may occur (Flow Science, 2015):

- 1) When all four corners of a cell face are inside the geometry, then the entire face is defined within the geometry.
- 2) If all corners are outside the geometry, then the entire face is considered to be outside the geometry. This leads to the non-resolution of objects that are smaller than the cell size. The area fraction generator does not recognize pieces of the geometry that aren't included in a single cell corner, defrauding the geometry's full resolution. This often occurs in spherical objects that are smaller than a grid cell.
- 3) In the case where some corners are inside and others are outside the geometry, the intersection of the geometry with face edges is simulated. Area fractions are defined from these intersection points by assuming straight-line connections between intersection points within the face. When the geometry boundary is curved in the cell, the straight-line assumption entails a small error in the fractional area. The accuracy in this approximation improves with the refinement of the grid.

Figure 33 illustrates how the FAVOR™ method defines a geometry within the grid, showing all three situations mentioned above. On the left is the actual geometry and on the right is the resolution of the geometry by the FAVOR™ method and, therefore, it is the geometry the software will consider in the simulation.

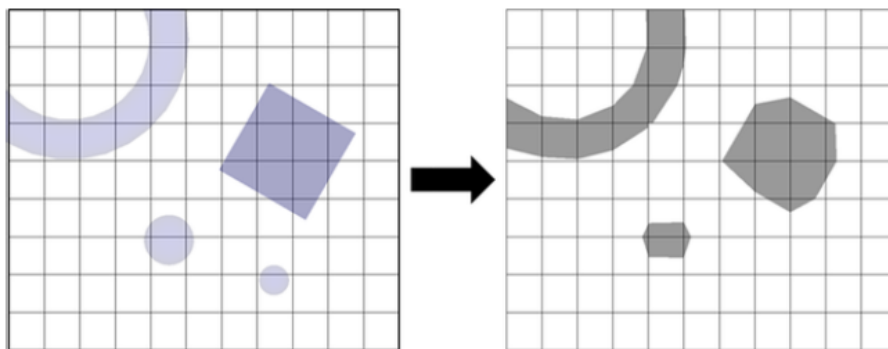


Figure 33 – FAVOR™ method (Flow Science, 2015).

### **3.6.4 Boundary conditions**

The proper specification of initial and boundary conditions is crucial in the definition of any CFD problem. Regarding the initial conditions, the initial values of all flow parameters must be specified by the user at all of the domain's solution points. This is a rather simple procedure, requiring only the initialization of the appropriate data arrays into the CFD code. The choice and implementation of proper boundary conditions, however, aren't as straightforward. Instead of simply introducing the previously known initial flow parameters, the user must assume what type of condition defines the flow in each boundary and choose which of the CFD software's pre-defined boundary condition best approaches each case (Versteeg & Malalasekera, 1995). *FLOW-3D*<sup>®</sup> contains 10 available boundary conditions: symmetry, wall, continuative, periodic, specified pressure, specified velocity, grid overlay, outflow, wave and volume flow rate (Flow Science, 2015).

Considering the simulations that will be conducted, only the boundaries that will be used will be explained. The wall boundary is used to bound fluid and solid regions. For that, it applies a no-slip condition, which defines that the tangential fluid velocity is equal to the wall velocity, and the velocity condition normal to the boundary is set to zero. The symmetry boundary condition is used to reduce the computational effort associated to the problem by applying a zero-gradient condition at the boundary and by also setting the velocity component normal to the boundary to zero. The specified velocity boundary, as the name indicates, defines the flow's velocity vector and scalar properties at a flow inlet. This boundary condition is only useful when the velocity is previously known at the inlet. The specified pressure boundary is used to specify the pressure value at the boundary. This is useful when neither the flow rate nor the velocity are known at the inlet or outlet, since the flow is caused by a pressure difference (e.g. in a blower door test or in a buoyancy driven flow). When the fluid elevation is known, this boundary condition is also used, since the pressure at the boundary will follow a hydrostatic distribution (Flow Science, 2015).

# Chapter 4

---

Case Study



## Chapter 4. Case Study

### 4.1 Building description

The experimental procedure was performed in an actual Passive House, located in Oliveirinha, a small Portuguese town in the Aveiro district. Figure 34 contains two pictures of the dwelling's main facade, one showing the house when this study began and the other showing it after completion.



Figure 34 – Studied Passive House dwelling.

It is part of a small complex of 8 lots (Figure 35), all destined for residential buildings with 2 floors (ground and 1<sup>st</sup> floor). However, only the dwelling in study contains a passive design. At the moment of the procedures, only three dwellings were raised.



Figure 35 – Complex where the studied dwelling is inserted (in red).

All buildings are being built by a company named Modiko<sup>®</sup>. They use a patented construction system, based on light steel elements, referred to as *Light Steel Frame (LSF)*. The system consists of the interconnection of various prefabricated, standardized Modiko<sup>®</sup>

elements, such as steel profiles (for beams and pillars), walls and other accessories, which are later assembled on ground (Modiko®, 2014). The house contains a flat roof and an underground garage disconnected from the building. In terms of architecture, it consists of two singular rooms, two suites, a living room, a kitchen and two independent sanitary facilities. Figure 36 and Figure 37 present the building's ground floor and 1<sup>st</sup> floor plans respectively.

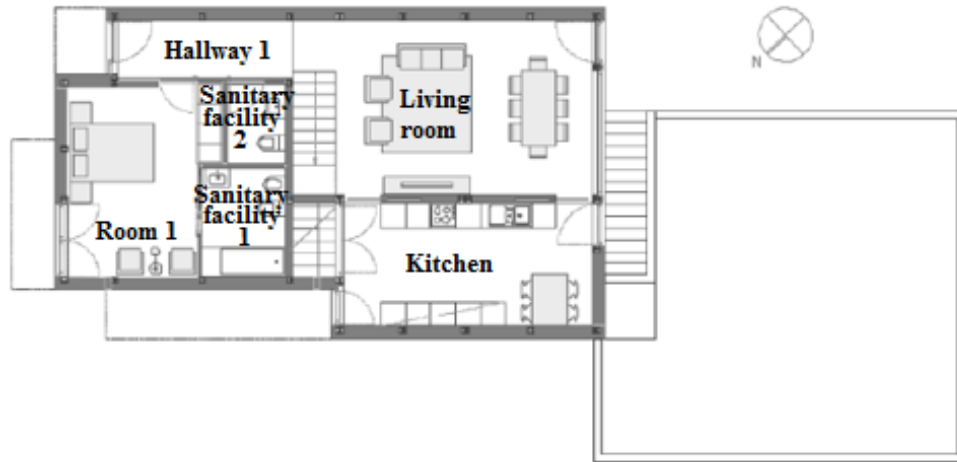


Figure 36 – Plan view of the ground floor.

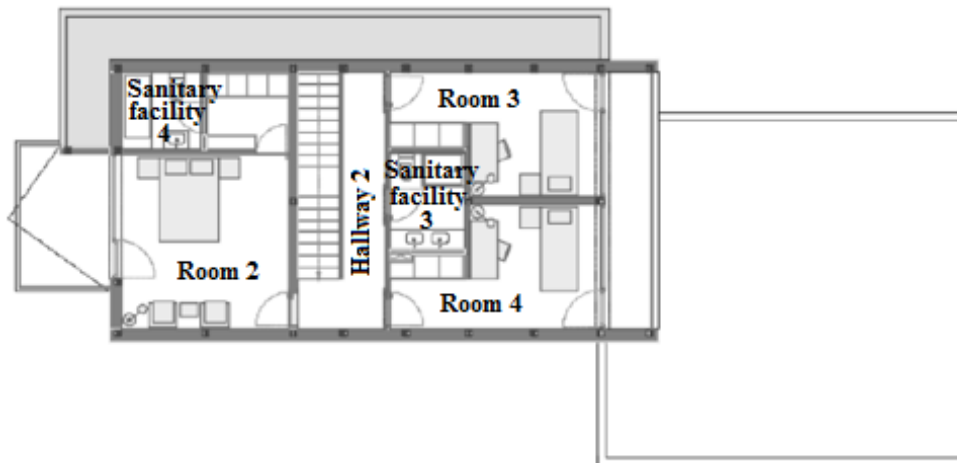


Figure 37 – Plan view of the 1<sup>st</sup> floor.

The house with a passive design resulted from an optimization of the regular Modiko® design. Table 9 presents the design characteristics of the original dwellings compared to the Passive House where the ventilation studies were performed.



Table 9 – Design characteristics of the original house compared to the Passive House.

<b>Modular Construction</b>	<b>Original House</b>	<b>Passive House</b>
Construction type	Concrete ground slab + LSF	Concrete ground slab + LSF
Treated floor area (m <sup>2</sup> )	139.24	141.62
U <sub>ground slab</sub> [W/(m <sup>2</sup> .°C)]	0.457-0.478 (XPS=3cm)	0.306-0.315 (XPS=10cm)
U <sub>wall</sub> [W/(m <sup>2</sup> .°C)]	0.327 (EPS=6cm)	0.211 (EPS=12cm)
U <sub>roof</sub> [W/(m <sup>2</sup> .°C)]	0.350 (EPS=5cm)	0.181 (EPS=12cm)
U <sub>window</sub> [W/(m <sup>2</sup> .°C)]	1.73-1.79	1.59-1.67
Ventilation system	HVAC	HRV and bypass for free cooling
Night ventilation	No	Yes
Heating/Cooling generation	Central unit (air to air)	Compact heat pump (air to air)
DHW source	Boiler and solar thermal	Compact heat pump and solar thermal
Lighting type	Halogen	LED
n <sub>50</sub> (ach <sup>-1</sup> )	0.6	0.6
Heating demand [kWh/(m <sup>2</sup> .year)]	44	14
Cooling demand [kWh/(m <sup>2</sup> .year)]	18	-
Overheating (%)	24.5	8.6
Total primary energy [kWh/(m <sup>2</sup> .year)]	167	74

The heating and cooling demand and the percentage of overheating were calculated according to PHPP8. Considering the pressurization values (0.6 ach<sup>-1</sup> for each house), it represents the maximum design reference value used in PHPP8. However, in locations with temperatures above 0°C in the winter, as in the central coast of Portugal, a pressurization test result of 1 ach<sup>-1</sup> is generally sufficient to achieve the heating criterion (Passive-on, 2007). A pressurization test was performed in the Passive House after completion, and the result was 0.9 ach<sup>-1</sup>.

## 4.2 Experimental analysis

The experimental study consisted of two separate experimental procedures. The purpose was to start with a simple procedure, which would result in a simple numerical simulation, and then extend it to a higher scale experiment. The ventilation phenomenon would then be analysed, at first, in a single compartment inside the house and then extended to a full-scale ventilation system analysis. In the first case, the airflow will be caused by a blower door and

in the second the experiment will be conducted with the dwelling's mechanical ventilation system in function.

#### **4.2.1 Experimental procedure 1 – blower door**

At the moment of this first procedure, the housing wasn't yet completed, since plasterboard work wasn't totally finished. However, partition walls already delimited the division in study. The ductwork for the ventilation system was already installed, lacking the ventilation unit (which is only installed later on) and the inlet and outlet grids, meaning that the edge of each duct is directly opened to the indoor divisions through holes in the plasterboard, as shown in Figure 38.



Figure 38 – Hole for the ventilation duct.

As mentioned before, the experimental procedure consists of a blower door test performed in a limited space inside the dwelling, in order to create an airflow through the division, which will then be monitored. The space where it was performed intends to be a sanitary installation connected to a closet in the 1<sup>st</sup> floor, as indicated in red in Figure 39.

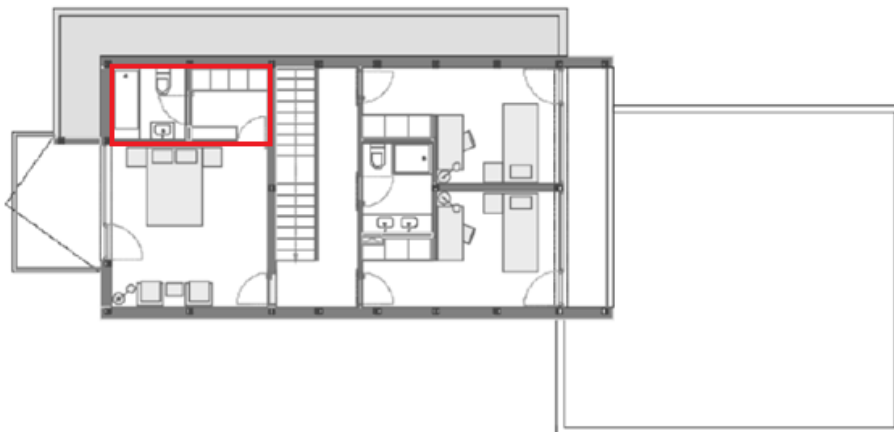


Figure 39 – Identification of the space in study where the blower door test was performed (in red).

Before conducting the experiment, the space was properly measured, to make sure that the drawings possess the correct measures. Its exact dimensions are (4.025 x 1.860 x 2.415 m). A 3D model of the studied space is presented in Figure 40. Note that the bathroom (on the left) and the closet (on the right) are separated by two plasterboard walls, with an opening between them where a door will be installed. The entry to the closet is also a simple opening. That entry is where the blower will then be installed. It is also possible to visualize the opening for the ventilation duct in the bathroom's ceiling, which is an 80 mm hole. An insulation tape was used to close all other openings/holes present in the plasterboard and all water supply and sanitation pipes that were open in the sanitary facility. This allowed a higher control over the airflow.

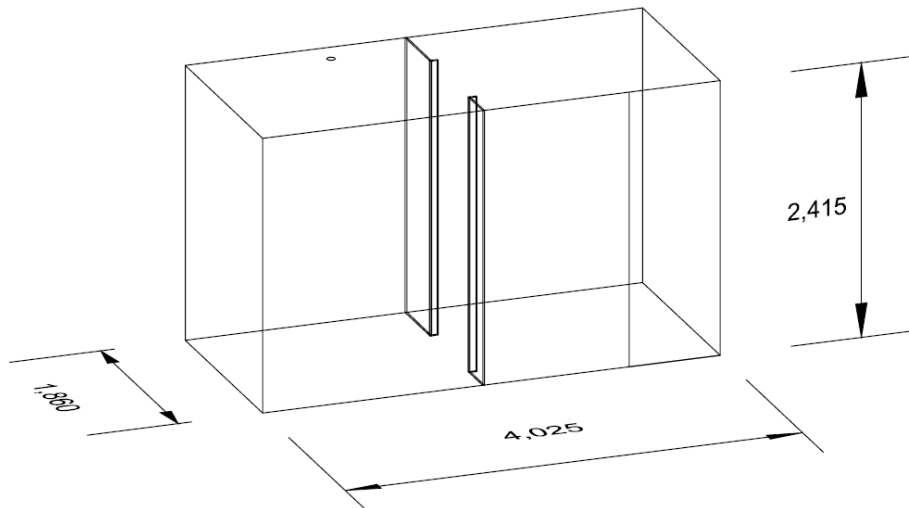


Figure 40 – 3D model of the space where the blower door test was conducted.

The goal of this experiment was to measure the air velocity in a, as much as possible, controlled environment. For that, a digital anemometer was used. Figure 41 shows a picture of that anemometer.



Figure 41 – Digital anemometer used to register air velocities in experimental procedure 1.

This anemometer is a product of PCE instruments. The model is a PCE-423 and contains the technical specifications presented in Table 10.

Table 10 – Technical specifications of the anemometer used in experimental procedure 1.

Sensitivity Range	m/s	0.1 - 25.0
Resolution	m/s	0.01
Precision	Air velocity	$\pm 5\% \pm 0.2\text{m/s}$

The blower door was installed as shown in Figure 42. During the experiment, various pressure differences specified in the blower were tested in order to find the most suitable airflow.



Figure 42 – Blower door installed to conduct the experiment.

The experimental procedure consisted in setting the blower in depressurization and registering the air velocity at different points. Depressurization means that the blower is pushing air out of the space, leading air to enter through the ventilation opening in the ceiling, as illustrated in Figure 43. Thus, the opening will be considered the air inlet and the blower the outlet.

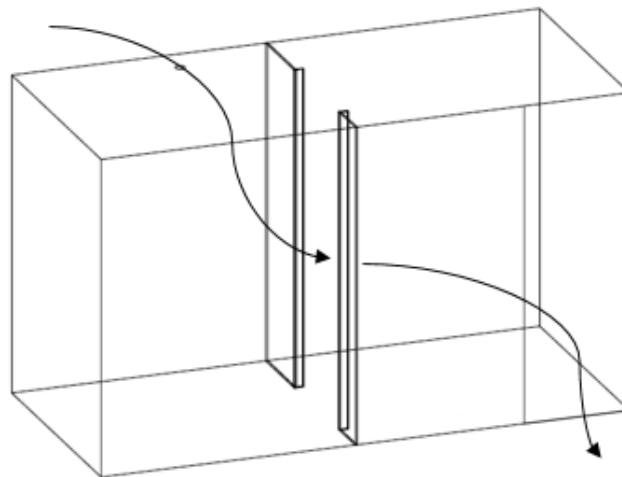


Figure 43 – Illustration of the expected airflow caused by a depressurized blower installed at the door.

A preliminary experiment was performed in order to test the anemometer's sensitivity. For that, the blower was initially set in depressurization at a pressure difference of -50 Pa and the anemometer was held by hand at different points. It was intended to delimit the airflow path through the room, from the inlet to the outlet, registering velocity values throughout that path, however, only near the inlet and outlet was it possible to register values. For that matter, the pressure difference was successively elevated to increase the airflow velocity. Pressure differences of -60, -70, -80 and -90 Pa were tested, but the anemometer's sensitivity was never able to register values away from the inlet and outlet, since the room's area was too large causing the airflow to scatter and drop the velocity to values under the limit of sensitivity of the anemometer. Therefore, in the absence of a more sensitive equipment, it was decided to monitor various points below the inlet and around the outlet, where the velocities were within the anemometer's acquisition range.

A grid was made using a thin black string, to mark the exact points where the anemometer would make registrations. That way, there would be higher precision when comparing experimental and numerical results, since the location of the points in the experimental grid would match the cells in the grid defined in the CFD software. Figure 44 shows part of the grid that was installed below the ventilation opening. More points were also marked at lower and wider positions.



Figure 44 – Part of the grid used to mark the exact points where the anemometer registered values below the ventilation opening.

This grid was installed below the air inlet, where most of the values were registered. It is important to mention that these points weren't selected randomly. In fact, the points were marked in strategic spots that actually follow the airflow caused by the blower. The pressure difference set at the blower was -80 Pa. Six specific heights were chosen, each with a series of points. Figure 45 represents the plan views of each height, specifying the selected points. The x0y referential is also indicated. Note that these points are below the air inlet, therefore, in the sanitary installation.

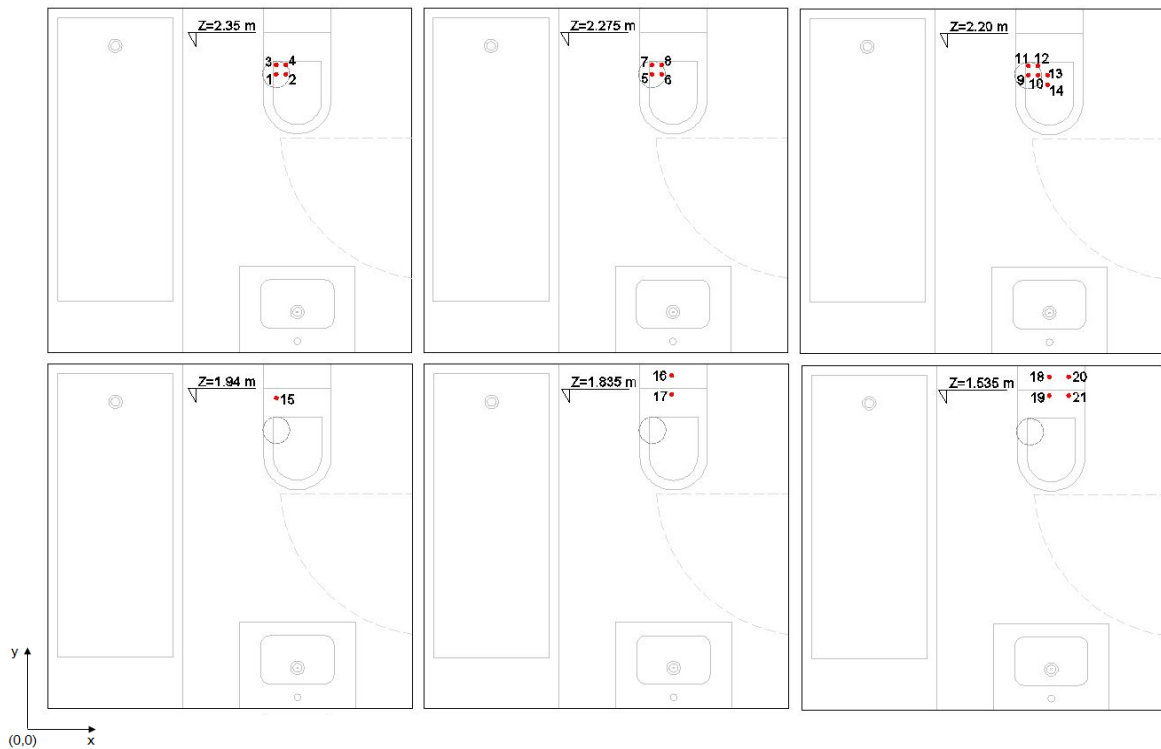


Figure 45 – Plan views of each height with the identification of the registration points below the air inlet.

The plan coordinates ( $x$ ,  $y$  and  $z$ ) of each point are presented in Table A1 of Appendix A. A factor that influenced the direction of the airflow was the slope that the duct presents at the opening, as shown in Figure 46. This slope deviates the flow, leading it towards the upper wall, and is then redirected towards the outlet. Points 15 to 21 presented in Figure 45 demonstrate that, since they are near the upper wall and, therefore, deviated from the path to the outlet. This deviation is more significantly noted at lower heights, since immediately below the inlet, the flow is still relatively vertical.



Figure 46 – Slope of the ventilation duct.

The velocity value at the outlet was also measured. For that, the anemometer was placed near the blower's opening, where the air was being sucked out. Note that, as mentioned before, the blower was installed in the entry door to the closet, therefore, the measurement was made inside the closet. Considering the same referential as before and the same origin point (0,0), the coordinates of the outlet point are given in Table A2 of Appendix A.

#### 4.2.2 Experimental procedure 2 – mechanical ventilation system

By the time of this procedure, the house was already at a whole different stage of completion compared to the previous. In fact, it was practically ready to be inhabited. The data collection had to be done at this stage, considering that the mechanical ventilation system had to be fully functional and being active for a few days to assure a stabilized airflow in the building. This procedure contemplated two separate data collections. One focused on the indoor air temperature and the other on the air velocities caused by the ventilation system. Regarding the temperature data collection, numerous thermo hygrometers (Figure 47) were placed

throughout the house, at different heights. The thermo hygrometer is a model Testo 174H-Mini. In each position, air temperature and relative humidity were registered.



Figure 47 – Thermo hygrometer used in experimental procedure 2 (Testo, 2015).

The technical specifications of the thermo hygrometers used are presented in Table 11.

Table 11 – Technical specifications of the thermo hygrometers used in experimental procedure 2.

Sensitivity Range	T (°C)	-20 - +70
	RH (%)	0 - 100
Resolution	T (°C)	0.1
	RH (%)	0.1
Precision	T (°C)	± 0.5
	RH (%)	± 3%

While the temperature data was being collected, a different anemometer (Figure 48) from the one used in experimental procedure 1 was used to register air velocities in each of the ventilation system’s grids.



Figure 48 – Anemometer used in experimental procedure 2 (Testo, 2015).

The change in anemometer was simply due to the equipment’s availability. This anemometer was a Testo 435 model and possessed the technical specifications present in Table 12.

Table 12 – Technical specifications of the anemometer used in experimental procedure 2.

Sensitivity Range	m/s	0.0 - 20.0
Resolution	m/s	0.01



The existence of the ventilation grids (Figure 49) is actually a big difference between this procedure and the previous, considering that, in the first, the air inlet was simply a hole in the plasterboard. However, these grids are in fact a relevant factor in the ventilation system.



Figure 49 – Ventilation grid.

Before starting the registrations, it was assured that the ventilation system was set at a previously known velocity. This system is comprised of 4 different levels, each with a specific air velocity. The level that was used was level 3, which, according to the mechanical engineer responsible for the design of the system, blows and pushes air at 3.4 m/s at the ventilation unit. This means that air is expected to lose velocity in its path through the ventilation ductwork. This part of the experimental data collection was very similar as the one performed using the blower door, placing the anemometer in various points around the grids. Due to the lack of sensitivity of the anemometer for very low velocities, similarly to what occurred in the experimental procedure 1 with model PCE-423, only points immediately surrounding the grids were measured. In this case, the problem is greater than in experimental procedure 1, since the air velocities are lower.

As mentioned earlier, this ventilation system is composed by air suppliers in rooms, living room and hallways and air extractors in the kitchen and sanitary facilities. In the air supply grids, considering that here the air velocities are higher, 9 points were considered: points 1 to 4 around the grid, and points 5 to 9 at the center of the grid at different heights. In the air extraction grids, the air velocities were lower, and, therefore, the anemometer could not register as many points as around the air supply grids, so only 5 were considered: the same 4 points around the grid and only point 5 immediately below the center of the grid. These points are illustrated in Figure 50. All points were then measured and duly noted.

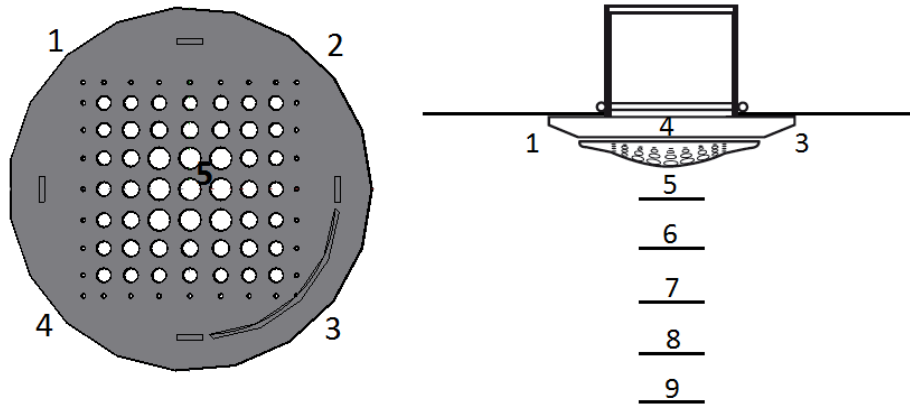


Figure 50 – Representation of each measuring point.

### 4.3 Numerical analysis

As mentioned before, the CFD software used to perform the numerical simulations was *FLOW-3D*<sup>®</sup>, version 11.0.3. Considering the experimental procedures mentioned, various numerical simulations were performed. For experimental procedure 1 (blower door in a sanitary facility), 1 simulation was performed, and for experimental procedure 2 (mechanical ventilation system of the entire house) 6 simulations were performed. From the 6 simulations of the second procedure, 5 of them include the mesh convergence process without the ventilation grids (Figure 49) and the last simulation will include these ventilation grids.

#### 4.3.1 Numerical procedure 1 – blower door

This numerical simulation consisted essentially of 4 steps: definition of the geometry, definition of the computational mesh (although in Chapter 3 the term “grid” was mostly used in this context, in order to avoid confusion with the mechanical ventilation’s grids, the term “mesh” will be adopted from this point further), definition of flow and fluid properties, and definition of boundary conditions.

##### Geometry definition

The space in study is, as mentioned before, a sanitary installation connected to a closet inside the Passive House dwelling. Since the model’s geometry is quite simple, the software’s internal primitive geometries were used to create the physical three-dimensional model of the space in study. Figure 51 illustrates the model in *FLOW-3D*<sup>®</sup>’s graphical interface.

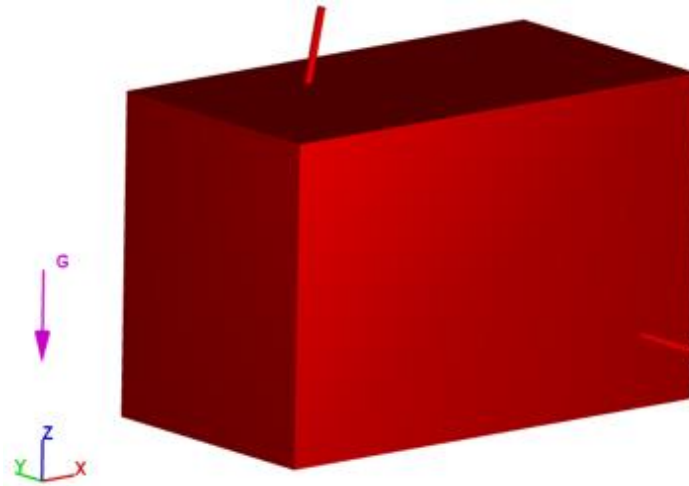


Figure 51 – 3D model of the space in study.

The interior partition walls were approximated as baffles, since they are very thin and, this way, a very small cell size is avoided. By defining these thin walls as baffles, they are considered surfaces instead of volumes, therefore, they do not affect the volume fraction at each cell, since the baffle's geometry snaps directly into the grid lines of the mesh (Flow Science, 2015). Figure 52 presents the partition walls approximated as baffles (in dark blue) that were defined within the 3D model shown in Figure 51.

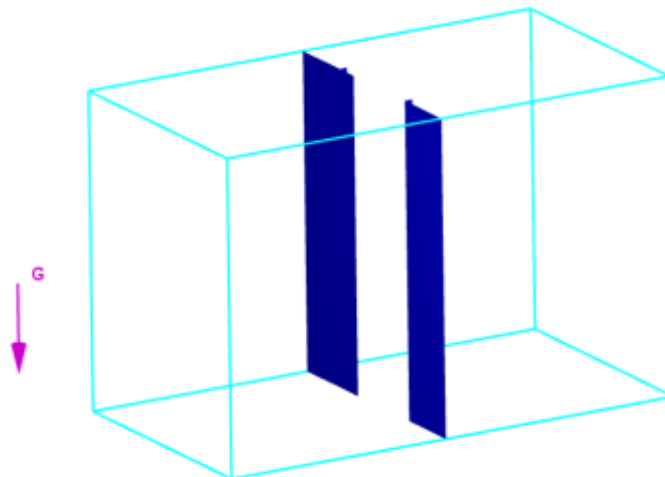


Figure 52 – Partition walls approximated as baffles.

In order to create the geometry, multiple subcomponents were grouped into a main component, in order to form a unique object. For that, 4 subcomponents were considered, which were either defined as solids or holes. Solids add material inside the geometry of the subcomponent, in order to define a solid object, while a hole removes material from the

current subcomponent to another, in order to open holes in solid geometries (Flow Science, 2015). The 4 subcomponents are described below:

- i) Subcomponent 1 intends to define the walls that outline the space in study. For that, this subcomponent was considered a solid. Note that this creates a full solid object, to which will then be subtracted the inside space through another subcomponent defined as a hole.
- ii) Subcomponent 2 intends to define the outlet. For that, a cylindrical element was created with the same diameter as the extraction point of the blower, which is 80 mm. This subcomponent is defined as a hole, which means that it will subtract the material from the wall defined in subcomponent 1, allowing air to be extracted through that wall.
- iii) Subcomponent 3 defines the air inlet. The same method was used as in subcomponent 2, defining a cylindrical element with the same diameter as the ventilation opening in the roof, which is 75 mm. In this case, however, the duct's slope had to be considered. For that, the slope was measured at the house and inserted in subcomponent 3. It presents an angle of  $2^\circ$  in the  $x$  direction and  $7^\circ$  in the  $y$  direction. There were some difficulties with this measurement, since it was made after the ductwork was completed and the plasterboard installed, therefore, the considered values are, in fact, very close approximations.
- iv) Subcomponent 4 defines the void space within the walls. The size of this subcomponent corresponds to the interior dimensions of the sanitary facility and the closet. Therefore, it was defined as a hole within subcomponent 1 and it is where the air will flow.

By applying a transparency to the model, it is possible to visualize its full extension, including each subcomponent that define the geometry and the partition walls, as shown in Figure 53.

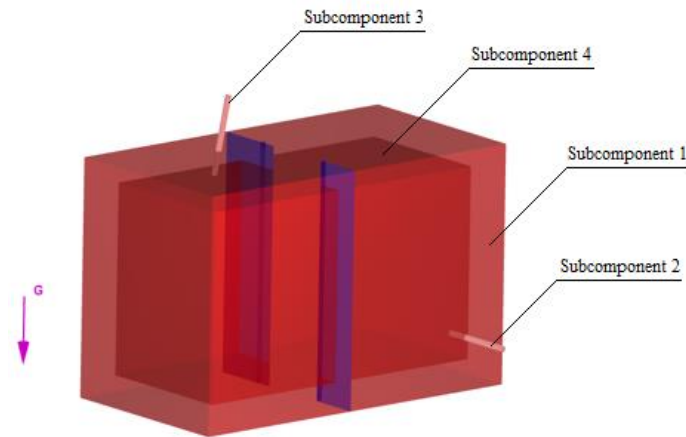


Figure 53 – 3D model representing all subcomponents that define the geometry in study.

### Mesh definition

A single mesh was generated, subdivided into multiple mesh planes. These planes delimit each subcomponent and baffle at all three directions ( $x$ ,  $y$  and  $z$ ). Instead of defining the number of cells in each direction, the size of each cell was specified and considered equal to 0.03875 m. This cell size was chosen considering the smallest mesh plane that defines the partition walls which measures 0.0775 m, and, therefore, the selected cell size was half of that measurement. A convergence test was not performed in this case, considering the limited geometry of this model. In fact, the cell size considered is already very small as will be confirmed in the convergence test done in the following procedure. This resulted in a total cell count of 662,096 cells. Figure 54 illustrates the mentioned mesh planes and the respective computational mesh. In addition to the mesh convergence, a time convergence of the solution is also required. This convergence in time was observed, demonstrated by the mass-averaged mean kinetic energy stability graphic (Figure 55) and the mass-averaged turbulent energy stability graphic (Figure 56).

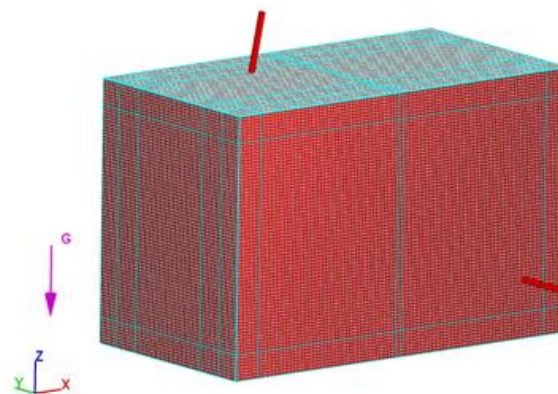


Figure 54 – Mesh definition of the region in study.

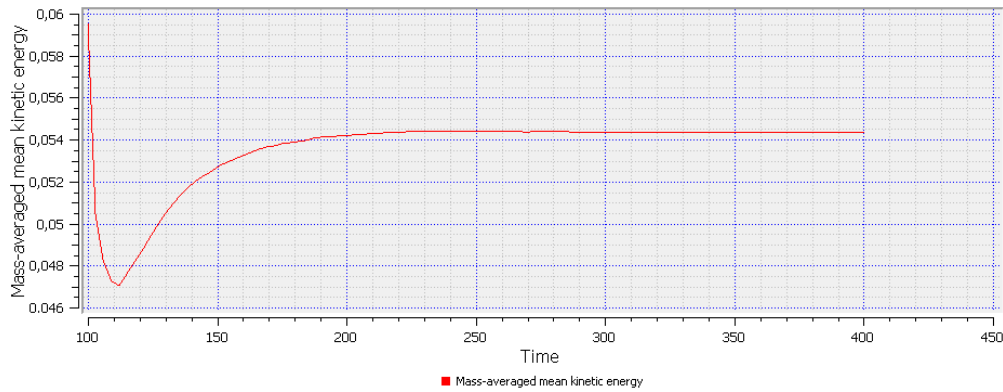


Figure 55 – Mass averaged mean kinetic energy of the solution.

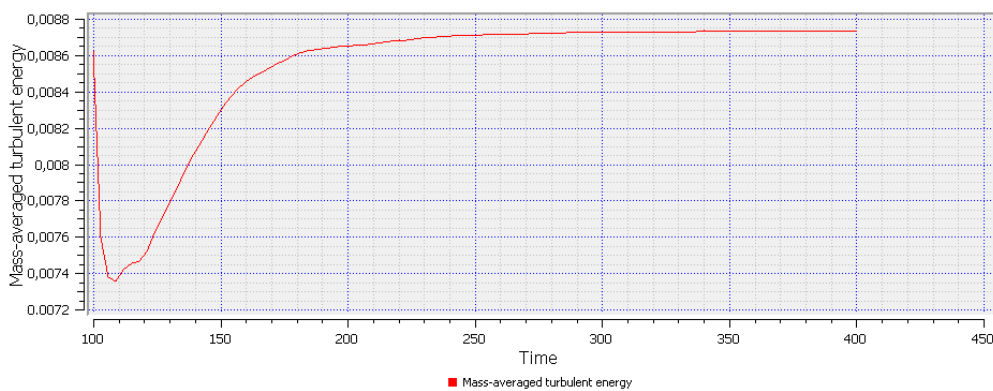


Figure 56 – Mass-averaged turbulent energy of the solution.

### Flow and fluid properties

The first property that characterizes the flow indicated in the simulation was its incompressibility. A parameter used to define a fluid’s compressibility is the Mach number. This parameter can be given by (Balachandran, 2006):

$$M = \frac{u}{c} \quad (67)$$

Where  $u$  is the flow velocity and  $c$  is the velocity of sound. For a Mach number below 0.3, the flow can be considered incompressible. This occurs when the flow velocity is very low, and therefore, density effects are negligible (Balachandran, 2006). In this particular case, the maximum air velocity value measured in the experimental procedure was used to determine the Mach number. The flow velocity that was considered was the maximum velocity obtained in the experimental procedure, which was 6.10 m/s (which is presented in Table B1 of Appendix B) and considering the velocity of sound 340 m/s, the ratio is equal to 0.0179, which is far below 0.3. It is then confirmed that, in this case, the incompressibility assumption is absolutely valid.

A turbulence model must also be specified. For this simulation, considering the higher accuracy mentioned in subsection 3.4.1, the renormalized group, or RNG k- $\epsilon$  model was used.

The gravity force component was defined as -9.8 m/s in the  $z$  direction and, finally, the fluid properties were assigned. For that, a default fluid from *FLOW-3D*<sup>®</sup>'s fluid database was used. In this case, the fluid is air at 15° C and presents the following properties:

- Density: 1.225 kg/m<sup>3</sup>.
- Viscosity: 1.781E<sup>-5</sup> kg.m<sup>-1</sup>.s<sup>-1</sup>.
- Specific heat: 718 m<sup>2</sup>.s<sup>-2</sup>.°C<sup>-1</sup>.
- Thermal conductivity: 0.02346 kg.m.s<sup>-3</sup>.°C<sup>-1</sup>.

#### Boundary conditions

Considering the 10 boundary conditions available in the *FLOW-3D*<sup>®</sup> software mentioned in subsection 3.6.4, only the symmetry and the specified pressure boundary conditions were needed to perform this specific simulation, as described below:

- Specified pressure. This condition was used in two specific boundaries, at the air inlet and outlet. At the outlet, which corresponds the minimum  $y$  plane (the air outlet is located at the door, where the blower is installed), a specified pressure of -80 Pa was inputted. At the inlet, to which corresponds the maximum  $z$  plane (the air inlet is located in the roof), a specified pressure of 0 Pa was inputted. These two pressures intend to simulate the pressure difference of -80 Pa that the blower introduces between the space in study and the environment around it. The negative pressure was defined at the outlet, in order for the air to flow from the inlet to the outlet.
- Symmetry. This condition considers a symmetry in the boundary where it is being set, in order to define the same conditions in the regions beyond that boundary. This results in a reduction of the computational effort. This way, the symmetry boundary condition can be applied in any surface where no specific condition is required (such as velocity or pressure). Therefore, this condition was set in all boundaries except at the inlet and outlet mentioned before.

Figure 57 illustrates the boundary conditions applied in each surface of the model, where the blue “P” at the top corresponds to the 0 Pa specified pressure, the green “P” in front

corresponds to the -80 Pa specified pressure and the “S” in every other surfaces corresponds to symmetry boundaries.

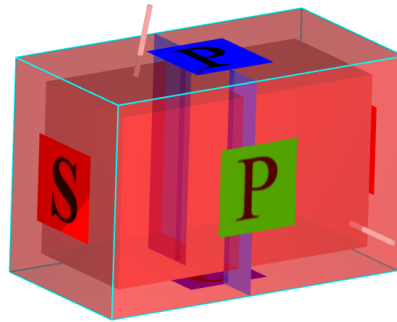


Figure 57 – Boundary conditions applied to the model.

#### 4.3.2 Numerical procedure 2 – mechanical ventilation system

To perform this simulation, the same 4 steps were conducted as in procedure 1. In this case, the geometry definition was more laborious considering that the whole building was modelled, including the ventilation ductwork. Considering the mesh definition, its refinement process was more complex since the physical model is widely bigger, requiring therefore a much higher number of cells. Another difficulty was related to the existence of ventilation grids which require a much smaller cell size, compared to the other elements of the building. Their definition requires a higher computational capacity leading to an elevated simulation time. For that reason, it was not possible to include the ventilation grids into the simulations. Considering their significance in the airflow velocity field, it is acknowledged that their absence will certainly influence the software’s validation. Therefore, the inclusion of these grids is still in progress and will be presented in future developments.

##### Geometry definition

To create the physical model of the house, the same method was used as in procedure 1. That is, using *FLOW-3D*<sup>®</sup>’s internal primitive geometries, the indoor divisions were done by creating solid subcomponents and then subtracting hole subcomponents to create the void spaces. The house is composed of two suspended ceilings with approximately 50 cm each, where the ventilation ductwork was installed. The spaces within the suspended ceilings were considered solid elements. Partition walls were, as before, approximated as baffles to avoid an even higher number of cells. Figure 58 illustrates the 3D model of the building in *FLOW-3D*<sup>®</sup>’s graphical interface.



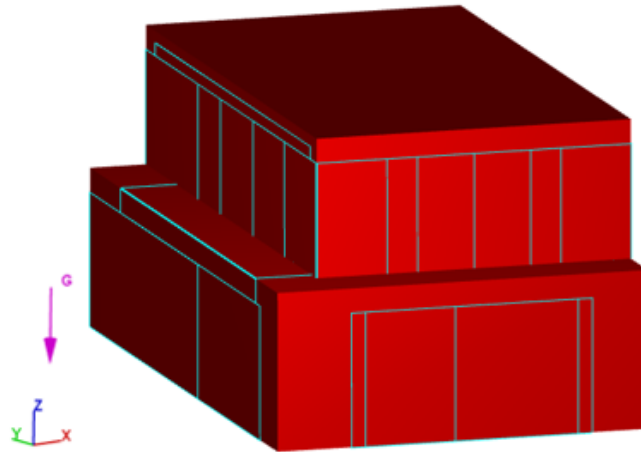
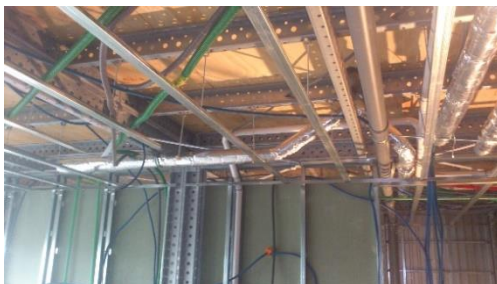


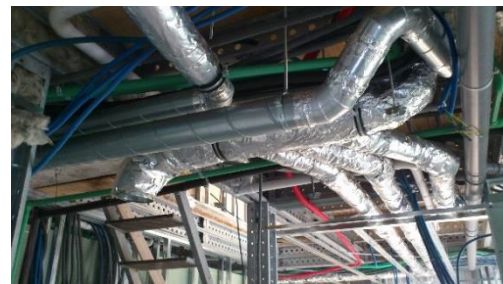
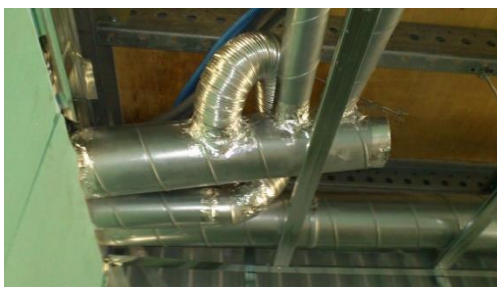
Figure 58 – 3D model of the studied house.

It is important to mention that the glazing was not considered in order to simplify the model. Although acknowledging its importance considering possible solar gains in those areas, in terms of thermal fluctuations it is not significant since the windows possess high levels of insulation due their low coefficients of thermal transmission. Besides that, the window blinds were closed, in order to further reduce solar gains.

The ventilation ductwork was done using Autodesk's AutoCAD software. It was done according to the ventilation project and pictures that were taken previously to the plasterboard being installed. Figure 59 shows some relevant pictures which served as basis to accurately draw the ventilation ductwork.



a) Deviation to avoid sanitation pipes

b) 1<sup>st</sup> floor air supply collector

c) Abnormal layout of the duct

d) 2<sup>nd</sup> floor air extraction collector

Figure 59 – Pictures of details which helped to accurately draw the ventilation ductwork.

For this simulation, only the supply and extraction related tubes were modelled. The sets of tubes responsible for admitting outdoor air and exhausting air out of the building weren't considered, since they are irrelevant to the simulation. The analysis that is intended only covers what happens inside the building, and, therefore, the admission and exhaustion will simply be simulated through boundary conditions. Figure 60 illustrates the entire ductwork that was created.

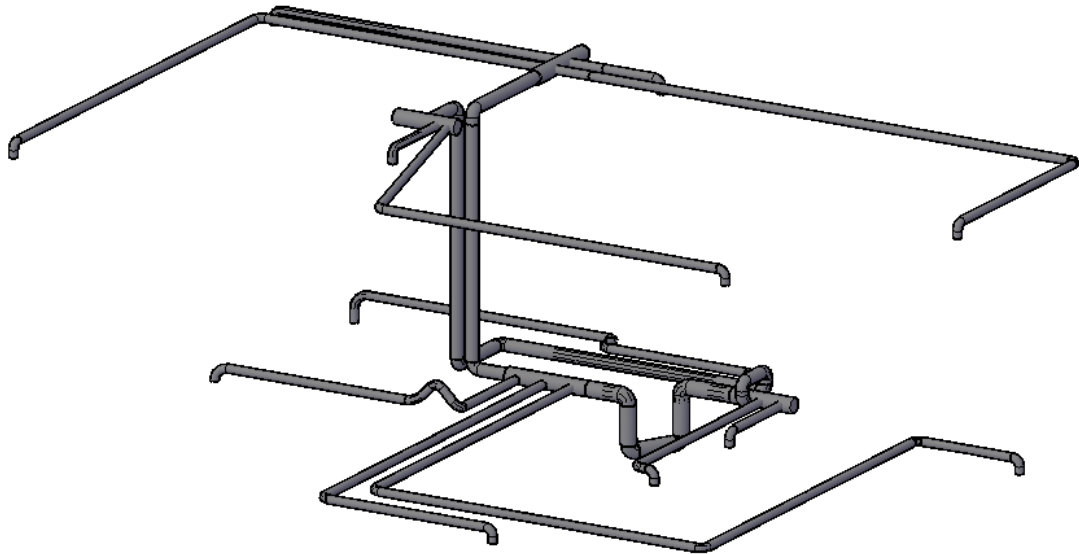


Figure 60 – Ventilation system ductwork modelled using AutoCAD software.

The entire system begins at the ventilation unit, where the two sets of ducts are connected, one for air supply and the other for air extraction (again, excluding the air admission and exhaustion). Just off the unit, both ducts possess a diameter of 160 mm and each connects to its respective air collector at that floor. From there, each duct splits into various ducts with a diameter of 80 mm in order to connect to the various divisions of the house (rooms, living room and hallway for supply and kitchen and bathrooms for extraction). Out of each collector, a duct with 125 mm connects to the first floor. There, each duct connects again to its respective upstairs air collector which then splits into 80 mm ducts for each division. As mentioned before, this entire layout is found above the ceiling of each floor. The system was exported as an STL file and imported into *FLOW-3D*<sup>®</sup> as a hole subcomponent, inside each 50 cm suspended ceiling (which were previously defined as solid subcomponents). Figure 61 illustrates the ductwork at the suspended ceilings in *FLOW-3D*<sup>®</sup>'s interface.

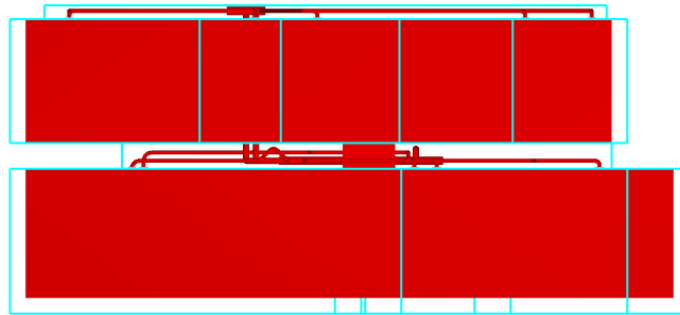


Figure 61 – Position of the ductwork within the suspended ceilings (direction y of the house).

By applying a transparency to the 3D model, a better visualization of its interior content can be obtained, as shown in Figure 62, where interior partition walls and the ventilation ductwork can be seen.

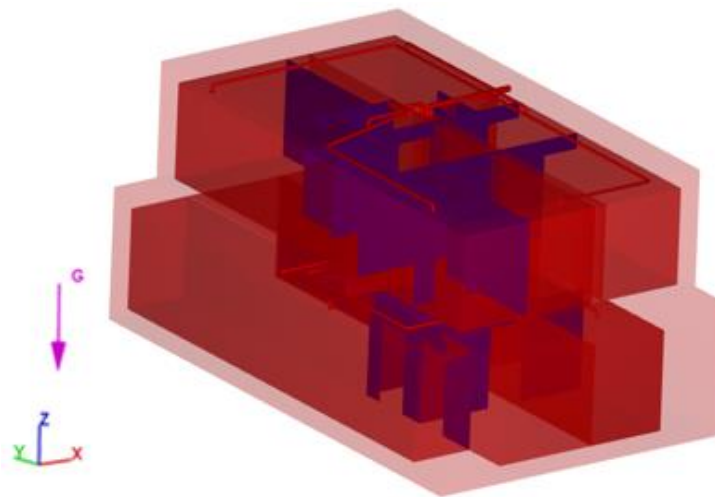


Figure 62 – Interior content of the studied house's 3D model.

### Mesh definition

In the definition of the mesh, 3 main elements were considered: the indoor compartments, the ventilation ductwork inside each suspended ceiling and the ventilation inlets and outlets, which are presented in an increasing order of refinement, due their increasing level of detail. A convergence test was performed in order to choose the best cell sizes without requiring too much simulation time and capacity. The process consisted in defining a relatively coarse mesh and performing the simulation. Once it stabilized, the velocity results in 3 different plans were extracted, describing the airflow behaviour in all three directions:  $x$ ,  $y$  and  $z$ . These plans are located in specific positions in order to capture the behaviour below and around the ventilation inlet in the living room. This process was repeated as the mesh was being refined until the velocity results of all points between two consecutive simulations,

presented a low relative difference. Once it was met, the results were considered to have converged and the mesh would be used in the final simulation. To achieve convergence, 5 simulations were needed. In each, the cell sizes of 3 multi-block meshes were varied: the grid inside the suspended ceiling to define the ventilation ductwork (mesh 1), the grid of the indoor space of each compartment of the house (mesh 2) and a small grid around the ventilation inlets and outlets (mesh 3), in order to attenuate the difference between the cell sizes of mesh 1 and 2 and also to allow more results to be extracted in those areas. Figure 63 illustrates these meshes. The relation in the cell size between mesh 1 and mesh 3 and between mesh 3 and mesh 2 was always kept below a 2 to 1 ratio, as recommended for adjacent multi-block meshes.

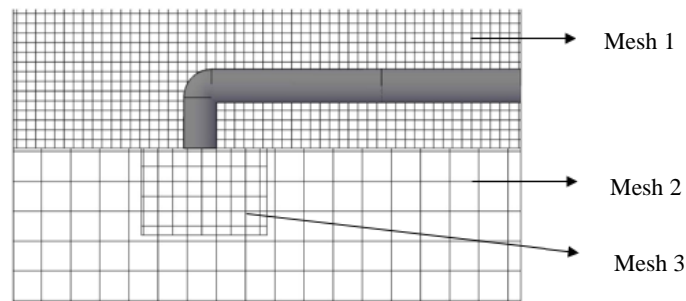


Figure 63 – Grids considered in the convergence test.

The cell sizes of each multi-block mesh for the 5 tests are presented in Table 13. Note that they all possess cubic cells, therefore, the size presented corresponds to the  $x$ ,  $y$  and  $z$  sizes.

Table 13 – Cell sizes of each multi-block mesh for the 5 tests.

	Test 1	Test 2	Test 3	Test 4	Test 5
Cell size mesh 1 (m)	0.050	0.040	0.035	0.030	0.030
Cell size mesh 2 (m)	0.200	0.140	0.120	0.120	0.090
Cell size mesh 3 (m)	0.100	0.070	0.060	0.060	0.045
Number of cells	844,935	1,666,267	2,360,691	3,458,934	3,870,716

The  $z$  plan was used as reference, considering that it presents the most evident convergence. Figure 64 presents the velocity results in the living room below the air inlet from the floor to the ceiling (considering that the inlets are installed in the ceiling). Note that, considering different meshes in each simulation test, the more refined meshes present a higher number of results since they have a higher number of cells.

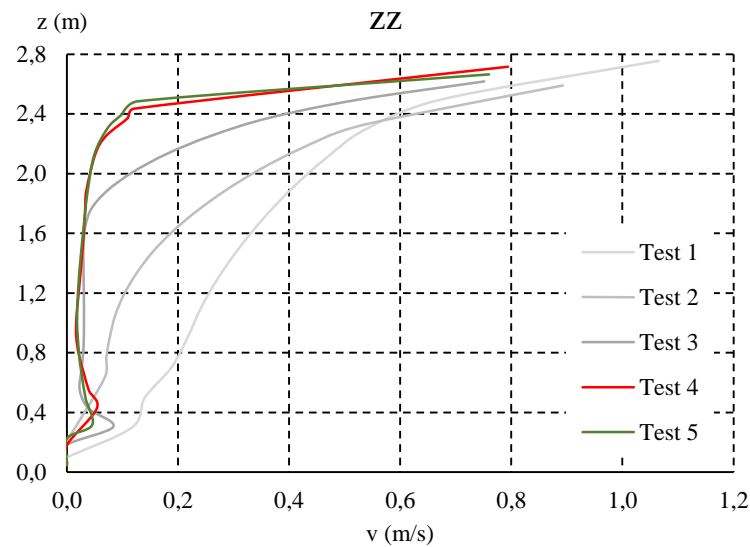
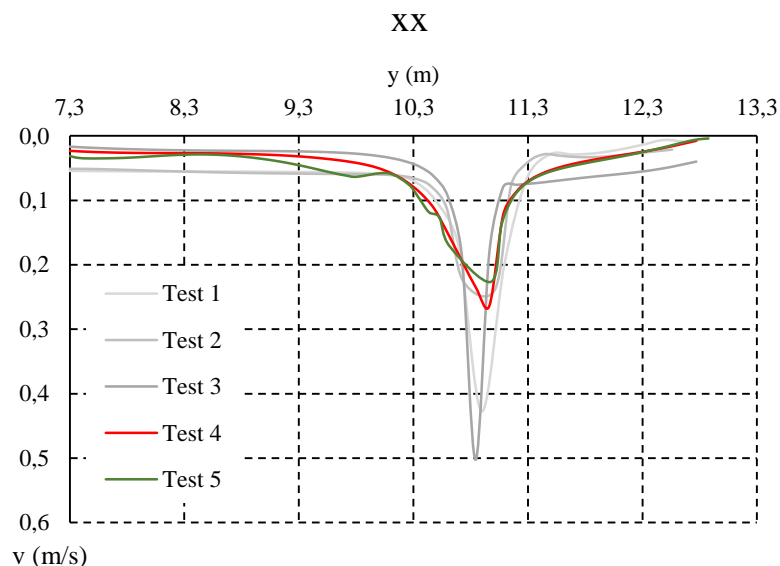
Figure 64 – Convergence process in the  $z$  plan.

Figure 64 indicates low velocity values near the floor, which slowly rise towards the inlet, with a more significant increase above 2 m in height (the inlet is at 2.8 m). Tests 4 and 5 were considered to have converged, therefore, the mesh that was used in the simulation was the one from test 5. The relative difference between both simulations varied from 0.5 to 15%, with a mean relative difference of 7%. Figure 65 and Figure 66 present the convergence tests in the  $x$  and  $y$  plans respectively. The mean relative difference in the  $x$  plan is 16%, while in the  $y$  plan it is 10%.

Figure 65 – Convergence test in the  $x$  plan.

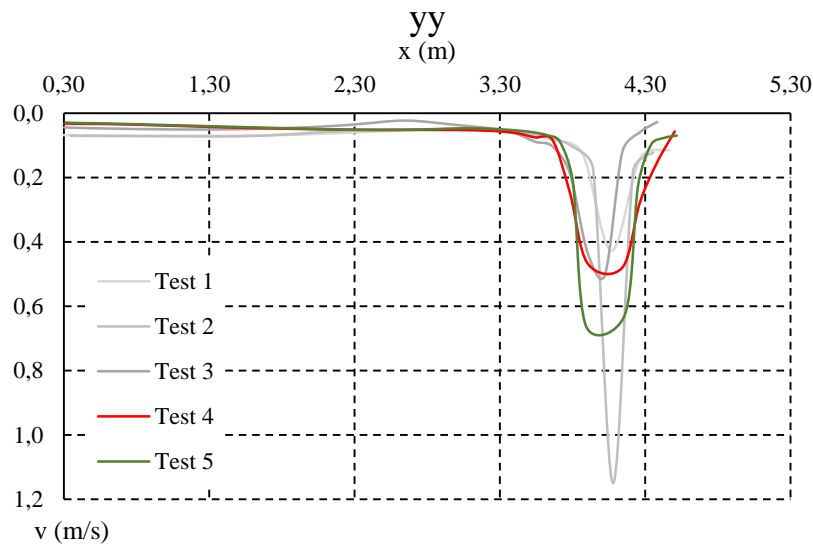


Figure 66 – Convergence test in the y plan.

These plans are located at a height of  $z = 2.75$  m. In these plans, the air velocity is barely null until approximating the air inlet, increases drastically (approximately at  $x = 4.0$  m and  $y = 10.8$  m), and decreases once again moving away from the inlet. In the y plan, the curves of tests 4 and 5 are very similar in form, only diverging in their maximum velocity value. In the x plan, the slightly elevated mean relative difference can be explained by the fact that many of the points present very low velocities (below 0.05 m/s in some cases), which culminate in high relative differences even for small amplitudes between both simulations. Figure 67 illustrates the numerical mesh that was used to extract the results.

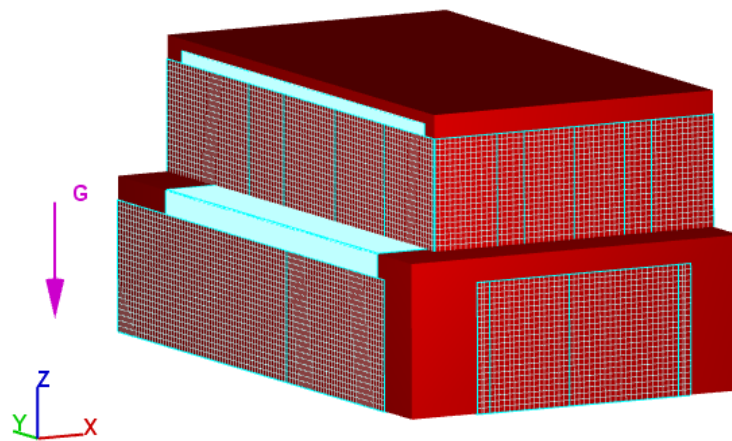


Figure 67 – Grid definition of the modelled house.

In terms of convergence in time of the solution, the model presented the mass-averaged mean kinetic energy and the mass-averaged turbulent energy stability graphics shown in Figure 68 and Figure 69 respectively.

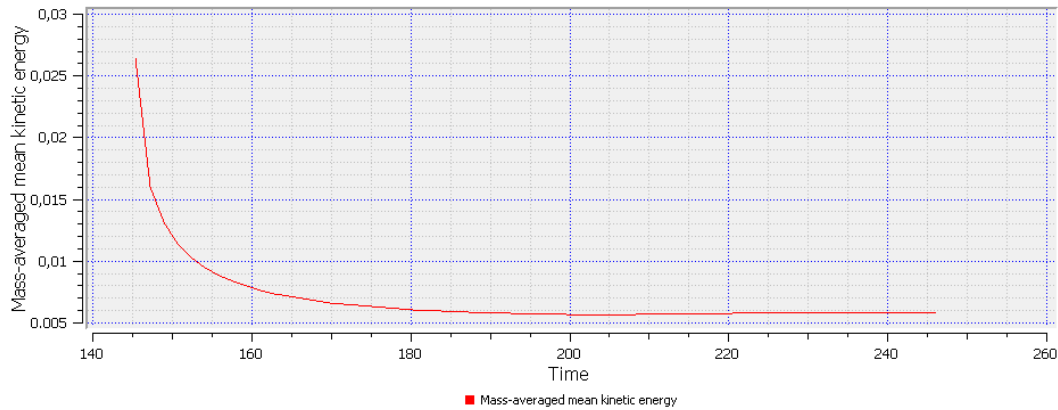


Figure 68 – Mass averaged mean kinetic energy of the solution.

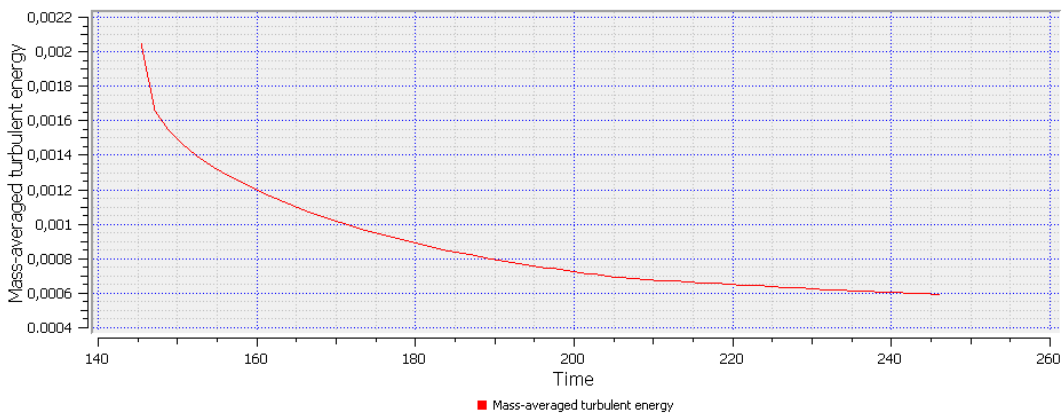


Figure 69 – Mass-averaged turbulent energy of the solution.

### Flow and fluid properties

In this section, both flow and fluid properties were defined as in the previous simulation. Considering that the expected air velocities are lower than the ones in the previous procedure, the incompressibility assumption is fully valid. The RNG k- $\epsilon$  turbulence model was also used in this simulation and the same fluid properties were assigned as in the previous simulation.

### Boundary conditions

For this simulation, the boundary conditions were specified as type wall, symmetry and specified velocity. This last boundary type was used to define the velocity at which air is blown out of the ventilation unit into the supply ductwork and to define the velocity that the

unit pushes air from the extraction ductwork. As mentioned before, both these velocities were set to be 3.4 m/s and these boundaries delimit the ventilation unit. The wall boundary condition was set at every outdoor wall and floors. Considering the symmetry boundary, which was already mentioned in the previous simulation, was used at all other boundaries, that is, all boundaries that delimit interior divisions and boundaries that are in contact with each other.



# Chapter 5

---

Results Analysis



## Chapter 5. Results Analysis

### 5.1 Procedure 1 – blower door

The analysis of this first procedure was done solely considering velocity results. Its purpose is to validate the use of *FLOW-3D*<sup>®</sup> for this type of simulations, by comparing the experimental and numerical data.

Considering the experimental part of this procedure, the inconstant flow caused by the blower affected the accuracy in the registrations. Instead of marking a constant velocity value at each point, the minimum and maximum velocities that the air reached were noted, then the amplitude between them and consequently their average value ( $v_{med}$ ) were calculated. The variation in the flow exists, however, considering the inconstant flow produced by the blower, the amplitude between the minimum and maximum values is not too excessive, never exceeding 0.5 m/s. The mean results are presented in Table 14. The full extent of the results, including the minimum values, maximum values and amplitudes are presented in Table B1 of Appendix B.

Table 14 – Average velocity values measured at each point.

Height	Point	$v_{med}$ (m/s)	Height	Point	$v_{med}$ (m/s)
1 (Z=2.35m)	1	5.85	4 (Z=1.94m)	15	0.41
	2	3.70		5 (Z=1.82m)	16
	3	0.55	17		1.60
	4	1.24	6 (Z=1.54m)	18	0.75
2 (Z=2.28m)	5	2.83		19	0.32
	6	2.98		20	1.38
	7	4.50	21	0.42	
	8	3.22	7 (Z=0.36m)	22	4.66
3 (Z=2.20m)	9	0.52			
	10	2.96			
	11	2.44			
	12	2.96			
	13	2.79			
	14	0.34			

As expected, the highest velocity value was registered right below the inlet, which is the first point, with an average velocity of 5.85 m/s. The velocity is inversely proportional to the area, therefore, inside the duct, the air flows at a very high velocity, which still remains high immediately outside the duct. With the decreasing height of the registrations, the velocity values also gradually decrease. These registrations also demonstrate the deviation towards

the upper wall caused by the duct's slope, since point 14 possesses a very low velocity. Point 14 would be expected to have a high value, since it should be right through the flow's path. However, points 16 and 17, for instance, present much higher values, since the deviation directs the flow towards the upper wall where those points are located. Finally, and as expected, the velocity at the outlet (point 22) presents the second highest value, registering an average 4.66 m/s, since it is the point where the air is being extracted, entering a cross section with a small area.

*FLOW-3D*<sup>®</sup> possesses a data visualization tool which allows to present the velocity results in different two-dimensional plans for the three directions using a colour bar scale. Various plots were extracted which help understand the airflow field caused by the blower. For each direction, 3 images of 3 different plans were chosen to visualize the flow. It is possible to see that higher velocities are obtained near the air inlet and gradually decrease towards the outlet. These plots also show the deviation in the flow towards the upper wall caused by the duct's slope. Figure 70 presents results in different  $z$  plans, Figure 71 in different  $y$  plans and Figure 72 in different  $x$  plans. The values in the  $z$  and  $x$  plans show better the flow's deviation towards the wall, while the  $y$  plan follows the flow towards the outlet. The  $z$  and  $y$  plans also show the partition walls which obstruct the airflow.

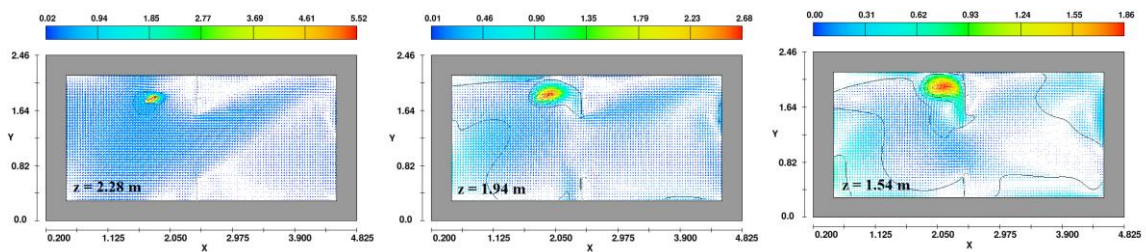


Figure 70 – Numerical velocity field (m/s) in the chosen  $z$  plans.

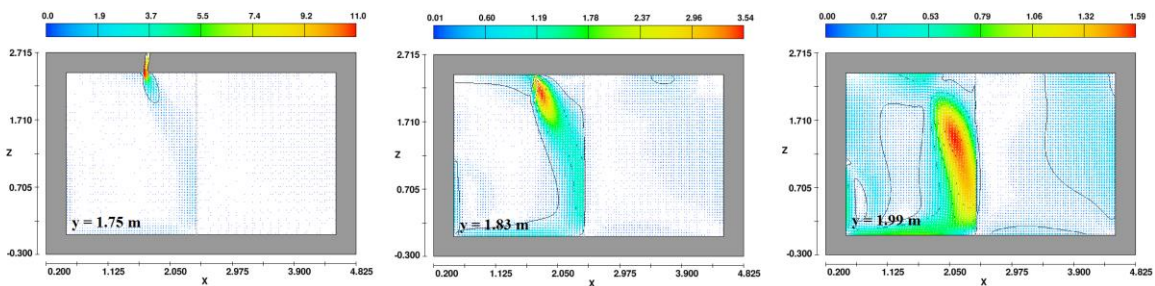


Figure 71 – Numerical velocity field (m/s) in the chosen  $y$  plans.

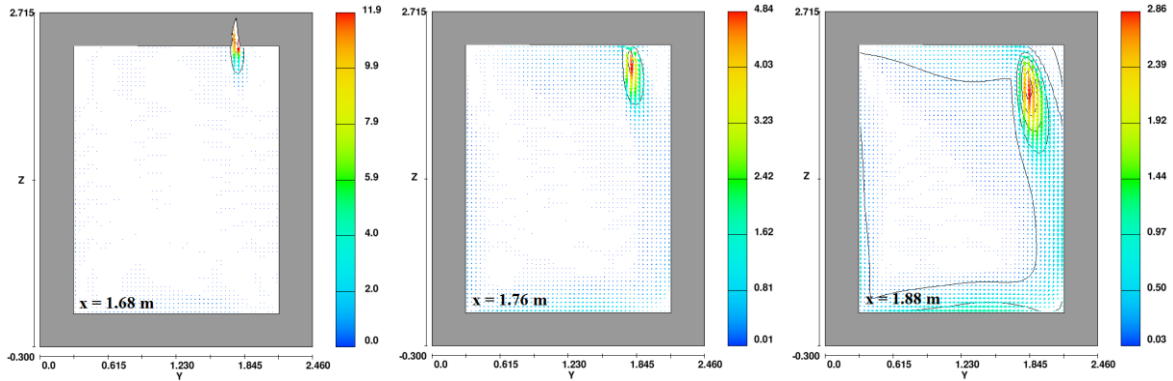
Figure 72 – Numerical velocity field (m/s) in the chosen  $x$  plans.

Figure 73 shows what happens at the outlet in the 3 directions, which is where the air is being extracted by the blower. It is possible to see that the air arrives at a low velocity, which dramatically increases when entering a significantly smaller cross-section.

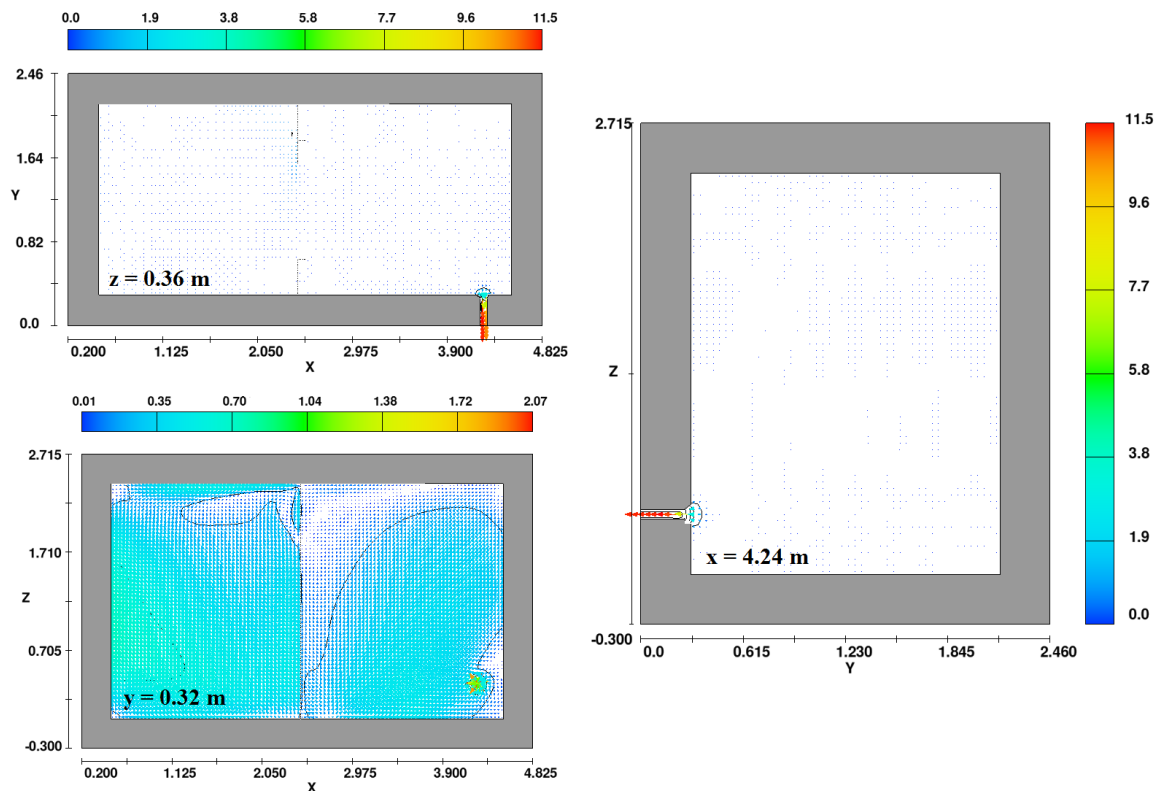


Figure 73 – Numerical velocity results (m/s) at the air outlet.

FLOW-3D<sup>®</sup> presents the velocity results in three components:  $u$ ,  $v$  and  $w$ , which correspond to the decomposition of the velocity vector in the  $x$ ,  $y$  and  $z$  directions respectively. In order to compare these velocities with the experimental results, the velocity's resultant force had to be calculated. This parameter was designated velocity magnitude. The resultant velocity

magnitude for each point (illustrated in Figure 45) and the amplitude and relative difference between the *FLOW-3D*<sup>®</sup> simulation results and the average experimental velocity values are presented in Table 15. Instead of comparing the numerical results with the average velocity values, but with its closest value between the minimum, maximum and average value, the error would be smaller, however, statistically, the average value is more correct.

Table 15 – Analysis between experimental and numerical data in procedure 1.

Point	Velocity magnitude	Average experimental velocity results	Amplitude	Relative difference	Point	Velocity magnitude	Average experimental velocity results	Amplitude	Relative difference
	(m/s)	(m/s)	(m/s)	(%)		(m/s)	(m/s)	(m/s)	(%)
1	5.92	5.85	0.07	1	12	2.98	2.96	0.02	1
2	3.42	3.70	0.28	8	13	3.03	2.79	0.24	9
3	1.00	0.56	0.44	78	14	0.46	0.34	0.12	34
4	1.36	1.24	0.12	10	15	0.43	0.40	0.04	10
5	2.90	2.83	0.07	2	16	0.45	1.69	1.24	73
6	3.28	2.98	0.30	10	17	1.30	1.60	0.30	19
7	3.89	4.50	0.60	13	18	0.48	0.75	0.27	35
8	3.18	3.22	0.04	1	19	0.36	0.32	0.04	13
9	0.53	0.52	0.01	2	20	0.77	1.38	0.61	44
10	3.03	2.96	0.07	2	21	0.72	0.45	0.27	60
11	2.53	2.44	0.09	4	22	3.54	4.66	1.12	24

Compared to the experimental results obtained using the digital anemometer, the results of the simulation are in fact fairly similar. In terms of amplitude, the difference between both results is, in almost every case, low. Out of 22 points measured, only points 3, 7, 16, 20 and 22 exceed an amplitude of 0.30 m/s. Almost half of the measured values present an amplitude below 0.10 m/s. Only for points 16 and 22 the amplitudes exceed 1.00 m/s. Analyzing relative differences, only points 3, 14, 16, 18, 20 and 21 exceed 25%, while 14 out of 22 points (64% of the results) present a relative difference below 15%. The high error associated to points 16 and 20 may be related to their proximity to the bathroom's upper wall. By not considering the 3 points with higher relative differences (points 3, 16 and 21), admitting that they are result of numerical errors, the average relative difference of all other measured points is 13%, which is an acceptable error.

The results were also analyzed graphically, presenting the variation in the experimental results (minimum, maximum and average velocity values) and values obtained through the numerical simulation, as shown in Figure 74.

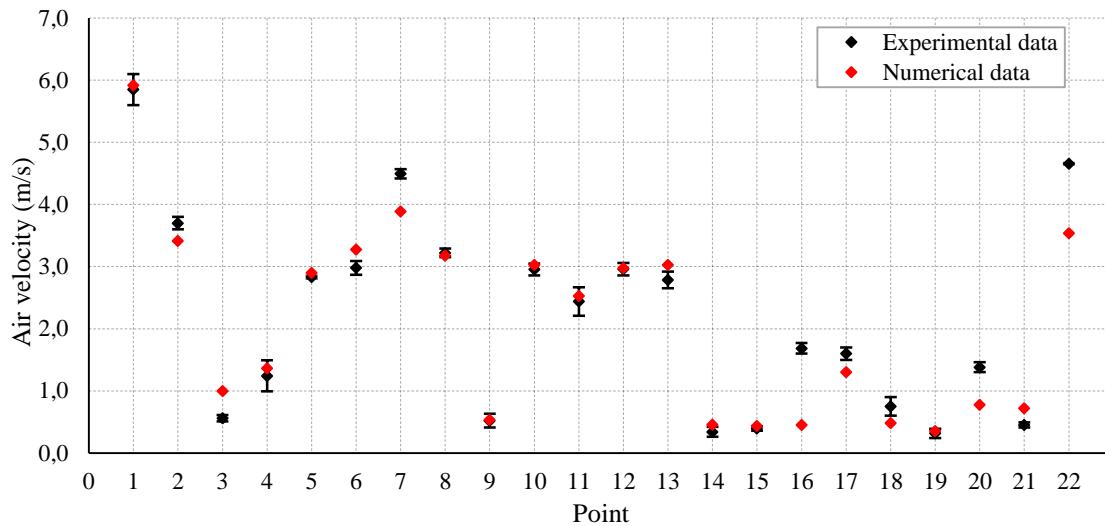


Figure 74 – Graphical analysis of the velocity results obtained experimentally by the blower door test and through numerical simulation.

Although it is safe to say that the results are quite acceptable, there is no absence of error, as was expected. The error in the results can be explained through numerous factors. Firstly, it is a fact that experimental equipment and numerical models can never be 100% accurate. However, after properly acknowledging these errors, other factors might be much more influential in the results, both during the experimental and numerical procedures. During the experimental data collection, errors can be caused by the user who handled the anemometer. Despite the extreme care presented during the experiments, the position where the anemometer was placed could distance a few millimeters or even centimeters from the exact position of its corresponding cell inside the numerical mesh. The blower door itself may also be a cause of discrepancies. Not only was it incapable of creating a constant airflow, as was mentioned earlier, but even the established pressure difference of -80 Pa can vary slightly from the pressure that was actually caused by the blower. Considering the numerical simulation procedure, there may be small differences between the physical 3D model done in the software's geometry creator and the actual geometry of the studied space, especially considering that an approximation was made in order to simulate the duct's slope at the inlet.

## 5.2 Procedure 2 – mechanical ventilation system

This procedure is similar to the previous, where velocities obtained from the *FLOW-3D*<sup>®</sup> simulation are compared with experimental data. Note that, considering the absence of results with the ventilation grids, only results without the grids will be presented. It is expected, for that reason, natural discrepancies in the numerical results.

As mentioned in the description of the experimental procedure, the digital anemometer was placed under each ventilation grid of each compartment and velocity values were registered. In living compartments (supply), where the velocities are higher, 9 points were registered, while in service compartments (extraction), only 5 were noted, as depicted in Figure 50. Table 16, Table 17 and Table 18 present the experimental results.

Table 16 – Experimental velocity results for the living room and rooms 1, 2 and 3.

Living room (S)			Room 1 (S)			Room 2 (S)			Room 3 (S)		
Point	z (m)	v (m/s)	Point	z (m)	v (m/s)	Point	z (m)	v (m/s)	Point	z (m)	v (m/s)
1	2.795	1.4	1	2.795	0.0	1	5.695	0.9	1	5.695	1.1
2	2.795	0.8	2	2.795	1.1	2	5.695	1.1	2	5.695	1.0
3	2.795	0.9	3	2.795	1.4	3	5.695	0.0	3	5.695	0.0
4	2.795	1.6	4	2.795	1.1	4	5.695	1.1	4	5.695	1.1
5	2.760	1.7	5	2.760	2.0	5	5.660	1.4	5	5.660	1.1
6	2.700	1.3	6	2.700	1.2	6	5.650	1.3	6	5.600	0.8
7	2.650	1.1	7	2.650	1.2	7	5.600	1.2	7	5.550	0.7
8	2.550	0.6	8	2.550	1.0	8	5.550	0.8	8	5.500	0.5
9	2.450	0.5	9	2.450	0.4	9	5.500	0.0	9	5.450	0.0

Table 17 – Experimental velocity results for room 4, the upstairs hallway and kitchen.

Room 4 (S)			Hallway 1 (S)			Hallway 2 (S)			Kitchen (E)		
Point	z (m)	v (m/s)	Point	z (m)	v (m/s)	Point	z (m)	v (m/s)	Point	z (m)	v (m/s)
1	5.695	0.8	1	2.795	1.1	1	5.695	1.0	1	2.795	0.7
2	5.695	0.7	2	2.795	0.8	2	5.695	1.0	2	2.795	0.6
3	5.695	0.0	3	2.795	0.0	3	5.695	0.0	3	2.795	0.0
4	5.695	1.0	4	2.795	1.3	4	5.695	1.1	4	2.795	0.0
5	5.660	1.3	5	2.760	1.6	5	5.650	1.2	5	2.760	1.2
6	5.650	1.2	6	2.700	1.2	6	5.600	1.0			
7	5.600	1.2	7	2.650	0.8	7	5.550	0.9			
8	5.550	1.1	8	2.550	0.6	8	5.500	0.8			
9	5.450	0.9	9	2.450	0.0	9	5.450	0.6			



Table 18 – Experimental velocity results for the 4 sanitary facilities.

Sanitary facility 1 (E)			Sanitary facility 2 (E)			Sanitary facility 3 (E)			Sanitary facility 4 (E)		
Point	z (m)	v (m/s)	Point	z (m)	v (m/s)	Point	z (m)	v (m/s)	Point	z (m)	v (m/s)
1	2.795	0.0	1	2.795	0.6	1	5.695	0.0	1	5.695	0.0
2	2.795	0.0	2	2.795	0.0	2	5.695	0.0	2	5.695	0.0
3	2.795	0.0	3	2.795	0.0	3	5.695	0.0	3	5.695	0.0
4	2.795	0.0	4	2.795	0.8	4	5.695	0.0	4	5.695	0.0
5	2.760	1.3	5	2.760	1.3	5	5.660	0.7	5	5.660	0.9

These results indicate, firstly, that the air velocities supplied by the mechanical ventilation system are significantly lower than those caused by the blower door at a pressure difference of -80 Pa. Not only is the velocity at which the air exits the ventilation unit (3.4 m/s) already lower than the highest value caused by the bower (5.85 m/s), the results indicate that the air velocity can decrease up to 67% by traveling through the ventilation ductwork and crossing the ventilation grid, since the lowest value of point 5 (which is immediately below the grid) in supply compartments is 1.1 m/s in room 3.

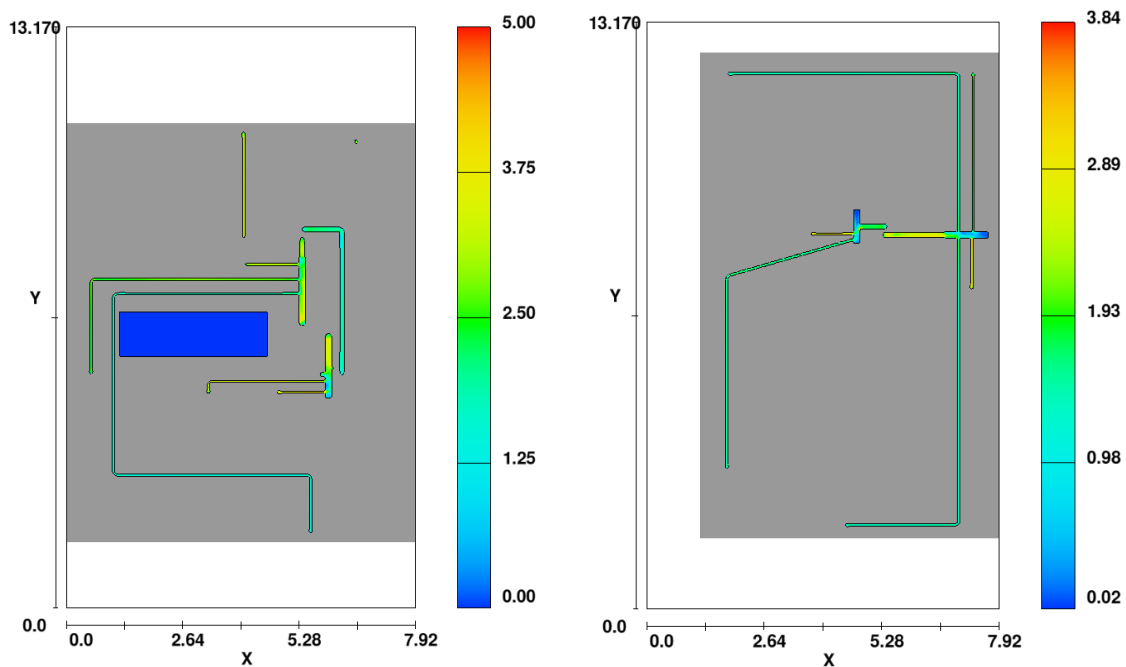
As expected, points 5 to 9 at the centre of each supply grid present a decreasing velocity value as the registrations move away from the grid.

Note that, except for the living room and room 1, point 3 of all grids present a velocity of 0 m/s. This is explained by the fact that this point was located immediately in front of one of the grid's fixators which blocked the airflow, as shown in Figure 50 of the experimental procedure description. Figure 75 shows that fixator. In the living room, point 3 was measured slightly aside from the fixator, therefore the velocity is not null, while in room 1, the fixator is located at point 1 (the exact position of each point was duly registered, in order to accurately compare the experimental and numerical results, since these fixators were also introduced in the modelling of the grids).



Figure 75 – Grid's fixator that blocks the airflow at point 3.

The velocities registered in service compartments (extraction grids) are significantly lower than those from living compartments (supply grids), since, in this last case, registrations are done downstream of the flow, which means that air is coming from a small cross-section tube (velocities are even higher inside the ductwork), while in extraction grids, registrations are done upstream of the flow, meaning that air comes from a large space (where velocities are lower) into the small cross-section tube. The fact that most values around the grids in the sanitary facilities are null, is related to the lack of sensitivity of the used digital anemometer. Using *FLOW-3D*<sup>®</sup>'s data visualization tool, two-dimensional plans of the model were extracted to demonstrate visual velocity results and better understand the airflow behaviour inside the ventilation ductwork, near the grids and throughout the building's compartments. Figure 76 shows the airflow across the ventilation ductwork in the 1<sup>st</sup> and 2<sup>nd</sup> floors.



a) 1<sup>st</sup> floor suspended ceiling.

b) 2<sup>nd</sup> floor suspended ceiling.

Figure 76 – Velocity results (m/s) inside the ventilation ductwork.

Although no registrations were done inside the suspended ceilings (where the ductwork is installed), it is still relevant to visualize these areas to make sure that they are properly represented and that no interruptions in the airflow path to each compartment are observed. In the 1<sup>st</sup> floor it seems to exist an interruption (at  $x = 4.02$  m plan), however, that is related to the ductwork design, more specifically, due to a deviation to avoid sanitation pipes above the living room, as demonstrated in Figure 59a). This area is presented in detail in Figure 77,

showing how the flow passes through it. Inside the ductwork, velocities vary from approximately 1 to 3.5 m/s.

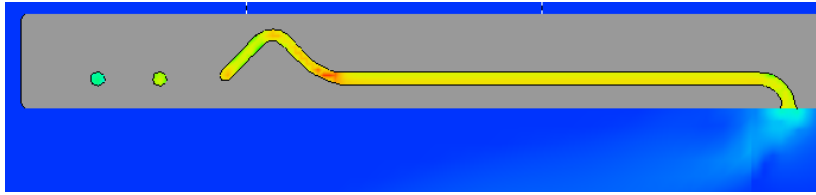
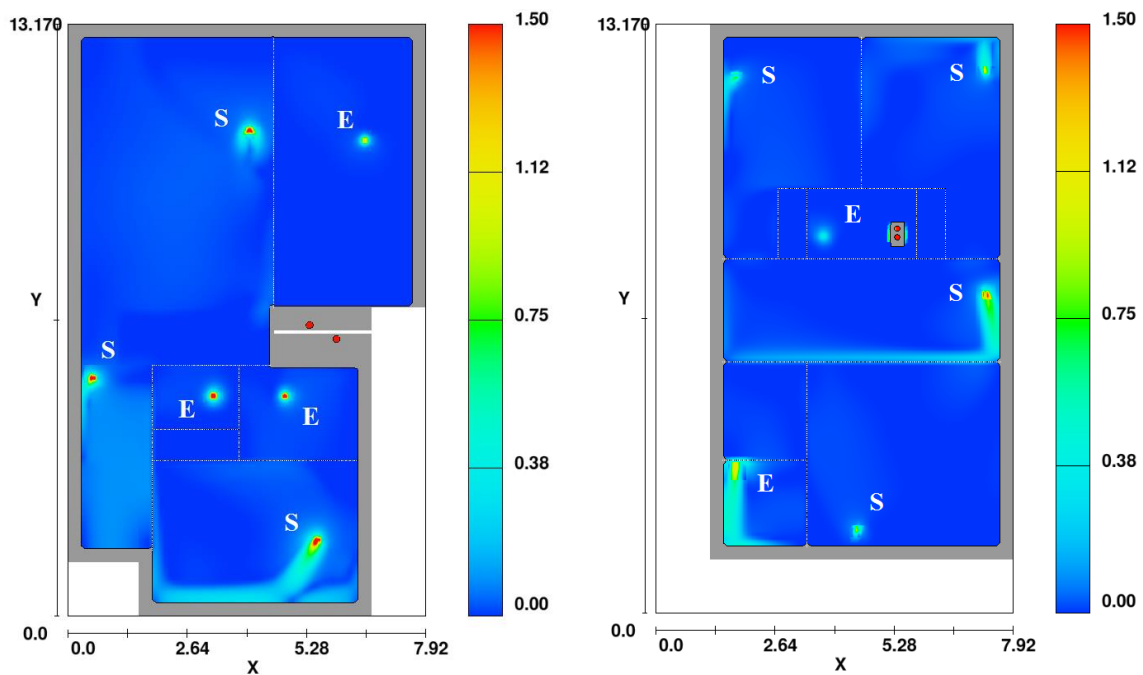


Figure 77 – Sectional detail of the ventilation duct at  $x = 4.02$  m.

Higher velocities than the 3.4 m/s that exit the ventilation unit occur during the ductwork, considering the constant cross-section variations of the tubes. In the 2<sup>nd</sup> floor, it is also possible to see how low air runs inside the air collectors, considering their bigger cross-sections. Immediately below the ventilation openings, the air supply (S) and extraction (E) can be visualized in a  $z$  plan as shown in Figure 78.



a) 1<sup>st</sup> floor at  $z = 2.79$  m.

b) 2<sup>nd</sup> floor at  $z = 5.60$  m.

Figure 78 – Air velocities (m/s) at supply and extraction points in different  $z$  plans.

These images show that air velocities are higher in supply grids than in extract grids, as explained in the analysis of the experimental results. In these areas, air velocities can vary approximately from 0.5 to 1.5 m/s.

Velocity vectors can be introduced in order to visualize the direction of the airflow. In supply grids, air flows into the compartment, while in extraction grids, air flows out of them, as shown in Figure 79.

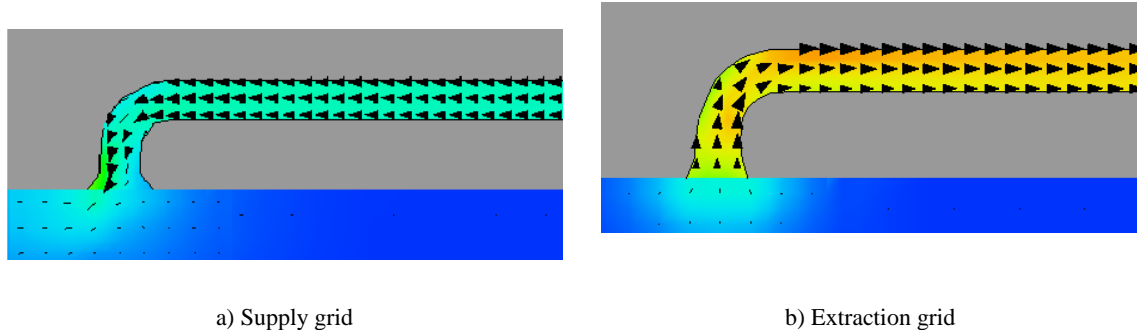


Figure 79 – Airflow directions in supply and extraction grids.

Finally, Figure 80a) presents a more general image of the model at plan  $y = 1.89$  m, where it is possible to see the air supply in room 2 and airflows in other compartments captured in that sectional plan. Note that, to better visualize the flow inside the compartments, the colour scale was altered, by limiting it to 1.5 m/s. This was done considering the velocity difference between the air inside the ductwork, which is significantly higher (around 3 m/s), and inside the compartment (varying from 0.03 m/s to 1.5 m/s). Figure 80b) contains a sectional plan at  $y = 8.43$  m, that shows the air extraction in sanitary facility 4 and the airflow through the ductwork travelling from the 1<sup>st</sup> to the 2<sup>nd</sup> floor.

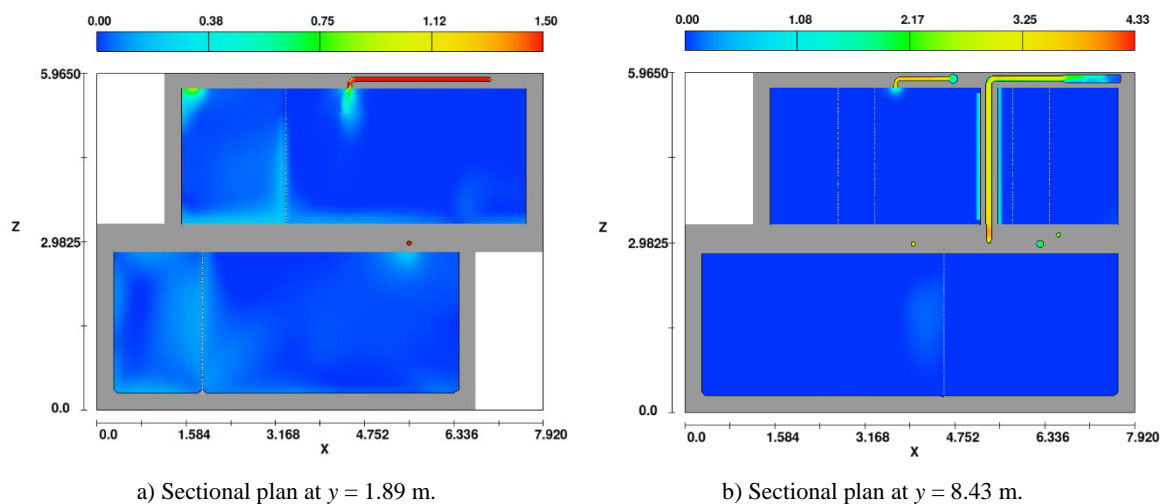
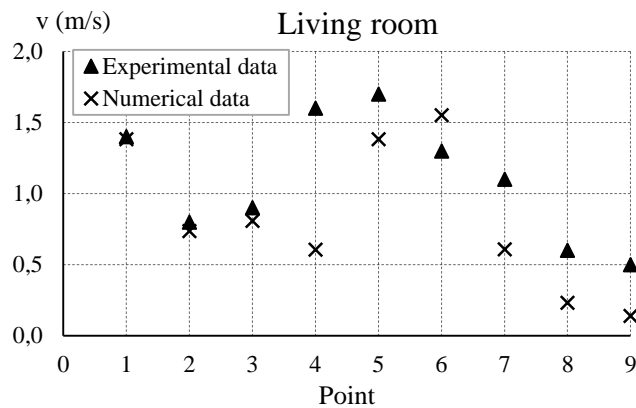


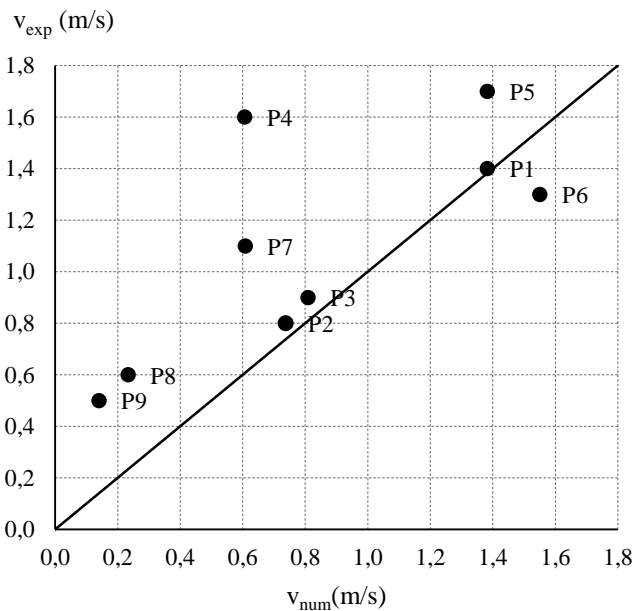
Figure 80 – Sectional plans to illustrate the airflow velocities (m/s) in different areas of the model.

In this simulation, considering the elevated number of points measured, the numerical results will be directly presented graphically for each division (according to Figure 36 and Figure 37), where a comparison between them and the experimental data is done. Figure 81

demonstrates the results in the living room. In this case, two approaches were done: a more intuitive comparison between the experimental and numerical velocity values in Figure 81a) and another approach that better demonstrates the error between the results in Figure 81b). The second approach was only presented for the living room, while the graphics for other living compartments are presented in Figure C1 to Figure C6 of Appendix C. The numerical results in comparison with the experimental data following the first approach for the rest of the living compartments are presented in Figure 82 to Figure 87.



a) Experimental and numerical velocities for each point.



b) Experimental vs numerical velocities for each point.

Figure 81 – Graphical analysis of velocity results in the living room.

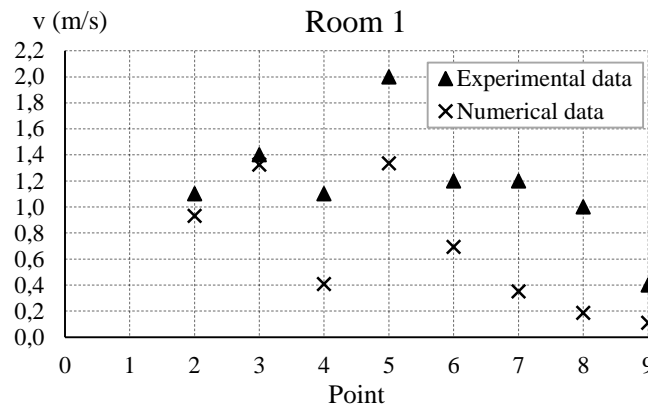


Figure 82 – Graphical analysis of velocity results in room 1.

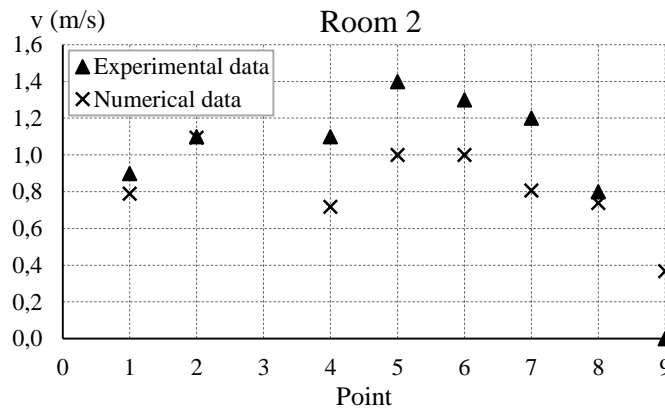


Figure 83 – Graphical analysis of velocity results in room 2.

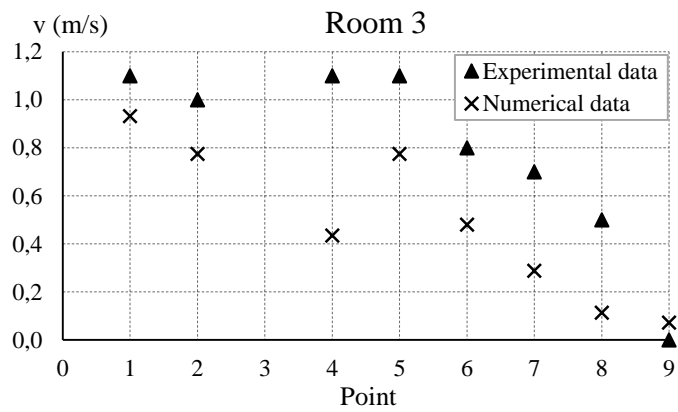


Figure 84 – Graphical analysis of velocity results in room 3.

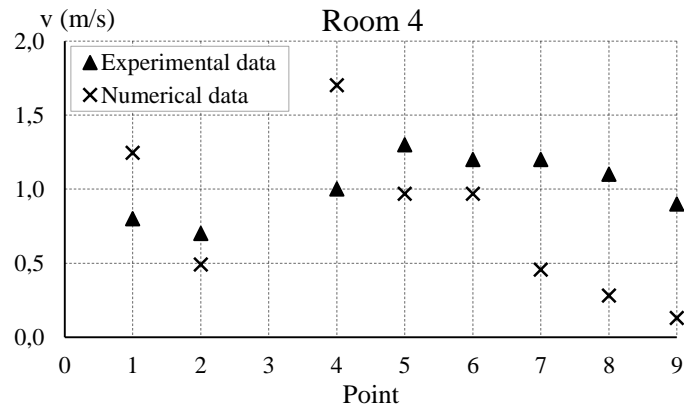


Figure 85 – Graphical analysis of velocity results in room 4.

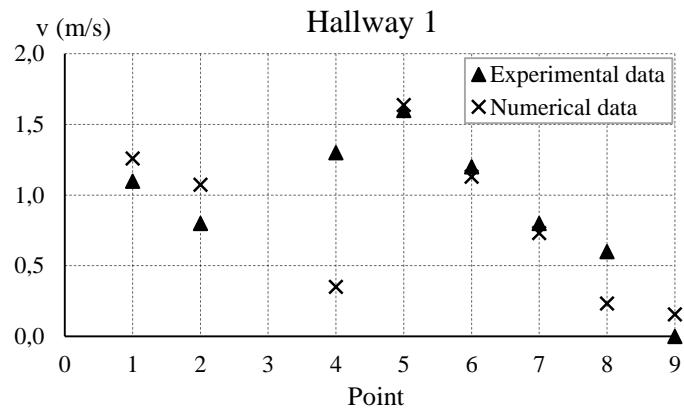


Figure 86 – Graphical analysis of velocity results in hallway 1.

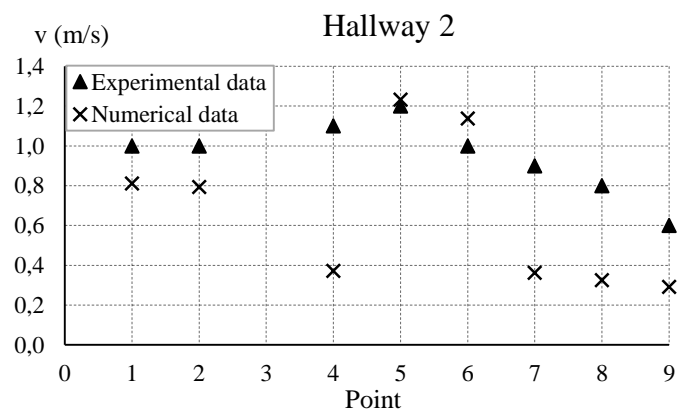


Figure 87 – Graphical analysis of velocity results in hallway 2.

Considering what was mentioned earlier regarding point 3 and the grid's fixator, since the grids were not used in this simulation, the numerical results would never match the experimental data. In this last case, the velocity is always null because the fixator blocks the airflow. For that reason, the numerical results in point 3 were not considered and assumed

null as well, except for the living room where no point is located in front of the fixator and in room 1 where the fixator is located in front of point 1, which was, therefore, also assumed null. Regarding the results obtained in living compartments, despite some discrepancies in the exact value obtained numerically, it is evident that they present the same order of magnitude (except in a few isolated cases) and a very similar behaviour.

Figure 88 to Figure 92 graphically present the numerical results in comparison with the experimental data for service compartments. In this case, only the first approach to the representation of the results was used, since the other approach would not make sense considering that only one point can truly be analysed.

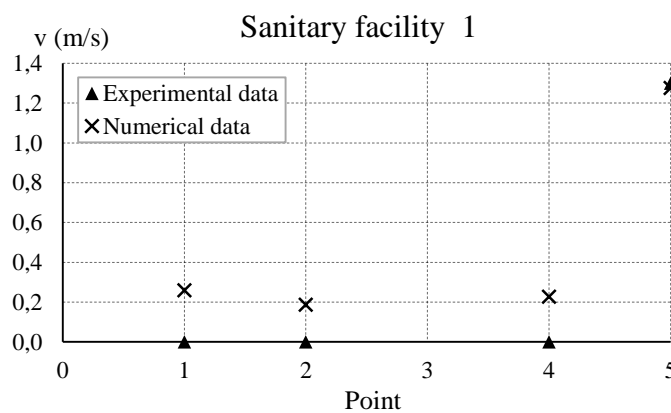


Figure 88 – Graphical analysis of velocity results in sanitary facility 1.

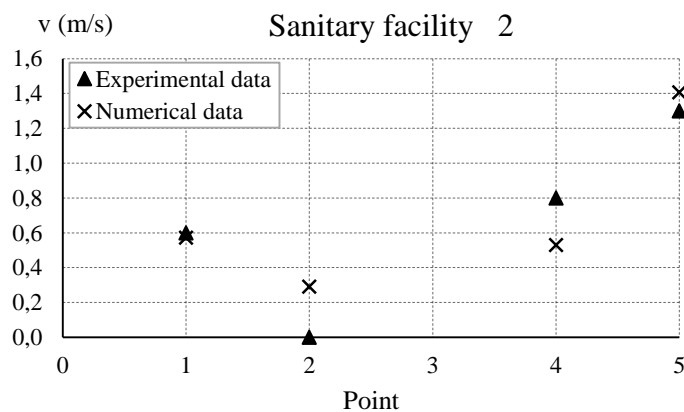


Figure 89 – Graphical analysis of velocity results in sanitary facility 2.



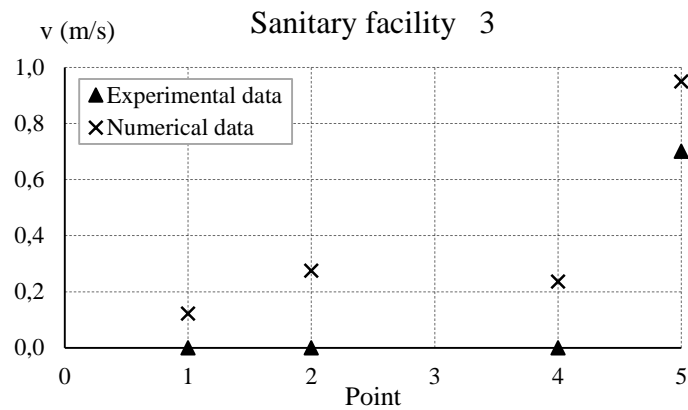


Figure 90 – Graphical analysis of velocity results in sanitary facility 3.

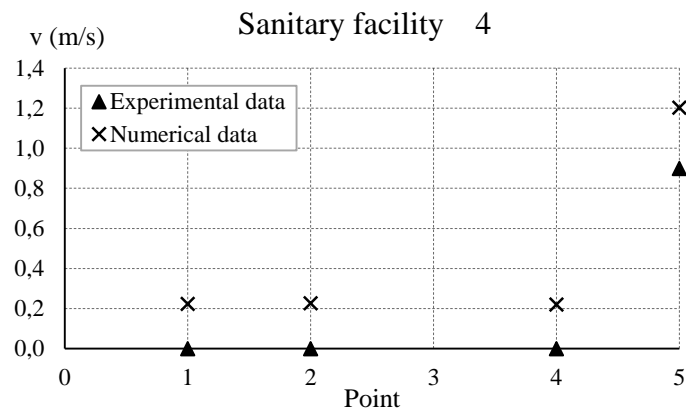


Figure 91 – Graphical analysis of velocity results in sanitary facility 4.

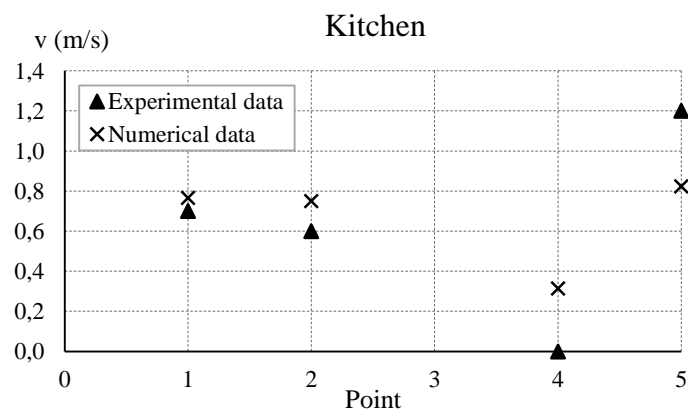


Figure 92 – Graphical analysis of velocity results in the kitchen.

The analysis of service compartments is necessarily different considering the low velocity values registered. Note that, in the sanitary facilities, the difference in the results is directly connected to the lack of sensitivity of the anemometer that was used. The experimental data resulted in 0 m/s registrations around the grid (points 1 to 4), while the simulation resulted

in low values. Points 5 however, which are exactly at the center of each grid, obtained closer results. Once again, the results between experimental and numerical data present the same order of magnitude and a similar behaviour.

After graphically analysing the results, a more objective analysis was performed by presenting the amplitudes and relative differences between experimental and numerical data. The variation range (minimum and maximum) and average value of each parameter are presented in Table 19. The experimental values of 0 m/s that resulted from the anemometer's lack of sensitivity were not considered, since these values cannot be compared with numerical results. The sensitivity range of the anemometer (as proven during the experimental process and not from the equipment information) was only above 0.4 m/s, therefore, considering that the numerical results point to values below 0.3 m/s in sanitary facilities, it is understandable. For that reason, since only point 5 of sanitary facilities 1, 3 and 4 presented a value above 0 m/s, in these cases, only that result is presented, instead of a variation of results.

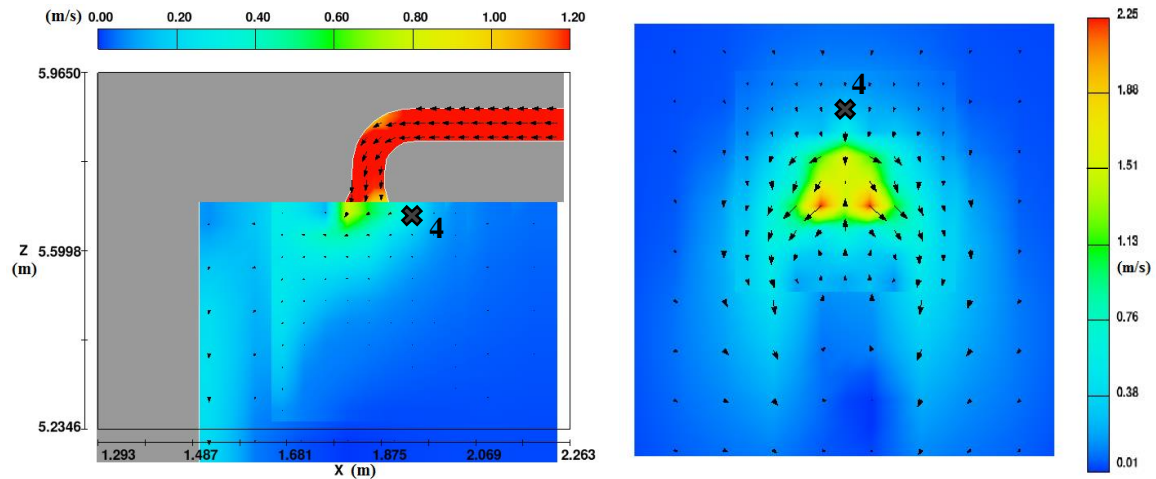
Table 19 – Analysis between experimental and numerical results in procedure 2.

Compartment		Amplitude variation range (m/s)	Average amplitude (m/s)	Relative difference variation range (%)	Average relative difference (%)
Living compartments	Living room	0.02 - 0.99	0.33	1 - 72	33
	Room 1	0.08 - 0.85	0.51	5 - 81	48
	Room 2	0.01 - 0.40	0.24	1 - 35	20
	Room 3	0.07 - 0.66	0.36	15 - 77	43
	Room 4	0.21 - 0.82	0.53	19 - 86	53
	Hallway 1	0.04 - 0.95	0.28	2 - 73	29
	Hallway 2	0.03 - 0.73	0.33	3 - 66	37
Service compartments	Kitchen	0.07 - 0.38	0.20	9 - 31	22
	Sanitary Facility 1	0.02	0.02	2	2
	Sanitary Facility 2	0.03 - 0.27	0.14	5 - 34	16
	Sanitary Facility 3	0.25	0.25	36	36
	Sanitary Facility 4	0.30	0.30	34	34

Although presenting points with an elevated level of accuracy, where approximately 30% of the results present a relative difference below 15%, there is still an elevated amount of simulation values that significantly differ from experimental data. The most extreme cases occur in rooms 1, 3 and 4 where the average relative differences exceed 40%. These elevated percentages can, however, be explained by the fact that this study deals with low values

(below 1 m/s) causing the slightest variation to immediately present an elevated percentage of error, as was mentioned in procedure 1. The proof of this explanation lies in the amplitudes obtained, where the average amplitude between numerical and experimental values never exceeded 0.55 m/s and where over 50% of the results presented an amplitude below 0.30 m/s, which, at a human scale of sensitivity, is not noticeable.

Of course, and as mentioned before, the simplification of the model in study by not introducing the ventilation grids has an evident influence on the results, since the model deviates from reality. To obtain the most accurate results, the model must be as close to the actual building as possible, which, due to numerous limitations, was not possible. A recurring fact in the numerical velocity results in living compartments is that they are, in the great majority of cases, lower than the experimental data, which is clearly seen in the graphical analysis of the results that was presented by both graphical approaches. In fact, in the second approach (mainly present in Appendix C), it is even more evident. The absence of the grids can, in fact, explain this event, since in supply grids the registrations are done downstream of the flow, therefore, by crossing the grid's small cross-section, the air velocities increase. Since the model does not include the ventilation grids, this increment on the flow velocity does not occur, meaning that lower velocities resultant from the simulation are justifiable. Another discrepancy related to the absence of the ventilation grids is found in points 4 of almost all living compartments. By analyzing the graphics of Figure 81 to Figure 87, it is clear that the discrepancies between experimental and numerical data in points 4 are substantially higher than in other points. This happens because air tends to enter in each room with a certain direction, influenced by the direction of the ductwork at the entrance of the room. What happens is that the ventilation grid forces a more distributed air ventilation, which is why the experimental velocities in points 1 to 5 are very similar. Without the grid, air is not properly distributed when entering a room, maintaining the direction of the ductwork. In most of the cases, point 4 is actually away from that direction, which makes the numerical velocities in points 4 far lower than the experimental values. Figure 93 illustrates this phenomenon, showing how point 4 is located away from the airflow due to the absence of the ventilation grid and, therefore, explaining the higher discrepancy between experimental and numerical data in point 4, for different compartments. The only compartment where this does not occur is in room 4, where the ventilation grid is placed differently.



a) Room 3 in plan  $y = 12.02$  m.

b) Living room in plan  $z = 2.795$  m (below the inlet).

Figure 93 – Velocity field in different compartments with indication of the position of points 4.

It can also be mentioned that the phenomenon mentioned above demonstrates the importance of the ventilation grids regarding comfort levels, considering that the purpose of the ventilation system is to supply air as equally as possible to all areas of a room. Without the grids, air does not distribute and tends to only supply in a certain direction. It is even more serious when the air is supplying directly towards a wall, as would happen, for example, in room 3, as shown in Figure 93a) and in most cases, as shown in Figure 78. If it was admitted that point 4 is not comparable numerically and experimentally and, therefore, was not considered, the mean relative differences in all living compartments would drop between 2 to 8%.

In service compartments, the same does not occur, since the registrations are upstream of the flow, before reaching the grid. This means that the absence of the grid does not have such a high influence in these compartments, as shown by the generally lower relative differences. Other model related discrepancies can be used to explain some less accurate results, such as the ventilation ductwork, where an approximation was done based on the ventilation project on paper (which may not fully correspond to the actual ductwork done on site) and photos. The tubes' lengths can vary slightly from reality and eventual inclinations were impossible to consider. This can highly influence the head loss of the flow inside the tubes. A possible deviation between the real and theoretical air velocity value at the exit and entrance of the ventilation unit (supply and extraction velocities) can also occur. Even the geometry of the building can be a source of error.

Numerical errors during the simulation can eventually occur, thus the need for its validation, especially in the prediction of a turbulent flow as in this case. The characteristics of the fluid, such as its viscosity defined in the fluid properties may also be slightly different. Errors can also be related to the acquisition of experimental data, due to human and equipment factors. In fact, as mentioned in the description of the experimental procedures, the anemometers used lack accuracy and sensitivity, leading to discrepancies.

### 5.3 Thermal comfort evaluation

An evaluation over the thermal comfort of the building was performed, as will be presented next. It is important to mention that, at the time of the thermal experimental registrations used to perform this evaluation, the building was not yet being lived in and a full understanding of the thermal settings of the mechanical ventilation system was lacking. Therefore, the thermal conditions that are found after the house is inhabited, are slightly better than those presented in this study. Nevertheless, it is possible to obtain a close prediction. Considering the methods presented in subsection 2.5.3, although the adaptive model from the EN 15251 is recommended by the Passive House Institute for South European climates, this model requires weekly information on the running mean outdoor temperatures, which is not available. The available thermal and velocity information in this work represent an ideal stationary condition, therefore, the analytical approach from ISO 7730 will be used to determine the PMV and PPD indices to thermally categorize the building. Local discomfort parameters will also be analysed.

For that, Equations 2 to 8 are used to determine the PMV index, which is then used to calculate the PPD through Equation 9.

Table 20 shows the parameters that were obtained experimentally ( $t_a$ ,  $RH$ ), numerically ( $v_a$ ) and through tabulated values ( $M$ ,  $I_{cl}$ ). Considering that the value of the mean radiant temperature ( $\bar{t}_r$ ) can only be obtained using a black-globe thermometer, which is unavailable, according to Rodrigues *et al.* (2009) this value is generally very close to the air temperature ( $t_a$ ), therefore, in the present work, it was decided to considerer them equal to each other.

Although possessing experimental velocity results, these were only measured near the ventilation openings, since the anemometer lacked the sensitivity to register values throughout the room. That issue is not verified in the numerical results, where velocities are predicted for each of the model's cells. Although the validation of the model presented

elevated relative differences between the experimental and numerical airflow velocity data, these were highly influenced by the absence of the ventilation grids. In this sense, the influence is much higher close to the ventilation grids than away from the openings, that is, where the residents spend most of their time. For that reason, the velocity results were used to predict the building's thermal comfort. Each room temperature and relative humidity was considered the average value of all registrations throughout the room and air velocities were extracted from the *FLOW-3D*<sup>®</sup> results in the exact same points where temperature registrations were made. From there, the average velocity of those points was calculated and considered the room's air velocity. Regarding the metabolism rate, it was considered that the residents are seated and relaxed and since the registrations were done in the summer, it was considered that they were wearing light summer clothing. The analysis was only performed in living compartments, where thermal comfort is more important. Note that, due to their proximity and the fact that they are connected, the living room and hallway 1 were considered the same compartment in terms of thermal analysis.

Table 20 – Thermal comfort evaluation according to ISO 7730-2006.

Main Parameter		Living Compartments					
		Living Room + Hallway 1	Room 1	Room 2	Room 3	Room 4	Hallway 2
Air temperature ( $t_a$ )	(°C)	25.6	24.5	25.5	25.6	25.3	24.5
Air velocity ( $v_{ar}$ )	(m/s)	0.05	0.05	0.04	0.03	0.02	0.03
Relative Humidity (RH)	(%)	57	59	60	56	59	63
Metabolism rate (M)	(W/m <sup>2</sup> )	58.15	58.15	58.15	58.15	58.15	58.15
Clothing insulation ( $I_{cl}$ )	(m <sup>2</sup> .°C/W)	0.078	0.078	0.078	0.078	0.078	0.078
Mean radiant temperature ( $t_r$ )	(°C)	25.6	24.5	25.5	25.6	25.3	24.5
PMV	(-)	-0.123	-0.470	-0.024	-0.051	-0.158	-0.451
PPD	(-)	5.311	9.607	5.012	5.053	5.519	9.243
Category	(-)	<b>A</b>	<b>B</b>	<b>A</b>	<b>A</b>	<b>A</b>	<b>B</b>

The mean temperatures registered in the Passive House varied from 24.5 to 25.6 °C, which is expected considering the summer conditions and the mechanical ventilation system. Thermal comfort is also influenced by the air velocity. Calm air is a term designated to

classify a comfortable air velocity, which is considered 0.10 m/s and is associated to air velocities near walls, where convective fluxes are more recurrent (Frota & Schiffer, 2006). For that reason, a comfortable air velocity inside compartments where residents spend most of their time and where convective fluxes are not felt, is below 0.10 m/s. The velocities obtained in each compartment are, therefore, considered comfortable. Note that velocities of such order of magnitude would always be below the available anemometer's range, rendering impossible the use of experimental data for this analysis. Regarding the relative humidity registered in each compartment, this should be between 30% and 70%, which is the case, as the registrations indicate values around 60%. Following Table 6 of sub-section 2.5.3, regarding thermal comfort evaluation, each compartment was thermally categorized. As mentioned before, category A is considered the most comfortable and category C the least comfortable. The results indicate that 4 of the 6 compartments are classified as category A, while the other two are category B. This means that, in every case, all PPD indices are below 10%, which indicates that over 90% of people would feel comfortable in each of the building's compartments. Of course, although the results indicate high levels of comfort, as a Passive House, it would be expected that all compartments achieved a category A classification. However, as mentioned in the beginning of this analysis, the thermal conditions at the time of the experimental data acquisition were not as favourable as they are now, namely regarding the efficiency of the ventilation system. Nevertheless, it is possible to affirm that high levels of thermal comfort are, in fact, achieved in the studied Passive House.

Local discomfort parameters were also analysed for the compartments mentioned earlier. In this case, however, it was not possible to analyse the 4 parameters mentioned in sub-section 2.5.3 (radiant temperature asymmetry, air draught, warm and cool floors and vertical air temperature difference). The radiant asymmetry, in first case, was always an impossibility, considering what was mentioned regarding the lack of instrumentation. Plus, at the time of the data acquisition, it was not expected to perform a local discomfort analysis, which is why other parameters are also lacking, such as the superficial floor temperature (which would have needed a thermo graphic camera to register those values). Even regarding the vertical air temperature difference, this would require registrations at a regular person's head level (around 1.70 m from the floor) and knee level (around 40 cm from the floor), while the only available registrations are at the floor level and 1.55 m above it. Nevertheless, considering

the existence of these registrations, they were still used to perform a prediction (with an associated error) on levels of local discomfort. The draught rate (based on numerical velocity values) and the vertical air temperature difference were analyzed as presented in Table 21.

Table 21 – Local discomfort parameters calculated according to ISO 7730-2006.

Local discomfort	Index	Compartment					
		Living Room + Hallway 1	Room 1	Room 2	Room 3	Room 4	Hallway 2
Draught	DR (%)	0.00	0.00	0.00	0.00	0.00	0.00
	Category	A	A	A	A	A	A
Vertical air temperature difference	PD (%)	0.44	0.48	0.37	0.41	0.41	0.33
	Category	A	A	A	A	A	A

The 2 local discomfort parameters calculated in this work demonstrate elevated levels of comfort. Regarding the draught rate, there is a clear indication that uncomfortable air draughts do not occur in the building, since the air velocities inside it are comfortably low, leading to a category A classification in every compartment. The vertical air temperature difference measured, although the registrations should have been around 20 cm higher, the results are very far from uncomfortable levels. In fact, the highest measured temperature difference is of 0.5°C (resulting in a PD of 0.48%), which corresponded to a category A classification in room1, while, to reach category B, that difference would have to be of 2.7°C (resulting in a PD of 3.1%), proving that although this is an approximation, the real values would always correspond to high levels of comfort.



# Chapter 6

---

Final Considerations



## Chapter 6. Final Considerations

### 6.1 Conclusions

The study developed in this dissertation intended to combine two separate areas that can, in fact, complement each other, which are the study of thermal comfort in Passive Houses and the use of CFD software. It contributed for a further implementation of the Passive House concept as a goal to achieve a NZEB status and therefore reduce energy needs in the construction sector. The fluid mechanics area of study was used to study ventilation phenomena inside a Passive House, by using the CFD commercial software *FLOW-3D*<sup>®</sup>. This allowed not only to predict interior airflow behaviour in such low energy buildings in order to evaluate its levels of comfort, but, at the same time, validate the numerical model by comparison with experimental data gathered on site.

Firstly, an overview on the modern energy crisis in the construction sector was addressed and the evolution of the Portuguese legislation in effort to attain the European demands was presented, where it was possible to conclude that Portugal is taking proper measures to achieve such goals. However, the NZEB status is not yet mandatory. Nevertheless, the Passive House concept is gaining roots in the country, especially with the help of studies such as this one. Therefore, a brief description of the Passive House concept was done, by presenting its origins, the requirements needed to obtain the certification and the main principles that help achieve this energy standard. While describing each of the 5 principles, these being: a continuous thermal insulation, the elimination of thermal bridges, the use of high insulated windows, rigorous airtightness and the use of a highly efficient heat recovery ventilation system, this dissertation then focused on this last principle. Ventilation principles were explained, the risk of overheating events were mentioned and how night-time ventilation can prevent them and, finally, heat recovery ventilation system in Passive Houses was addressed. An important part of this study lied on the thermal comfort achieved in these buildings, and how a proper and efficient ventilation has a crucial role in that achievement. For that, an assessment on this subject was performed, and methods for evaluating comfort were presented, with particular emphasis to the analytical approach, where thermal indices such as the PMV, PPD and local discomfort indices were described in order to further be used in the analysis of the case study.

In order to validate the *FLOW-3D*<sup>®</sup> simulations, acquisition of experimental data had to be done. For that, an initial data acquisition was done inside the Passive House in study by installing a blower door in a single sanitary facility and registering air velocities with a digital anemometer. Later, a similar procedure was done after the mechanical ventilation system was installed, where air velocities and temperatures were measured at the full-scale of the building. Both situations were modelled separately in *FLOW-3D*<sup>®</sup> and velocity results were extracted. Temperature data was not introduced in the numerical models.

Several conclusions were obtained by comparing experimental and numerical data in both situations. Firstly, it is clear that a simpler procedure, with a simpler model, which was the case of the blower door, is less prone to errors. In this case, 64% of the numerical results presented a relative difference below 15% when compared to experimental data, and 73% of them, below a 25% relative difference, which indicates an elevated accuracy. This model was, therefore, concluded to be properly validated. Regarding the full-scale model of the house, more complex features arose. Here, only 30% of the results presented a relative difference below 15%. Nevertheless, absolute differences in terms of amplitudes between numerical and experimental values were acceptable and it was possible to conclude that, regardless of the high percentages of relative differences, in many cases connected to the fact that this study dealt with low velocity values (mostly below 1 m/s), the simulation still presented accuracy in terms of order of magnitudes of the velocity values and also demonstrated the same airflow behaviour as verified in the experimental procedure. This case also allowed other conclusions to be drawn. The most important aspect regarding the discrepancies in the results, is related to the ventilation grids in the supply and extraction openings. Initially, these were intended to be introduced in the simulation. Therefore, a proper model of the grids was made, however, the mesh refinement needed to properly define their geometry proved to be a limitation in terms of time. The fact that these grids possessed a very small geometry, containing holes with diameters below 1 cm, required a mesh with extremely small cells. This comprised two problems: first, the high number of cells led to a very long simulation time and computer capacity needed and second, the optimum cell size ratios between multi-block meshes became overly difficult to obey. Simulations were therefore performed without the use of these grids, although it was acknowledged that their absence significantly influences the simulation results, since the proper definition of a combination of very big and very small geometries is, in fact, a limitation of the default mesh

type. The conforming mesh concept is the most viable option in order to define such geometries, however, the simulation time is still extensive. Future developments of the model are intended to be performed and, therefore, obtain a more accurate validation.

Regarding the thermal comfort analysis of the studied Passive House, both experimental and numerical data were used to perform a prediction. Thermal data was gathered on site, since the defined numerical model did not include this kind of information, while air velocities were used from the numerical simulation after its validation. In fact, although the absence of the ventilation grids influenced the velocity results near these openings, away from them, where the residents spend most of their time, the numerical velocities are assumed to be fairly accurate. Combining experimental and numerical data, it is possible to conclude that this Passive House achieves high levels of comfort. Analysing PPD indices, 4 out of 6 compartments presented a category A classification, meaning that less than 6% of the population would feel thermally uncomfortable in those compartments, while the remaining 2 compartments presented a category B classification, meaning that less than 10% of people would feel thermally uncomfortable inside them. It was also mentioned that the thermal conditions inside the house during the data acquisition were slightly worse than those found inside it after it became inhabited, which means that after this analysis, all compartments may obtain the highest classification. Regarding local discomfort, only the air draught rate and the vertical air temperature difference were possible to analyse, due to the lack of thermal information to classify the building in terms of radiant asymmetry and floor temperatures. In both calculated parameters, a category A classification was obtained in every compartment, indicating the inexistence of air draughts and very low temperature differences between the floor and a person's neck.

## **6.2 Future developments**

During this study, some features regarding the numerical simulation were not considered in order to simplify the model. Therefore, this sub-chapter intends to describe these features and present further developments that may be considered in future research.

The performed thermal comfort analysis was based on experimental data gathered by thermo hygrometers, such as room temperatures and relative humidity. A future development of this work is to introduce all thermal properties into the numerical model and, therefore, perform the same analysis done in this work, but based on thermal numerical results. This is

particularly important in order to predict the levels of comfort before having the ventilation system functioning. Considering the simulations performed in this dissertation, in order to render the full-scale model of the house more accurate, a simulation of the glazed windows can be done in order to take into account solar and heat gains from these elements, which would also allow the evaluation of radiant asymmetries. Plus, all heat sources inside the dwelling can be considered, including human and service compartment activities, such as cooking and showers. This way, the internal heat gains that characterize a Passive House will be modelled.

Considering that the ventilation inlet and outlet grids were not introduced in the simulations due to the computation time required to fully define their geometry, the introduction of these elements can be done in order to obtain more accurate velocity results. In fact, this process was already initiated in the framework of this dissertation. The ventilation grids were done using AutoCAD software. Figure 94 presents one of the 12 identical grids that were created and imported to *FLOW-3D*<sup>®</sup> as solid subcomponents.

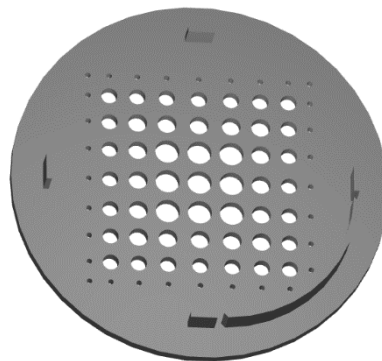


Figure 94 – Model of a ventilation grid.

In order to accurately define the geometry of the ventilation grids, the conforming mesh concept is believed to be the most viable. It is applied when a very small geometry within a large model is needed to be defined. In this case, the conforming mesh option would be applied so that meshes conform to a solid, in order to accurately capture a very thin solid region surrounded by fluid (Flow Science, 2015). This concept, however, still requires an elevated simulation time, which rendered this part of the simulation unobtainable to this dissertation, due to time restrictions.

The model that was created did not consider any air leakage/renewal. The entire envelope was considered totally airtight, however, a blower door test was performed in order to

calculate the air renewal rate and obtain the Passive House certification. That value can be used to simulate leakage areas and obtain a higher approximation of the studied house. Finally, the experimental data acquisition process can be performed with better equipment, since the anemometer that was used presented a low sensitivity and the thermo hygrometers were slightly limited. Plus, since this dissertation lacked information to properly perform a prediction over the building's level of local discomfort, such as mean radiant temperatures and floor temperatures, a black globe thermometer and a thermo graphic camera, respectively, can further be considered in order to determine this thermal information. To obtain higher accuracy in the prediction of the vertical air temperature difference, registrations should be done at the level of a person's head and knees. The temperature registrations could also be object of a longer and constant monitoring, leading to more accurate results and which would also allow to perform a thermal comfort evaluation according to the EN 15251 Standard, as recommended by the Passive House Institute.





# References

---



---

## References

- ADENE. (2013). Implementing the Energy Performance of Buildings Directive (EPBD). Retrieved September 16th, 2015, from: <<http://www.epbd-ca.org/Medias/Pdf/CA3-BOOK-2012-ebook-201310.pdf>>.
- Aelenei, L., Aelenei, D., Gonçalves, H., Lollini, R., Musall, E., Scognamiglio, A., Cubi, E., & Noguchi, M. (2012). Design issues for net zero-energy buildings. ZEMCH 2012 International Conference, Glasgow.
- Aelenei, L., Gonçalves, H., & Aelenei, D. (2013). The nZEBs in the near Future: Overview of definitions and guidelines towards existing plans for increasing nZEBs.
- Almeida, E. (2013). Casas passivas: conceito Passivhaus em climas mediterrâneos. MSc. thesis, Universidade de Aveiro, Portugal (in Portuguese).
- Antón, N. D., & Vogt, A. (2011). *Guía del estándar Passivhaus – Edificios de consumo energético casi nulo*. Chapter: La envolvente opaca y el aislamiento: Minimizar pérdidas. Madrid: Fundación de la Energía de la Comunidad de Madrid (in Spanish).
- Artmann, N., Manz, H., & Heiselberg, P. (2008). Parameter study on performance of building cooling by night-time ventilation. *Renewable Energy*, 33(12), 2589-2598. doi: 10.1016/j.renene.2008.02.025.
- Badescu, V., Laaser, N., & Crutescu, R. (2010). Warm season cooling requirements for passive buildings in Southeastern Europe (Romania). *Energy*, 35(8), 3284-3300. doi: 10.1016/j.energy.2010.04.013.
- Balachandran, P. (2006). *Fundamentals of compressible fluid dynamics*. India: PHI Learning.
- Carvalho, R. (2002). *Acções hidrodinâmicas em estruturas hidráulicas: Modelação computacional do ressalto hidráulico*. PhD. thesis, Universidade de Coimbra, Portugal (in Portuguese).
- Chen, Q. (2009). Ventilation performance prediction for buildings: A method overview and recent applications. *Building and Environment*, 44(4), 848-858. doi: 10.1016/j.buildenv.2008.05.025.

Crook, B., & Burton, N. C. (2010). Indoor moulds, sick building syndrome and building related illness. *Fungal Biology Reviews*, 24(3), 106-113. doi: 10.1016/j.fbr.2010.05.001.

Decreto-Lei n° 79/2006 de 4 de Abril. Regulamento dos Sistemas Energéticos de Climatização (RSECE). Diário da República n° 67 – I Série A, pp. 2416-2468.

Decreto-Lei n° 80/2006 de 4 de Abril. Regulamento das Características de Comportamento Térmico dos Edifícios (RCCTE). Diário da República n° 67 – I Série A, pp. 2468-2513.

Decreto-Lei n° 118/2013 de 20 de Agosto. Diário da República n° 159 – 1ª Série, pp. 4988-5005.

EN ISO 10211. (2007). Thermal bridges in building construction – Heat flows and surface temperatures – Detailed calculations.

EPBD. (2010). Directive 2010/31/EU of the European Parliament and of the Council of 19 May 2010 on the energy performance of buildings (recast). *Official Journal of the European Union*.

Feist, W. (2006). Ventilation in Passive House – only High Efficiency Will Work.

Retrieved October 28<sup>th</sup>, 2014, from:

<[http://passiv.de/former\\_conferences/Passive\\_House\\_E/passive\\_house\\_ventilation.html](http://passiv.de/former_conferences/Passive_House_E/passive_house_ventilation.html)>.

Ferziger, J., & Peric, M. (2002). *Computacional Methods for Fluid Dynamics* (3<sup>rd</sup> ed.). Germany: Springer. ISBN: 3-540-42074-6.

Figueiredo, A. (2014). *Dynamic Thermal Simulation of Passive Housing for Southern European Climate*. Seminar, Universidade de Aveiro, Portugal.

Flow Science. (2015). Flow-3D User Manual. Version 11.0.3, Flow Science.

Franke, J., Hellsten, A., Schlunzen, H., & Carissimo, B. (2007). Best practice guideline for the CFD simulation of flows in the urban environment. *COST Office*, (May), 1–52.

Frota, A. B., & Schiffer, S. R. (2006). *Manual de Conforto Térmico* (7<sup>th</sup> ed.). Brasil: Studio Nobel. ISBN: 85-85445-39-4.

Godish, T. (1994). *Sick buildings: definition, diagnosis and mitigation*. CRC Press.

- Gonçalves, H., & Graça, J. M. (2004). *Conceitos Bioclimáticos para os Edifícios em Portugal*. INETI, Lisbon, Portugal.
- Heiselberg, P. (2006). *Design of Natural and Hybrid Ventilation*. Department of Civil Engineering, Aalborg University. (DCE Lecture Notes; No. 5).
- IPHA. (2014). *Active for more comfort: Passive House* (2<sup>nd</sup> ed.). Germany: International Passive House Association.
- Jorge, A. (2013). *Convergência para NZEB de um edifício classificado*. MSc. thesis, Instituto Superior de Engenharia de Lisboa, Portugal.
- Keefe, D. (2010). Blower Door Testing. *JLC*. Retrieved November 14<sup>th</sup>, 2014 from: <<http://www.energyconservatory.com/sites/default/files/documents/blowerdoortestingjlc.pdf>>.
- Kleiven, T. (2003). *Natural Ventilation in Buildings: Architectural concepts, consequences and possibilities*. PhD. thesis, Norwegian University of Science and Technology, Norway.
- Kundu, P. K., Cohen, I. M., & Dowling, D. R. (2012). *Fluid Mechanics* (5<sup>th</sup> ed.). USA: Elsevier.
- Larbi, A. (2005). Statistical modelling of heat transfer for thermal bridges of buildings. *Energy and Buildings*, 37(9), 945-951. doi: 10.1016/j.enbuild.2004.12.013.
- Loomans, M. G. L. C. (1998). *The Measurement and Simulation of Indoor Air Flow*. PhD. thesis, Eindhoven University of Technology, Netherlands.
- Matias, L. (2000). *Seminário: Ambiente em edifícios urbanos*. Chapter: Conforto Térmico em Edifícios – Parte I: Conforto térmico em ambientes interiores. Lisboa: LNEC. ISBN: 972-49-1851-3.
- McLeod, R., Mead, K., & Standen, M. (2011). *Passivhaus Primer: Designer's Guide: A Guide for the Design Team and Local Authorities*. Watford: BRE (registered with the Passive House Institute as certifiers and designers for the Passive House Standard).
- Meireles, I. (2011). *Hydraulics of stepped chutes: experimental-numerical-theoretical study*. PhD. thesis, Universidade de Aveiro, Portugal.

Mlakar, J., & Štrancar, J. (2011). Overheating in residential passive house: Solution strategies revealed and confirmed through data analysis and simulations. *Energy and Buildings*, 43(6), 1443-1451.

Modiko. (2014). Processo construtivo. Retrieved April 9<sup>th</sup>, 2015, from: <<http://modiko.pt/sistema-modiko/conceito/>>.

Nicol, J. F., & Humphreys, M. A. (2002). Adaptive thermal comfort and sustainable thermal standards for buildings. *Energy and buildings*, 34(6), 563-572.

Norhidayah, A., Chia-Kuang, L., Azhar, M. K., & Nurulwahida, S. (2013). Indoor air quality and sick building syndrome in three selected buildings. *Procedia Engineering*, 53, 93-98. doi: 10.1016/j.proeng.2013.02.014.

Olesen, B. W. (2007). The philosophy behind EN15251: indoor environmental criteria for design and calculation of energy performance of buildings. *Energy and Buildings*, 39(7), 740-749. doi: 10.1016/j.enbuild.2007.02.011.

Oliveira, R. (2013). *Construir segundo requisitos Passivhaus: Modelação de pontes térmicas*. MSc. thesis, Universidade de Aveiro, Portugal.

Olsen, N. R. B. (1999). Computational fluid dynamics in hydraulic and sedimentation engineering. Department of Hydraulic and Environmental Engineering, The Norwegian University of Science and Technology, Norway. (DHEE Class notes). ISBN: 82-7598-041-0.

Passipedia. (2014a). Thermal bridges. Retrieved April 2<sup>nd</sup>, 2015, from: <[http://www.passipedia.org/basics/building\\_physics\\_-\\_basics/heat\\_transfer/thermal\\_bridges?s\[\]=thermal&s\[\]=bridge](http://www.passipedia.org/basics/building_physics_-_basics/heat_transfer/thermal_bridges?s[]=thermal&s[]=bridge)>.

Passipedia. (2014b). Passive House windows – requirements. Retrieved April 2<sup>nd</sup>, 2015, from: <[http://www.passipedia.org/planning/thermal\\_protection/windows/requirements\\_for\\_windows](http://www.passipedia.org/planning/thermal_protection/windows/requirements_for_windows)>.

Passipedia. (2015a). The world's first Passive House, Darmstadt-Kranichstein, Germany. Retrieved April 2<sup>nd</sup>, 2015, from:

<[http://www.passipedia.org/examples/residential\\_buildings/single\\_-\\_family\\_houses/central\\_europe/the\\_world\\_s\\_first\\_passive\\_house\\_darmstadt-kranichstein\\_germany?s\[\]=darmstadt](http://www.passipedia.org/examples/residential_buildings/single_-_family_houses/central_europe/the_world_s_first_passive_house_darmstadt-kranichstein_germany?s[]=darmstadt)>.

Passipedia. (2015b). The Passive House – definition. Retrieved April 2<sup>nd</sup>, 2015, from: <[http://passipedia.passiv.de/passipedia\\_en/basics/the\\_passive\\_house\\_-\\_definition](http://passipedia.passiv.de/passipedia_en/basics/the_passive_house_-_definition)>.

Passipedia. (2015c). PHPP – Passive House Planning Package. Retrieved April 2<sup>nd</sup>, 2015, from:

<[http://www.passipedia.org/planning/calculating\\_energy\\_efficiency/phpp\\_-\\_the\\_passive\\_house\\_planning\\_package?s\[\]=phpp](http://www.passipedia.org/planning/calculating_energy_efficiency/phpp_-_the_passive_house_planning_package?s[]=phpp)>.

Passipedia. (2015d). EnerPHit – the Passive House Certificate for retrofits. Retrieved May 13<sup>th</sup>, 2015, from:

<[http://www.passipedia.org/certification/enerphit;%20http://www.passiv.de/en/03\\_certification/02\\_certification\\_buildings/04\\_enerphit/04\\_enerphit.htm](http://www.passipedia.org/certification/enerphit;%20http://www.passiv.de/en/03_certification/02_certification_buildings/04_enerphit/04_enerphit.htm)>.

Passipedia (2015e). Thermal insulation. Retrieved September 24<sup>th</sup>, 2015, from: <[http://www.passipedia.org/planning/thermal\\_protection/integrated\\_thermal\\_protection?s\[\]=thermal&s\[\]=bridge](http://www.passipedia.org/planning/thermal_protection/integrated_thermal_protection?s[]=thermal&s[]=bridge)>.

Passipedia (2015f). General principles for improving airtightness. Retrieved April 2<sup>nd</sup>, 2015, from:

<[http://www.passipedia.org/planning/airtight\\_construction/general\\_principles/principles\\_for\\_improving\\_airtightness?s\[\]=red&s\[\]=pencil](http://www.passipedia.org/planning/airtight_construction/general_principles/principles_for_improving_airtightness?s[]=red&s[]=pencil)>.

Passive-On project. (2007). The Passivhaus standard in European warm climates: design guidelines for comfortable low energy homes – part 1. Passive-On project report. School of the built environment, University of Nottingham.

PHI. (2015a). Passive House Institute – Superior energy efficiency in buildings. Retrieved April 2<sup>nd</sup>, 2015, from:

<[http://www.passiv.de/en/01\\_passivehouseinstitute/01\\_passivehouseinstitute.htm](http://www.passiv.de/en/01_passivehouseinstitute/01_passivehouseinstitute.htm)>

PHI. (2015b). Passive House Institute – Passive House requirements. Retrieved April 2<sup>nd</sup>, 2015, from:

<[http://passiv.de/en/02\\_informations/02\\_passive-house-requirements/02\\_passive-house-requirements.htm](http://passiv.de/en/02_informations/02_passive-house-requirements/02_passive-house-requirements.htm)>.

Pinto, A. (2000). *Seminário: Ambiente em edifícios urbanos*. Chapter: Ventilação e Climatização – Parte III: Sistemas de climatização e ventilação mecânica. Lisboa: LNEC. ISBN: 972-49-1851-3.

Pinto, M., Freitas, V. P., & Viegas, J. (2007). Qualidade do ambiente interior em edifícios de habitação. *Engenharia e Vida*, 38, 34-43. Retrieved October 22<sup>nd</sup>, 2014, from: <[http://repositorio.ipv.pt/bitstream/10400.19/549/1/Engenharia%20e%20Vida\\_2007\\_MPinto.pdf](http://repositorio.ipv.pt/bitstream/10400.19/549/1/Engenharia%20e%20Vida_2007_MPinto.pdf)>.

Pordal, H. S. (2006). Practicing the science of computational fluid dynamics. *Stress Engineering Services, Inc, 10*.

Proença, M. C., & Cano, M. (2010). *Cadernos edifícios Número 6* (1<sup>st</sup> ed.). Chapter: Qualidade do ar interior. Lisboa: LNEC. ISBN: 978-972-49-2198-3.

Rodrigues, A. M., Piedade, A. C., & Braga, A. M. (2009). *Térmica de edifícios* (1<sup>st</sup> ed.). Amadora: Edições Orion. ISBN: 978-972-8620-13-4.

Ruivo, C. R. (2010). *Cadernos edifícios Número 6* (1<sup>st</sup> ed.). Chapter: Avaliação simplificada dos consumos de energia associados à ventilação. Lisboa: LNEC. ISBN: 978-972-49-2198-3.

Savage, B. M., & Johnson, M. C. (2001). Flow over ogee spillway: Physical and numerical model case study. *Journal of Hydraulic Engineering*, 127 (August), 640-649.

Schnieders, J., & Hermelink, A. (2006). CEPHEUS results: measurements and occupants' satisfaction provide evidence for Passive Houses being an option for sustainable building. *Energy Policy*, 34(2), 151-171. doi: 10.1016/j.enpol.2004.08.049.

Schnieders, J. (2003). Climate Data for the determination of Passive House Heat Loads in North Western Europe. PEP Project Information. EIE-2003-030.



- Sé, G. Ó. (2012). Guidelines for Blower Door Testing of Passive Houses. Retrieved November 3<sup>rd</sup>, 2014, from:  
<<http://www.greenbuild.ie/PassiveHouseBlowerDoorTesting.pdf>>.
- Shaviv, E., Yezioro, A., & Capeluto, I. G. (2001). Thermal mass and night ventilation as passive cooling design strategy. *Renewable energy*, 24(3), 445-452.
- Silva, M. (2013). *Modelação 3D de escoamentos em descarregadores de cheias com escoamento em superfície livre*. MSc. thesis, Instituto Superior Tecnico, Portugal.
- Sousa, J. R., Silva, S. M., & Almeida, M. G. D. (2012). Energy rehabilitation of Portuguese residential building stock through its transformation into NZEB. Seminário Reabilitação Energética de Edifícios, Universidade do Minho, Guimarães.
- Sousa, V. (2012). Introdução à dinâmica dos fluidos computacional. Instituto Superior Técnico, Lisboa. (Doctoral Program in Environmental Engineering, “Gestão Integrada de Sistemas de Saneamento” Lecture Notes).
- Testo (2015). Produtos. Retrieved December 10<sup>th</sup>, 2015, from:  
<<https://www.testo.pt/pt/home/produtos/produtos.jsp>>.
- Trend. (2014). Natural Ventilation. Retrieved October 24<sup>th</sup>, 2014, from:  
<<http://www.trendcontrols.com/en-GB/marketing/Documents/English%20Brochures/Eng%20Nat%20Vent%20Bro%20v1%20lo%20res.pdf>>.
- Valério, J. (2007). *Avaliação do Impacte das Pontes Térmicas no Desempenho Térmico e Energético de Edifícios Residenciais Correntes*. MSc. thesis, Instituto Superior Técnico, Portugal.
- Versteeg, H. K., & Malalasekera, W. (1995). *An Introduction to Computational Fluid Dynamics – The Finite Volume Method* (1<sup>st</sup> ed.). Harlow: Longman Scientific & Technical. ISBN: 0-582-21884-5.
- Viegas, J. C. (2000). *Seminário: Ambiente em edifícios urbanos*. Chapter: Ventilação e Climatização – Parte II: Contribuição da ventilação para a qualidade do ambiente interior em edifícios. Lisboa: LNEC. ISBN: 972-49-1851-3.

Wendt, J. (2009). *Computational Fluid Dynamics – An Introduction* (3<sup>rd</sup> ed.). Belgium: Springer. ISBN: 978-3-540-85055-7.

Wouters, P., & Santamouris, M. (2006). *Building Ventilation – The state of the art*. London: Routledge.

Zhai, Z. J., Zhang, Z., Zhang, W., & Chen, Q. Y. (2007). Evaluation of various turbulence models in predicting airflow and turbulence in enclosed environments by CFD: Part 1— Summary of prevalent turbulence models. *Hvac&R Research*, 13(6), 853-870

# Appendix

---



## Appendix A

Table A. 1 – Plan coordinates of each point measured near the inlet in experimental procedure 1.

Height	Point	x (m)	y (m)
1 (Z=2.35m)	1	1.685	1.770
	2	1.735	1.770
	3	1.685	1.820
	4	1.735	1.820
2 (Z=2.275m)	5	1.685	1.770
	6	1.735	1.770
	7	1.685	1.820
	8	1.735	1.820
3 (Z=2.2m)	9	1.685	1.770
	10	1.735	1.770
	11	1.685	1.820
	12	1.735	1.820
	13	1.785	1.770
	14	1.785	1.720
4 (Z=1.94m)	15	1.685	1.940
5 (Z=1.835m)	16	1.785	2.060
	17	1.785	1.960
6 (Z=1.535m)	18	1.785	2.060
	19	1.785	1.960
	20	1.885	2.060
	21	1.885	1.960

Table A. 2 – Plan coordinates of the outlet point in experimental procedure 1.

Height	Point	x (m)	y (m)
7 (Z=0.365m)	22	4.255	0.300

## Appendix B

Table B. 1 – Numerical range of the velocity results of experimental procedure 1.

Height	Point	x (m)	y (m)	Vmin (m/s)	Vmax (m/s)	Amplitude (m/s)	Vmed (m/s)
1 (Z=2.35m)	1	1.685	1.770	5.60	6.10	0.50	5.85
	2	1.735	1.770	3.60	3.80	0.20	3.70
	3	1.685	1.820	0.51	0.61	0.10	0.56
	4	1.735	1.820	0.99	1.49	0.50	1.24
2 (Z=2.275m)	5	1.685	1.770	2.80	2.86	0.06	2.83
	6	1.735	1.770	2.87	3.09	0.22	2.98
	7	1.685	1.820	4.42	4.57	0.15	4.50
	8	1.735	1.820	3.15	3.29	0.14	3.22
3 (Z=2.2m)	9	1.685	1.770	0.41	0.63	0.22	0.52
	10	1.735	1.770	2.86	3.05	0.19	2.96
	11	1.685	1.820	2.21	2.67	0.46	2.44
	12	1.735	1.820	2.86	3.06	0.20	2.96
	13	1.785	1.770	2.65	2.92	0.27	2.79
	14	1.785	1.720	0.26	0.42	0.16	0.34
4 (Z=1.94m)	15	1.685	1.940	0.36	0.43	0.07	0.40
5 (Z=1.835m)	16	1.785	2.060	1.60	1.77	0.17	1.69
	17	1.785	1.960	1.50	1.70	0.20	1.60
6 (Z=1.535m)	18	1.785	2.060	0.60	0.90	0.30	0.75
	19	1.785	1.960	0.24	0.39	0.15	0.32
	20	1.885	2.060	1.30	1.46	0.16	1.38
	21	1.885	1.960	0.41	0.49	0.08	0.45
7 (Z=0.365m)	22	4.255	0.300	4.64	4.67	0.03	4.66

## Appendix C

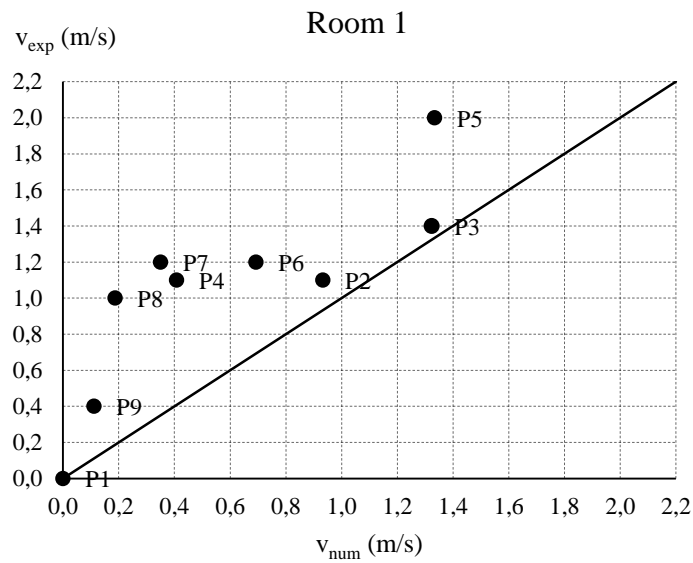


Figure C. 1 – Experimental vs numerical velocities for each point in room 1.

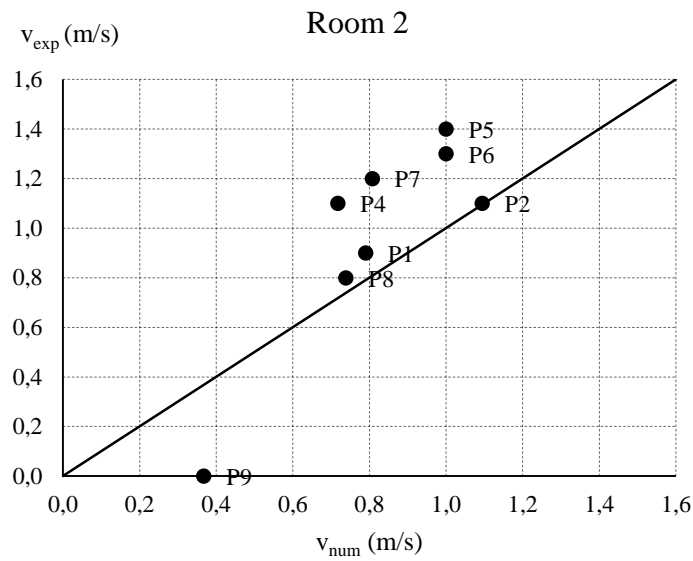


Figure C. 2 – Experimental vs numerical velocities for each point in room 2.

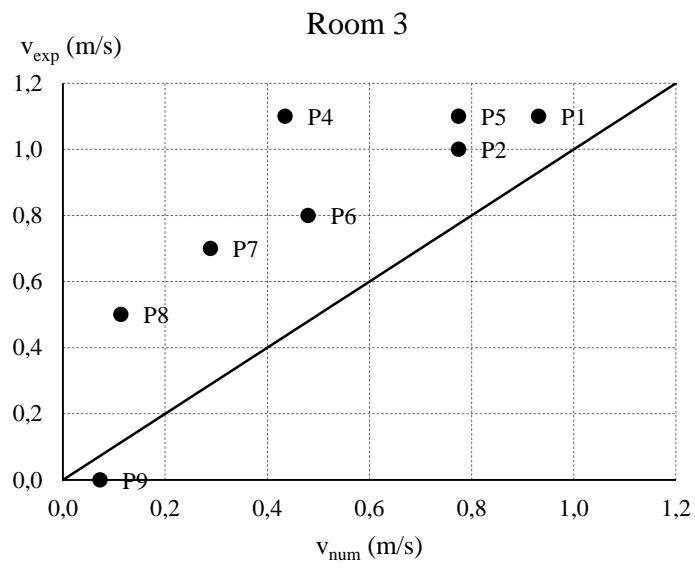


Figure C. 3 - Experimental vs numerical velocity results for each point in room 3.

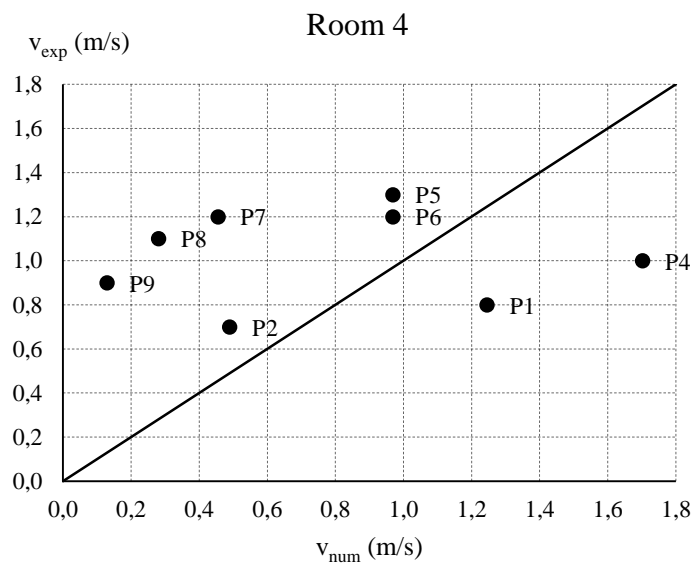


Figure C. 4 – Experimental vs numerical velocity results for each point in room 4.



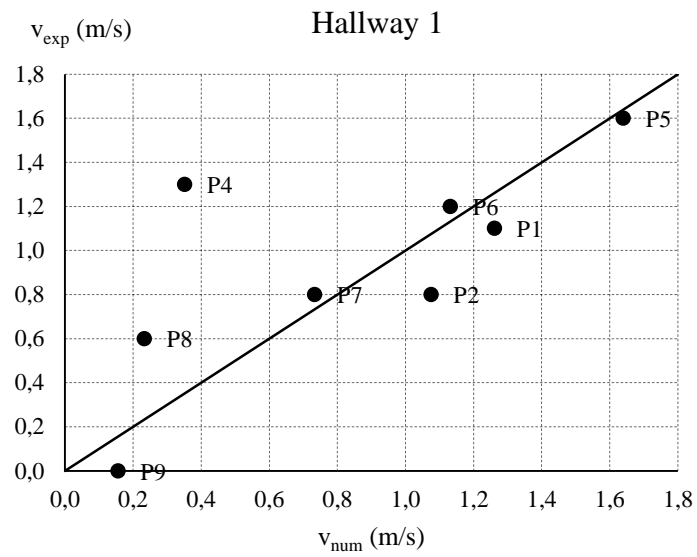


Figure C. 5 – Experimental vs numerical velocity results for each point in hallway 1.

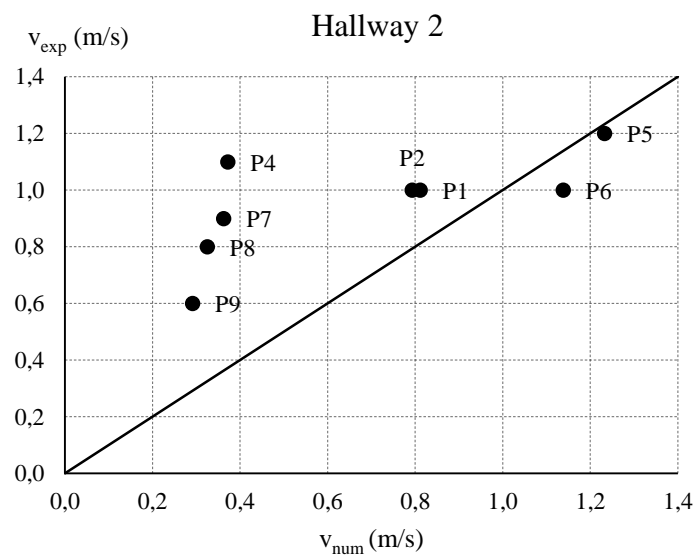


Figure C. 6 – Experimental vs numerical velocity results for each point in hallway 2.